Ministry of Higher Education and Scientific Research
University of Babylon -College of Science
Chemistry Department

Determination of poly nuclear aromatic hydrocarbons(PAHs)in surface water of Shatt Al-Hilla River and possibility of laboratory treatment for Anthracene

A Thesis Submitted to the Council of the College of Science, University of Babylon as a Partial Fulfillment of the Requirements for the Degree of Doctor of Philosophy
in Chemistry
By

Faiq Fathallah Karam Al-Syad

B. Sc. 1990-1991 **M. Sc. 2001-2002**

Supervisors

Prof. Dr. Falah Hassan Hussein & Assist. Prof. Dr. Sadiq Jaafer Baqir

2014 AC **1435 AH**

CHAPTER ONE

INTRODUCTION

1.1 General Introduction:

Polycyclic Aromatic Hydrocarbons (PAHs) or polynuclear aromatic hydrocarbons are an important group of environmental pollutants because of their prevalence and potentially adverse health effects. PAHs are ubiquitous environmental contaminants found in soil, air and aquatic environments [1-3]. PAHs emitted into the atmosphere as a result of industrial processes enter the surface water of rivers and lakes together with atmospheric deposition. They may also enter rivers directly along with municipal and industrial effluents [4].

Their concentrations range from not more than 10 ng/L in slightly contaminated water to over 1000 ng/L in heavily contaminated water [5, 6].

Some PAHs are mutagenic, and potent carcinogens and their presence in water can pose huge risks to both human health and aquatic organisms. The changes in PAH quantities in an environment are a reflection of biological degradation, evaporation, photochemical oxidation and adsorption to suspended matters. Photochemical oxidation and sedimentation cause a decrease in concentrations of the higher molecular mass of PAH. The lower molecular mass compounds are extensively degraded by microorganisms – bacteria, fungi and algae [7].

Both the European Union and the US Environmental Protection Agency (EPA) have listed them as priority pollutants. PAHs could exist constantly in the environment, especially in the presence of some substances that inhibit PAH degradation processes. For instance, Wild et al. (1991) reported that PAH degradation was significantly reduced in soil amended with Ni-rich sludge [8,9].

PAHs have often been found to coexist with some heavy metals due to similar contamination sources [10-13].

Natural organic matter (NOM) is known to have a binding preference towards PAHs [14,15]. This binding interaction can produce partitioning or adsorption phenomena, according to the nature of the organic matter [16].

The partitioning or distribution of non-ionic hydrophobic organic compounds like PAH compounds between water and sediment or soil has been shown to depend on the fraction of organic carbon in the sorbent and hydrophobicity of the compounds [17].

Concentrations of PAH compounds range between 0.1-830 ppb in surface waters. These contaminants in an aqueous medium can be absorbed by solid particles which form a suspension or colloidal solution. Condensed aromatic rings are mostly non-polar or very weak polar compounds; their solubility in water is very low and decreases as the number of aromatic rings increases. [18**]**

1.2. PAHs

PAHs are defined as compounds that consist of two or more fused aromatic rings, containing only hydrogen and carbon atoms [19, 20].

Activities such as agriculture and industrial production, combined with heavy urbanization and population growth, may negatively affect the aquatic environment, this effect including the degradation of wetland habitats and a heightened risk for humans and aquatic organisms [21- 23].

Most polycyclic aromatic hydrocarbons are suspected carcinogens and mutagens they are widespread in the soil, air and water [24-25].

These are formed mostly by the incomplete burning of organic materials [26,27]. These compounds may appear in the atmosphere either in the gas or particulate phase [28].

The distribution and concentration of polycyclic aromatic hydrocarbons are mentioned in many studies [29-32].

The occurrence of PAHs in rural sites in the USA and Canada was found to have meant a total concentration range from 26 to 90 ng/L [25].

The concentration and distribution of PAHs in an environment are often closely connected to local and regional sources; in addition to remote areas there can be sites of PAH deposition via atmospheric processes and long range transport. PAHs are formed during the incomplete burning of the pyrolysis process and chemical products by a series of complex reactions [33-37].

Due to the mutagenicity and carcinogenicity of these compounds, they were listed in several priority pollutant agencies such as the European Community (EC), the Agency of Toxic Substances and Disease Register (ATSDR), the Environmental Protection Agency (EPA), the International Agency for Research and Cancer (IARC) and in 1984

in the United States Environmental Protection Agency (USEPA) (US Environmental Protection Agency, 1984) [38].

Exposure of PAHs to humans is 88-98% connected with food [39]. Penetration of PAHs through food can follow two paths: the first is directly when smoking fish, for instance, and the second is indirectly from air or water.

PAHs are lypophylic compounds in nature and usually accumulate in the fatty tissues of organisms; as such they produced from the fatty tissues of fish at higher temperatures during the smoking process. The formation of polycyclic aromatic hydrocarbons is well-known to occur through the pyrolysis of fat at temperatures of more than 200°C [40, 41], and it is highly stimulated at temperatures of more than 700°C [42].

Pyrolysis of other organic compounds such as carbohydrates and proteins might be involved, but the highest concentrations of PAHs have been shown to arise from fat pyrolysis [43]. Consequently, if a fish is in direct contact with a flame, pyrolysis of the fat in the fish generates polycyclic aromatic hydrocarbons that become deposited on the fish. Previous studies proved that PAH production by cooking over charcoal (grilling or barbecuing) is a function of both the fat content of the meat/fish and the proximity of the food to the heat source [44, 45].

Seven PAH compounds have been classified by the United State Environmental Protection Agency (USEPA) as compounds of problematic human carcinogens [46]. These are Benzo[a]pyrene, Benzo[a]anthracene, chrysene, Benzo[k]Fluoranthene, Benzo[B]Fluoranthene, Dibenzo[a,h]anthracene, and indeno[1,2,3-cd]Pyrene. PAHs known for their carcinogenic, mutagenic and teratogenic properties are benz[a]Anthracene, chrysene, benzo[b]fluoranthene, benzo[j]fluoranthene, benzo[k]fluoranthene, benzo[a]pyrene, benzo[g,h,i]perylene, coronene, dibenz[a,h]anthracene, indeno[1,2,3-cd]pyrene and ovalene.

Polycyclic aromatic hydrocarbons are considered as the main classes of contaminants in the terrestrial environment [47].

The presence of PAHs in the environment at higher quantities is a result of human civilization. High concentrations of PAHs have been found in meat cooked at high temperatures such as barbecued or cooked meat and in smoked fish [48].

Evaluating the degradation of PAHs in the environment is extremely difficult. Many researchers have observed a stimulation of the PAH degradation rate in the presence of sulphate reducing conditions [49].

Ambrosoli et al. [50], noted that biodegradation of PAHs could proceed both by fermentative and respiratory metabolism. In a related study [51], researchers suggested that PAHs could also be degraded and then removed from an anaerobic system by the removal of PAHs from this system, which appeared to be slower than degradation in aerobic conditions. It has been suggested that PAHs are significantly degraded within a range of pH 6.0-8.0 using chemicals [52]. A related study showed that chemical oxidants such as Fentons reagents have demonstrated efficiency in destroying PAHs in soil [53]. Other researchers investigated titanium thin film photocatalytic reactors as a device for degrading PAHs in diluted water samples [54].

1.2.1 Properties of PAHs

PAHs are weakly volatile compounds and dissolve slightly in water; the solubility of these compounds decreases with an increase in the number of fused aromatic rings. They are lypophylic and dissolve well in organic solvents. All PAHs are have a high boiling and melting points. PAH compounds are chemically inactive but have the ability to bond to particulate matter. When adsorbed at the surface of dust particles these compounds are highly thermo-and photosensitive [55].
PAH compounds are classified as mutagenic and carcinogenic compounds; according to these properties it should be necessary understand their physical-chemicals transform through the atmosphere [56].

PAH compounds, which consist of two or three rings, are found predominantly in the gas phase, while those containing six or more fused rings principally adsorb to particles. Whereas PAHs consisting of four or five fused aromatic rings are partitioned between both phases to a degree dependent on environmental conditions and aerosols [57].

During their transport, PAH compounds are lost by both the gas-phase and heterogeneous photo-oxidation processes. Recent laboratory and modeling studies [58] suggest that heterogeneous reactions may be the dominant reactive atmospheric loss process for the larger PAHs prior to deposition.

High molecular weight PAHs, such as Benzo[a]Pyrene, Benzo[g,h,i]pyrelene and Benzo[b]Fluoranthene, primarily exist in the particulate phase in the air owing to their low vapor pressure. By contrast, low molecular mass PAHs with a higher vapor pressure are predominant in the gaseous phase. PAHs comprise a heterogeneous group of organic compounds with large differences in physicochemical properties such as vapor pressure, molecular weight and water solubility (Table 1.1).The fused rings can

be positioned in a linear, e.g. Anthracene, globular, e.g. Pyrene, or angular, e.g. Phenanthrene, arrangement (Fig. 1.1.) and generally the physicochemical properties for each compound are correlated to the number of fused rings in this compound, while minor differences within each ring-homologue is due to the arrangement of the rings. The physicochemical properties of the PAH compounds largely determine their environmental behavior. PAHs having a low molecular weight (LMW), which contain two or three fused aromatic rings, are more volatile and more water soluble, and hence more available, than those having a high molecular weight (HMW). PAHs containing fewer than three fused rings are primarily associated with particles. A higher abundance of LMW PAHs, as compared to HMW PAHs, makes them more likely to occur in various biological, photochemical and chemical degradation processes. PAH pollution in soil differs from water and air pollution in several ways. In air, most organic contaminants are degraded by reaction with hydroxyl-radicals, and thus their half-lives tend to be shorter in air than in either soil or water. In addition, air and water may mix with contaminants, resulting in the dilution of the PAH compounds into larger quantities and being transported to other parts of the environment. However, in soil and sediments, where PAHs are adsorbed to compartments of the soil and sediments, degradation, dilution and transport are limited [59].

Table 1.1 Selected properties of the 16 US-EPA PAHs [59].

PAHs Compound	Number of rings	Molecular weight	Aqueous solubility (mg/l)	Vapor Press. (Pa)	LogKow
Naphthalene (Nap)	2	128	31.00000	$1.0x10^{-2}$	3.37
Acenaphthylene (AcPY)	3	152	16.00000	$9.0x10^{-1}$	4.00
Acenaphthene (AcP)	3	154	3.80000	$3.0x10^{-1}$	3.92
Fluorene (Fl)	3	166	1.90000	$9.0\ x10^{-2}$	4.18
Phenanthrene (Phe)	3	178	1.10000	$2.0\ x10^{-2}$	4.57
Anthracene (Ant)	3	178	0.04500	$1.0\ x10^{-3}$	4.54
Pyrene (Pyr)	4	202	0.13000	$6.0\ x10^{-4}$	5.18
Fluoranthene (Flu)	4	202	0.26000	$1.2\ x10^{-3}$	5.22
Benzo[*a*]anthracene(B[a]A)	4	228	0.01100	$2.8\ x10^{-5}$	5.91
Chrysene (Chr)	4	228	0.00600	$5.7\ x10^{-7}$	5.91
Benzo[*b*]fluoranthene (B[b]Flu)	5	252	0.00150	-	5.80
Benzo[*k*]fluoranthene (B[k]Flu)	5	252	0.00080	$5.2\ x10^{-8}$	6.00
Benzo[*a*]pyrene (B[a]P)	5	252	0.00380	$7.0\ x10^{-7}$	5.91
Dibenzo[*a,h*]anthracene (DbA)	5	278	0.00060	$3.7\ x10^{-10}$	6.75
Indeno[1,2,3-cd]pyrene (InP)	6	276	0.00019	-	6.50
Benzo[*g,h,i*]perylene (BghiP)	6	276	0.00026	$1.4\ x10^{-8}$	6.50

Kow = Octanol /water partition coefficient.

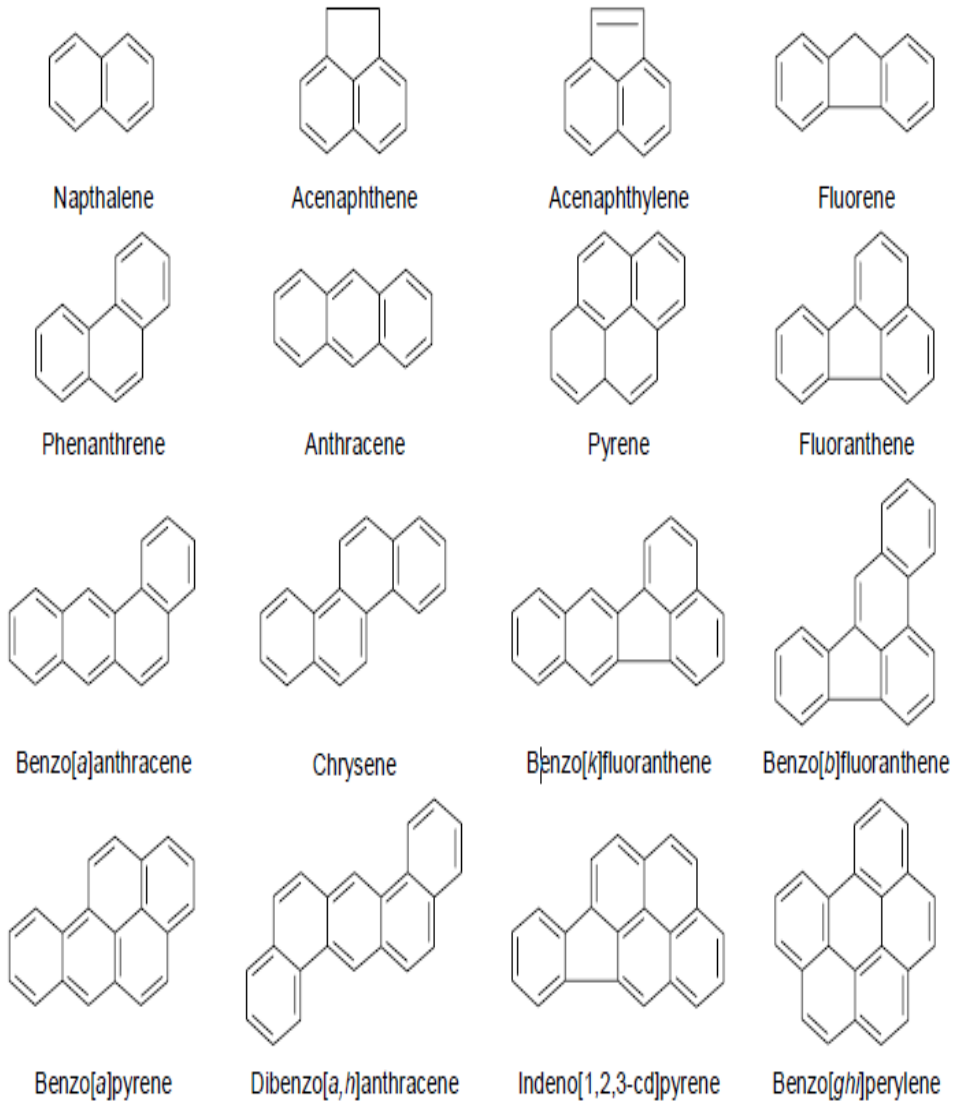

Fig. 1.1. Structures of the 16 US-EPA PAHs [59].

1.2.2 PAH Sources

The atmospheric input of semi-volatile organic compounds to the aquatic environment has been studied since the early 1970s [60 and reference there in]. During the past several decades, numerous studies have followed the level of pollution of PAH compounds in atmospheric deposition into the aquatic environment all over the world. Although PAHs can be transferred over long distances and deposited in more remote areas, the maximum deposition fluxes were monitored in the vicinity of industrial and urban areas [61,62].

Atmospheric deposition is considered as an important source of PAHs for surface water. The appearance of low molecular weight PAHs was reported to occur in the

atmosphere in the vapor phase, while multi-ring PAHs are bound to particles. Intermediate molecular weight PAHs are distributed between the vapor and particulate phase, depending on atmospheric conditions such as temperature [63]; in addition to the atmospheric input of PAHs through surface water, there are several sources such as urban run-off, municipal effluent, industrial effluent, oil leakage and oil spillage. PAH compounds have a relatively low solubility in water, but are highly lipophilic. Generally, the concentrations of PAHs in water are low [64]. The concentrations of PAHs in river sediments are generally much higher than in the surrounding body of water [65].
Domestic heating by wood combustion is among the main sources of emission of volatile organic compounds, particulate matter and polycyclic aromatic hydrocarbons, which are linked to harmful effects on human health [66].

The mutagenicity of the air in areas which use wood as fuel is widespread and is positively correlated with the PAH concentration in the air [67- 71]. The quantity of PAHs in the air is mainly due to incomplete burning of carbon and hydrogen-based fuels [72] such as vehicle fuels [73,74] and wood used for heating [75-78].

The emission of PAHs depends on many factors such as the amount of air/fuel [79] and the temperature of combustion. According to previous studies, wood combustion can produce more PAH emissions than any other type of fuel [80].

Other sources contributing to PAH emissions in the environment are as a result of a number of anthropogenic sources such as the combustion of organic matter, but also natural activities such as biogenic formation, volcanic eruptions, and others [81].

PAHs are very hydrophobic and tend to bind with particles [82]; due to their resistance to the degradation process (particularly when matched with particles), PAHs are subject to long transport, thus being detected even in remote areas, where primary emissions are limited. The production of PAHs in urban atmospheres is attributed to cooking activities, industrial activities, waste incineration and heating. Once in the atmosphere, polycyclic aromatic hydrocarbons will partition between the gas and particulate phase, with more hydrophobic and heavier ones tending to sorb exclusively onto particles. The penta and hexa ring PAHs are expected to sorb onto particles with an aerodynamic diameter of 0.5- 1.0 mm, because the latter deposit very slowly and remain in atmospheric dispersion for days [83].
The atmospheric deposition of combustion by products is a significant non-point source of PAHs to rivers, lakes [84] and coastal waters. Another non-point source is storm water runoff from watersheds [85].

Urban runoff from paved parking lots and roads occurs by washing particle-bound PAHs from the road surface [86] or direct leaching from bitumen and asphalt [87].

PAHs occur naturally in crude oil and coal they are often associated with the burning of fossil fuels. PAHs are thus ubiquitous environmental contaminants and elevated levels of site specific PAHs are generally near emission sources.
Domestic heating by wood combustion is among the main sources of the emission of VOC, PM and PAHs which are linked to harmful effects on human health. In previous studies, the mutagenicity of the air in regions which use wood as a fuel is widespread and is positively correlated with the PAH quantity in the air[88]. The concentration and composition of PAH profiles contaminating smoked meat products depend on several factors such as the type of food and its moisture content, and also the temperature associated with smoke generation, all of which have maximum effects. Benzo[a]pyrene concentration (one of the PAH compounds) has received particular interest due to its higher contribution to the overall burden of the occurrence of cancer in humans; therefore, it is used as a marker for the occurrence and effect of carcinogenic PAHs in food [89 and references their in].

The ambient PAH concentrations reported vary due to meteorological conditions and sampling locations. In general, their levels are higher in industrial regions than those in non-industrial regions, and are higher in urban areas than those in suburban areas. In addition, their levels are usually higher in winter than in summer [90].

PAH compounds are found in the atmosphere as by-products of the incomplete burning of almost any type of fuel. Therefore they exist in the environments of nearby urban and industrial areas rather than other places, and have been started to be widely investigated with regard to their environmental effects due to their well-known mutagenic and carcinogenic properties [91].
PAHs may enter the environment by adsorbing onto fine particulate matter through the atmosphere or via aquatic environments, transferring long distances, or by dissolution, resulting from more local sources. High molecular weight PAHs have been reported in the first case as opposed to low molecular mass PAHs, which are usually associated with the latter [92].

1.2.3 Health Effects of PAHs

Human health risk measurements has been used to determine if exposure to a chemical could cause a rise in the incidence of adverse effects on human health. The human population is suffering increased exposure to existing and new chemicals and

environmental toxins. Among the various environmental toxins, PAHs are an important class of environmental contaminants, and many PAHs are known or suspected carcinogens. Exposure to some of these compounds is well-known to cause cancer in mice and they are suspected to be carcinogenic compounds for humans [93]. The International Agency for Research on Cancer (IARC) concluded that some PAH compounds such as those produced by coke production and coal gasification have been deemed to be carcinogenic materials for humans in the data of carcinogenicity mechanisms [94, 95].

The carcinogenic and mutagenic effects of individual PAHs and PAH-containing products such as coal tars have been well investigated in several animals and in humans. PAHs are widespread environmental contaminants, and methods of monitoring human exposure to PAHs as a preventive health assessment are very important. The most frequent method for monitoring occupational PAH exposure is determining the concentration of airborne PAHs [96].

PAHs, and especially those with four or more fused aromatic rings and their metabolites, are considered as hazardous contaminants due to their toxicity, carcinogenicity and mutagenicity, and are classified as compounds with significant risks to humans [97, 98].

Benzo[a]anthracene and benzo[a]pyrene are formed when tobacco, gasoline, garbage or any plant material or animal burns, and being the most potent carcinogens, they can act both as promoters and initiators in the carcinogenic process. The carcinogenic effects of exposure to both compounds are mediated by their metabolic conversion, which might causes DNA adduct formation and mutations. Phenanthrene is a lower molecular weight PAH with three fused aromatic rings and is largely introduced into the environment through fossil fuel extraction, inhalation of polluted air, tobacco smoke, or ingestion of water contaminated with combustion effluents. While there is a large part of literature describing the toxicity and carcinogenicity of other PAHs, the toxicity data for Phenanthrene is limited because it is considered to have a non or only slightly toxic effect on humans. Naphthalene is used in the production of Naphthalic anhydride and mothballs, and exposure to this compound can cause severe DNA and oxidative damage. Recently, the US Environmental Protection Agency (EPA) and the Agency for Toxic Substances and Disease Registry (ATSDR) evaluated Nap exposure and determined that there is good evidence that Naphthalene exposure can lead to hemolytic anemia and liver, retinal, and neurological damage in animals. Since Naphthalene is a known carcinogen of the lung in rodents, it is classified as a possible human carcinogen [95].

Benzo (a)-Pyrene is a representative PAH that is generated as a product of combustion, and it exists in significant concentrations in cigarette smoke. According to different environmental protection and health organizations, such as the International Agency for Research on Cancer (IARC), many PAHs have carcinogenic, mutagenic and endocrine-disrupting properties [99].

Cioroiu et al., (2011) [100] have repeatedly reported human health damage associated with exposure to PAHs. Lung cancer, with an estimated 334,800 deaths (19.7% of the total number), was regarded to be the most frequent cause of cancer death in Europe, followed by colorectal cancer (207,400 deaths), breast cancer (131,900) and stomach cancer (118,200) [101]. It was reported that lung cancer affects mostly men [102].
Tobacco smoke is a main source of human exposure to PAH compounds. It was estimated that a smoker is exposed to about 1–30 $\mu g\, d^{-1}$ per pack of cigarettes [103]. In a study of 1,000,000 deaths in China, the risk of lung cancer was two to four times higher among smoking people compared to nonsmoking people who did not smoke, and this correlation was generally consistent in both urban and rural areas. In Romania, previous studies reported that the incidence of lung cancer compared with other types of cancers was higher, with over 10,000 new cases. Recent studies show higher levels of PAH compounds in human breast milk in environmental matrices [104] and in human blood.
Epidemiological investigations have demonstrated that exposure to urban particulate matter is associated with several adverse health effects. Exposure for a long time to high concentrations of particulate matter increases the chances of getting lung cancer, arteriosclerosis and respiratory diseases, whereas exposure for a short time can cause the exacerbation of different forms of respiratory disease, including asthma and bronchitis, as well as changes in heart rate variability [105]. The toxic effects of particulate matter are attributed to the small particulates with an aerodynamic diameter of less than 2.5 micrometers. Because of their large specific surface area, these particulates can adsorb different organic substances, such as PAHs, nitro aromatic hydrocarbons, and oxygenated aromatic hydrocarbons [106].

According to Calxton et al., (2004)[107], the mutagenicity of airborne particulates can result from about 500 or more identified compounds covered different chemical classes. Mutagenic non-substituted PAHs were the class most studied and their well-known compounds, recently, nitro-PAHs and oxy-PAHs have been shown to be very important due to their strong biological activity [108].

1.3 Preconcentration and Measurements Methods for PAHs in Water

The monitoring of polycyclic aromatic hydrocarbons is an important problem due to their well-known effects as mutagenic and carcinogenic compounds [109]. These compounds are found in several matrices, both biological and environmental.

Due to the abundance of PAHs in trace level concentrations and their wide distribution in water environments, it is necessary and vital to develop efficient methods for pre-

concentration and high selective and sensitive separation technique and analysis instruments.
The most frequent analytical methods for PAH compounds in surface water are high performance liquid chromatography–fluorescence detection (HPLC–FLD), or detection HPLC–UVDAD, (GC-MS), HPLC–ESI-MS and GC, which have also often been applied to measuring PAHs in water [110].

1.3.1 Extraction Techniques

PAHs are typically classified as non-polar compounds and they have excellent retention on reversed-phase adsorbents such as C18 bonded silica. Solubility of PAHs in water is very low; concentrations at the µg/L level are commonly encountered in the environment. Since PAH compounds are considered toxic at this level, their presence needs to be monitored. Recently, the development of pre-concentration steps in order to be implemented prior to the determination of trace level compounds were explored in considerable depth. With a view to eliminating, or at least minimizing, the use of different solvents employed in conventional liquid-liquid extraction, and which have been used by the EPA, other methods have been developed. Among them, membrane extraction, SPE and SPME are the most common ones.

Research activities are oriented towards the development of efficient, economical, and miniaturized sample preparation methods, SME and SPME have been developed, as compared with LLE and SPME, which is a solvent free process developed previously, this developing includes the simultaneous extraction and pre-concentration of analyte from the samples or the headspace of the sample. But SPME is considered expensive, its fiber is fragile, it has a limited lifetime, and sample carry-over can be problem. Recently new developing in an extraction method LLME system by which extraction is achieved into a single drop [111 and references there in].

The frequent methods for extracting PAHs from liquid and solid samples were SPE [112], LLE [113], and more innovative methods such as (SBSE) [114] and (SPME)[115].

The extraction of PAH compounds from water samples into a form that is pre-purified, concentrated and compatible with the analytical technique plays a key role in the precision and accuracy towards a new analytical methodology for the determination of PAHs in water samples. The single drop micro-extraction technique was developed as a solvent minimized sample pretreatment [116].

1.3.1.1. Solid Phase Extraction (SPE)

SPE is one of the fastest, most economic and cleanest pre-concentration methods for separating and concentrating trace metals from water [117].

The usual steps for sample preparation to determine the trace concentrations of analytes in complex samples include: the extraction of an analyte or analytes from the matrix, and subsequently their purification. SPE is commonly used for preparing the sample in the determination of PAHs, especially in drinking water [118].

The US-EPA prescribes LLE and SPE methods for pre-concentration polycyclic aromatic hydrocarbons in water samples. The extraction of polycyclic aromatic hydrocarbons from water samples, if it was compatible with an analytical system, can act as a key role for the determination of PAHs in water samples. The preferred method for analyzing PAHs in the aquatic environment is the SPE. The PAHs and SPE combine with column liquid chromatography, some whose derivatives represent a complex class LC or GC. Poppa et al., (2000) showed that fluorescence detection used on a 10 mL sample resulted in detection limits ranging between levels of (0.5-0.7) ng/L. The total analysis time was 50 min [119].

Solid phase extraction is a routine extraction method for contaminants that exist in trace metals in the environment. Recently, researchers used nano particles for sample extraction in SPE [120].

Nano-particle NPs offer higher significant surface area to volume ratio compared with traditional SPE sorbents. Other advantages for this type of sorbent, such as the short diffusion route, result in high extraction capacity, high extraction efficiency and rapid extraction dynamics [121].

Fe_3O_4 NPs has received increasing attention in recent decades due to its unique chemical and physical properties and high potential applications in different fields such as cell separation, drug delivery, magnetically assisted and protein separation [122, 123].

SPE because of its advantages of high recovery, short extraction time, high enrichment factor, low consumption of organic solvents, and ease of automation and operation, was universally used for the concentration of PAHs in water samples. In an SPE procedure, the choice of adsorbents was a very important factor for obtaining high enrichment efficiency. There are many materials used as SPE adsorbents for the pre-concentration of PAHs in water samples, including porous organoclay composite, matrix-immobilized organoclay, polyvinylidenefluoride, and bamboo charcoal. But C18 is the most common adsorbent chosen for extracting PAHs from water samples.

Oleszczuk and Baran [124] applied C18 as the SPE sorbent to determine PAHs in sewage sludge extracts. However, the recovery of large number of ring PAHs was not satisfactory in some cases and thus improvements were still needed. Solid phase extraction also requires a high level of expertise and the use of expensive cartridges [125].

1.3.1.2. Liquid-Liquid Extraction (LLE)

LLE is probably the most widely used technique for the extraction of PAHs from aqueous samples. However, LLE needs relatively large amounts of organic solvents and is a time-consuming as well as a labor-intensive method [126].

Despite researchers' trends towards a sample-handling focus on the development of faster, safer, cheaper and more environmentally friendly extraction methods, both LLE and SPE are still useful and widely accepted techniques for the exhaustive extraction of organic pollutants from water matrices. Traditional LLE does not fulfill the current requirements of green chemistry. However, it allows the application of the procedure to the raw sample without a filtration process, thus offering the possibility of extracting organic pollutants that tend to accumulate in the suspended solids [113].

The major disadvantage of the LLE method is that it needs large volumes of organic solvents and a long extraction time.

1.3.1.3. Solid Phase Micro-Extraction (SPME)

Solid phase micro-extraction has become a popular technique based on a single equilibrium at which the analyte partitions between a fiber coating and a matrix. A long sample preparation time, a limited fiber lifetime, and low recovery are common drawbacks that can be experienced with this technique. In recent years a new extraction method, SPME has been developed. It was initially investigated for the gas-chromatographic analysis of volatile and semi-volatile organic compounds. LC was described by Chen and Pawliszyn (1995), who used a specially designed interface [127].

Polycyclic aromatic hydrocarbons were selected as test analytes to evaluate this interface. Other SPME-LC couplings with various interfaces have been applied for the determination of PAHs [128].

SPME has been successfully applied to the analysis of environmental, biological, food, forensic and pharmaceutical samples. SPME is a solvent-free sample preparation technique, which combines isolation, sampling and enrichment in a single step. Thus, it has become an attractive alternative to most of the conventional sampling techniques. Besides its simplicity of use, fiber re-usability and a relatively short sample processing time are among the attractive characteristics of this technique. LC or GC, thus minimizing any potential analyte losses due to multi-step processes, can directly analyze an SPME fiber. Quantification in this technique is based on the amount of analyte extracted under appropriate conditions.

SPME is expensive technique, its fiber is fragile and has a short lifetime, and sample carry-over can cause problems [116].

1.3.1.4. Stir Bar Sorptive Extraction (SBSE)

SBSE has been developed to extract semi-volatile and volatile compounds from water [129].

This technique is based on the sorption of a polar species present in aqueous samples onto PDMS coated stir bar, thus partitioning the analytes occurring between the sample and the extracting phase. Stir bar coated with PDMS is introduced into the aqueous sample. After a stirring period, the stir bar is raised, rinsed, dried and placed

in an “injector tray.” The compounds are thermo-desorbed and analyzed by GC–MS. SBSE presents advantages over solid-phase extraction and liquid-liquid because no solvent is used, and small sample volumes can be analyzed since all the pre-concentrated analytes are desorbed. With respect to SPME, lower detection limits (sub-ng L^{-1} to ng L^{-1}), better recovery, and higher capacity can be achieved since extraction is performed with a larger amount of PDMS. SBSE is also characterized by its high reproducibility because of minimum sample preparation and manipulation [130].

SBSE technique has been developed and successfully applied to the enrichment and selective determination for organic compounds in water, urine, wine and other aqueous matrixes. Using magnetic power to stir the bar in a sample solution, target compounds can be enriched in the layer of SBSE, and then analytes can be liquid desorbed with organic solvents for HPLC analysis or thermally desorbed online with GC–MS. The typical coating material is PDMS in commercial stir bars. Compared with other sample preparation techniques, SBSE has many advantages, such as improved sensitivity, ease-of-use, high accuracy and low consumption of organic solvents [131].

SBSE is another micro-extraction method which has a similar extraction mechanism to that of SPME. The main difference between SBSE and SPME is that about a 50–250 times larger volume of extraction phase is employed in the SBME, which results in higher sample capacity and greater recoveries. Recently, SBSE has been successfully applied to organic compound analysis and elemental speciation in food, environmental and biological samples [132].

1.3.2 Analysis Techniques for PAHs in Water

The analysis of PAHs can be carried out by several analytical techniques, for example, gas chromatography with mass spectrometry or with a flame ionization detector and reverse-phase high performance liquid chromatography with a fluorescence detector, or with photo metrics [133].

Because of trace level concentrations of PAHs in complex water, an efficient pre-concentration technique is required, as well as a highly sensitive and selective method for separation and determination techniques. Several researchers have applied different techniques to measure PAHs in several media like: High Performance Liquid Chromatography / Fluorescence Detection, Ultraviolet Diode , Array Detection, Gas

Chromatography-Mass Spectrometry. Gas Chromatography (GC) and High Performance Liquid Chromatography coupled to Electro Spray Ionization Mass Spectrometry (HPLC-ESI-MS). PAHs in complex mixtures are usually determined by the gas chromatography technique (GC), or by high performance liquid chromatography (HPLC) with either UV-VIS diode array detectors (DAD) or fluorescence detectors [134].

1.3.2.1. High Performance Liquid Chromatography (HPLC)

HPLC is suitable for the analysis of compounds with higher boiling points and molecular weights, and has therefore been widely applied to PAH analysis. HPLC may be supplied with one of three detectors, namely DAD, UV, or FLD. FLD has the characteristics of high resolution, low detection limits and high sensitivity; therefore HPLC–FLD has higher sensitivity for the quantification of PAHs exhibiting fluorescent effects. HPLC connected with UV/VIS FLD and DAD has been used to analyze PAHs in soil and drinking water. The results were illustrat that DAD is useful for qualitative and quantitative analysis of PAH compounds in soil samples and an FLD detector is recommended for the analysis of PAH compounds in water samples. HPLC–DAD/FLD has been successfully equipped in the analysis of PAHs in sewage sludge samples and food supplement samples [135].

Among them, FLD has been found to be very suitable for the determination of PAH compounds in a variety of environmental samples due to the high fluorescence quantum yields of PAHs. FLD has a sensitivity of about 20–320 times more than UV detection, and about 0.8–50 times more than MS. Furthermore, the HPLC-FLD technique, which requires no carrier gas, allows the determination of non-volatility, thermally able to change molecules without derivatization. Because of all the advantages mentioned above, HPLC-FLD is a preferable technique for PAH analysis [133 and references there in].

1.3.2.2. Gas Chromatography (GC)

Methods used for the determination of PAH compounds by means of GC, frequently in conjunction with the tandem mass spectrometry technique (MS/MS), provide detection limits in the range of µg/L. In addition, the use of the HPLC technique with

fluorescence detection or diode array detection has been observed. Several methods were used for the quantification of PAHs by means of liquid chromatography–mass detection [136].

The most frequently-used detectors coupled to GC are mass spectrometry (MS), flame ionization (FID), electron capture (ECD) and tandem MS (MS/MS). The capillary GC method is a valuable alternative, sometimes a necessity for PAH analysis, considering that many PAH compounds cannot be easily detected in LC–FLD because of a too-low fluorescence signal. In particular, GC has a higher peak capacity in comparison with LC, and coupling to MS detectors is easier and relatively cheaper, thus enabling high sensitivity and selectivity. GC–MS enables the analysis of non-fluorescent PAH compounds, such as CPP and alkylated PAHs. Since PAH compounds are highly stable and produce mainly the molecular ion $[M–2H]^+$ or $[M–H]^+$ along with a few fragments, the single quadruple analyzes the frequency employed. However, some previous works report the use of a triple quadruple (QqQ) and ion trap (IT). Usually the single ion monitoring (SIM) acquisition mode is used to enhance sensitivity (amount in pg can be detected). A gas chromatography-flame ionization detector (GC-FID) is not suitable for such an analysis since it is not sensitive enough, and is subjected to background interferences. Very few papers report the use of a photo-ionization detector (PID), particularly since a PID is a non-destructive detector type, it is used coupled with an FID, and the response ratios of the two types of detectors can be used for identification purposes. However, more reliable results and higher sensitivity are obtained using mass spectroscopy (MS). As mentioned before, the GC technique has often been considered by the US Official Authority. This technique is not reliable enough, mainly because of several co-elution problems. Actually, several PAH pairs exist which cause critical resolutions such as: (1) Chr and triphenylene (2) Ant and Pyr, (3) BbFl, BjFl and BkFl, (4) CPP, BaA and Ch, (5) DBahA and IP, and (6) DBahP and DBacA. In fact, these unresolved pairs depend on the stationary phase used in a column, thus the selection of a suitable column is an important issue for perfect resolution, which has been discussed in previous dtudies. Generally, when performing GC analysis, the choice of a suitable injection system is of great importance, since discrimination can occur, particularly when less volatile compounds are being measured. Among the possible injection systems, the most employed for PAH analysis have been the split less injection mode, cold on-column injection, programmed-temperature vaporization (PTV) and large-volume injection (LVI). In particular, the combination of LVI and PTV has been widely applied to reduce injection discrimination and to increase sensitivity in environmental and food samples [137 and references there in].

1.3.2.3. Gas Chromatography-Mass Spectrometry (GC-MS)

Several techniques were proposed to assign a hydrocarbon spilled in an environment to its potential sources and it is broadly accepted that no single technique can solve this [138].

Comprehensive techniques for hydrocarbon fingerprinting include a combination of analytical techniques and chemometric tools for data evaluation. The use of GC–MS is essential, and represents the most powerful fingerprinting analytical technique available at present [139].
Numerous analytical methodologies have been reported in previous studies for the analysis of priority organic contaminant compounds in wastewater and natural water. The developed methods have generally been based on GC–MS rather than liquid chromatography–mass spectrometry (LC–MS), owing to the physicochemical properties of PAHs, and in particular due to their low solubility in water and their low polarity [140].

1.4 Treatment Methods for PAH Remediation

The main processes which successfully eliminate PAHs from the environment include microbiological transformation and degradation, bioaccumulation, biological uptake volatilization, photo-oxidation, and chemical oxidation. Photo degradation is an important transformation method for most PAHs in an environment. This is because it preferentially attacks the same tertiary carbon atoms in PAH compounds that tend to block biodegradation [141].

Photolysis and ozonation are the most important methods for the transformation of most PAHs adsorbed onto natural substances in the environment [142].
Photolysis of PAHs leads to the formation of photo-dimers and photo-oxidation products [143].
Photochemical behaviors of PAH compounds are dependent not only on their molecular structures, but also on the physicochemical properties of the substrate on which they are adsorbed. Using carbonaceous particles as a catalyst can inhibit the photo reactivity of PAHs, while using mineral particles can accelerate the photo reactivity of PAHs [144].
The ozonation of PAHs has been investigated on several substrates, including soot [145], Phenylsiloxane oil [146], octanol and decanol [147], Azelaic acid [148], NaCl [149], pyrex glass [150], mineral oxides [151] and different coated aqueous surfaces [152] under dark conditions.

Treatment processes usually employed for polluted soil include thermal desorption, chemical oxidation, incineration and biodegradation, but these processes do not always yield satisfactory results, particularly in the case of soils with low hydraulic permeability or those soils polluted by a mixture of inorganic and organic waste. Therefore, the development of technologies and processes for the simultaneous remediation of soil polluted by organic and heavy metals has emerged as an important role for current research in the soil remediation research field. Electro-kinetic remediation has been employed for the remediation of many soils polluted with heavy metals for the last twenty years with high efficiency. The implementation of electro-kinetic remediation for polluted soils involves inserting a series of cathodes and anodes into this soil and applying an electric potential between them [153].

1.4.1. Biodegradation of PAHs

Bioremediation techniques are routinely applied to recover soils contaminated by PAHs. These techniques are based on the well-established capability of soil microorganisms to remedy PAHs through growth-linked or co-metabolic reactions [154].

However, a major limiting factor in the bioremediation of PAH-polluted soils is the reduced bio accessibility that is often exhibited by these contaminants, which results in difficulty in predicting whether an acceptable end-point decontamination level can be achieved. Bio accessibility can be defined as the fraction of a contaminant that is potentially biodegradable over time in the absence of limitations to biodegradation other than restricted phase exchanges. Microorganisms can potentially overcome bio accessibility restrictions through several mechanisms, including bio surfactant production, attachment and chemo taxis [155].

Accessibility of bio degradation can also be increased in the soil externally, for instance, by adding surfactants [156].

Rhizoremediation, i.e., the use of ecosystem services provided by the plant rhizosphere to decontaminate polluted soils, has recently gained attention in relation to organic contaminants, such as PAHs. Translocation of dissolved pollutants in the rhizosphere and the microbial usage of root exudates as co-substrates in the biodegradation of PAHs have been proposed as mechanisms through which plants contribute to the elimination of PAHs [157, 158].

Bioremediation is an emerging clean-up technology for PAH polluted soil, which is a low-cost and environmentally friendly alternative for the decontamination of polluted soil [159].

However, PAHs polluted soil often suffers from organic matter and nutrient deficiency, which seriously limits the microbial degradation capacity in soil. Therefore, some readily available organic wastes, such as municipal solid wastes, manure and compost from different sources were added to the polluted soil to enhance the indigenous microbial degradation activity, as well as being introduced into exogenous PAH-degrading microbial strains, and hence promoted the PAH removal efficiency in soil [160].

Previous studies have demonstrated that organic amendments could stimulate the reduction of PAHs in soil by increasing microbial mineralization, as well as the formation of unextractable bound residues. Whereas some studies showed that the water-extractable organic matter (WEOM) from organic residue (e.g. humic substance) may play an important role through providing an available carbon source for soil microbial growth, as well as mobilizing PAHs from soil particles [161 and references there in].

1.4.2. Direct Photolysis

PAHs consist of multi-fused aromatic rings, almost existing as a complex mixture rather than single substances in the environment. The conventional treatment of surface water often includes coagulation, sedimentation filtration, flocculation and final disinfection. The addition of chlorine is frequently used for disinfection. Chlorine reacts with the natural organic matter present in water, which causes different type of cancers. The use of low-pressure ultraviolet (LPUV) photolysis for water disinfection has been widely described due to its efficiency. It has also been described to be very effective in achieving the degradation of a wide range of photo able organic micro-pollutants by UV fluencies. Different types of UV sources have been used to study the photolysis of polycyclic aromatic hydrocarbons such as low pressure lamps, medium pressure lamps, UV lamps that emit mainly radiation at 365 nm, higher than 290 nm, and Xe arc lamps simulating sunlight. The efficiency of the different UV lamps to degrade polycyclic aromatic hydrocarbons depends on the type of compounds and their capability to absorb radiation at certain wavelengths. For instance Miller and Olenjik, (2001)[162] observed that medium pressure UV lamps are more efficient than low pressure lamps for the photolysis of Benzo(a)Pyrene, but the opposite was

obtained for Chrysene using the same system. Therefore, the structure and properties of PAHs have an important thing in their photo degradation, since PAHs with a higher molecular weight, molecular polarizability, and heat of formation often have lower photolysis quantum yields. Few studies have addressed the efficiency of LP/UV photolysis to degrade PAHs, such as Anthracene, Fluorene, and Benzo (a) Pyrene, which are included in the list of priority substances mentioned above. Miller and Olenjik (2001) reported a fast degradation of Benzo (a) Pyrene spikes in a mixture of laboratory grade water and methanol using LP/UV lamps under different experimental conditions. Another study reported a more rapid degradation of Anthracene and Benzo (a) Anthracene than Pyrene and dibenzo [a,h]Anthracene using LP direct photolysis in laboratory grade water [163].

1.4.3. Advanced Oxidation Processes

Advanced oxidation processes (AOPs) refers to processes in which the oxidation of organic pollutants occurs primarily through reactions with hydroxyl radicals (·OH). In water treatment applications, AOPs usually refer to a specific subset of processes that involve O_3, H_2O_2, and/or UV light. Advanced oxidation processes are considered one of the most important methods to break down the contaminants and form friendly products. The effective force of these processes is production hydroxyl radical (·OH), which is regarded as a second strong oxidation component after fluorine and has an oxidation potential equal to 2.8 eV.

AOPs have been studied intensively for a long time. Various combinations of radiation, oxidants and catalysts have been developed for the removal of natural organic matter (NOM) and organic pollutants, e.g. UV/ O_3, O_3/H_2O_2, UV/ H_2O_2, UV/TiO_2, Fe^{2+}/ H_2O_2, vacuum ultraviolet (VUV) radiation or ionizing radiation and Fe^{2+}/ H_2O_2+ hv. These processes require the generation of highly reactive radical intermediates, in particular the ·OH^- radical. The appeal of AOPs is the possibility for donning complete oxidation or mineralization of organic pollutants through a process that operates near ambient pressure and temperature. The ·OH^- radical is well-known as one of the most powerful oxidant species.

The rate of reaction for a compound in ·OH- radical mediated oxidation is usually many orders of magnitude higher than the rate of reaction with molecular ozone under the same conditions. The reaction rate constants between organic species and the ·OH^- radical are in the range of 10^8 - 10^{10} M^{-1} s^{-1} [164]. The ·OH^- radical is a non-selective oxidant, and a very large number of reactions is possible. Once a free radical reaction has been initiated by ozone, photolysis, heat, hydrogen peroxide, etc., a series of

simple reactions will take place. The reactions of the ·OH^- radical with NOM proceeds in different ways: (i) by H-atom abstraction, which yields carbon-centred radicals, (ii) by the addition of the ·OH^- radical to double bonds and (iii) by a reaction mechanism where the ·OH^- radical receives an electron from an organic species. The carbon-centred radicals then react rapidly with oxygen to form new organic peroxyl radicals. The reactions of peroxyl radicals among themselves are able to produce aldehydes or ketones and/or carbon dioxide [165].

The rate of oxidation depends on radical contaminant concentrations and oxygen. Other factors affecting the radical formation are temperature, the presence of ions, pH, the type of contaminants, as well as the presence of scavengers in reactions such as with a bicarbonate ion [166].

Generally, NOM has been reported to decrease more when measured as UV254 than as dissolved organic carbon DOC in various AOPs studied, e.g. during UV/ H_2O_2 [167], Fenton processes [168] and TiO_2/UV [169].

The higher drop in UV254 values suggest that the chromophores present in the NOM macro-molecules, which consist mostly of a high molecular mass (HMM) of aromatic rings, are rapidly broken down into lower molecular mass by-products with no UV absorbance apparent. These by-products are thus less capable to attacks by the ·OH^- radical and therefore are not mineralized completely [170].

The intermediate fragments of organic species usually undergo a series of complicated reactions prior to mineralization. In addition, the preferential degradation of hydrophobic species has been observed in many investigations. Among several chemical techniques, (AOPs) have been very widely investigated. Initially widespread for the treatment the wastewater, they have been increasingly applied to solid matrices such as sludge’s, soils, and sediments [171].

AOPs in water treatment include the production of hydroxyl radicals (·OH) as intermediates species. UV-based AOPs traditionally required the oxidation processes in natural systems, such as sunlight in the atmosphere or on surface water. UV irradiation is well-established for the disinfection of water. The UV/H2O2 system provides the oxidation process through the generation of hydroxyl radicals through the photolysis of H_2O_2. This process degrades organic pollutants; including recalcitrant odorants such as 2-methylisoborneol (2-MIB) and geosmin mainly by the reaction, those pollutants with hydroxyl radicals, and partially by direct UV photolysis. Solution-phase AOPs are advantageous for pollutant removal because residual solids

are not formed as would occur with spent activated carbon from an adsorption process [172].

AOPs such as O_3/H_2O_2, H_2O_2/UV, O_3/UV and vacuum-UV (VUV) processes, constitute promising methods that are being investigated for the elimination or partial oxidation of NOM in raw water [173].

1.4.4. Photocatalyst Methods

In recent years, due to the release of toxic and persistent organic contaminants such as halogenated organic solvents, pesticides, polychlorinated biphenyls (PCBs) and PAHs into the aquatic environment from wastewater treatment plants and industrial or agricultural run-off, photo plants have drawn much attention, and is considered one of the most baffling problems facing environmental scientists today. Among several oxide semiconductor photocatalysts, titanium dioxide (TiO_2) has proven to be one of the most suitable for widespread environmental applications owing to its chemical and biological inertness, lower cost, strong oxidizing power, and long-term stability against corrosion and chemical corrosion [174].

Semiconductors are used for pollutant degradation in water to convert these pollutants into less harmful inorganic material. Both the catalysts titanium dioxide and zinc oxide have perfect photocatalytic properties made of these catalysts, thus being better for the photo degradation of water pollutants [175].

Attention has been focused in the past decade on using nano crystalline TiO_2 for the degradation of organic contaminates as a photocatalyst. TiO_2 has wide band gap of about 3.2eV semiconductor, corresponding to radiation in the region of near-UV range. The formation of an electron hole pair occurs within the conduction and valance bands of the semiconductor of TiO_2 after the absorption of UV radiation. Water molecules can be oxidized to a hydroxyl radical by a positive hole. Scheme 1.1 shows the mechanism diagram for the photodegradation of anthracene. The hydroxyl radical is frequently a powerful oxidant. The oxidation of organic pollutants seems to be mediated by a series of reactions started by a hydroxyl radical on the TiO_2 surface. A recombination of the hole and the separated electron can occur either on the surface or in the volume of the semiconductor particle accompanied by a release of heat. For the occurring photo oxidation reaction, both a UV light source and TiO_2 are necessary [176].

Heterogeneous photocatalysis of organic contaminants using TiO_2 under UV light and/or solar light has reported successful performances in various remediation systems

of contaminated soil. The addition of small amounts of TiO_2 significantly enhanced the photo degradation of pesticides such as p,p-DDT on soil surfaces. Photocatalytic degradation might be also an efficient way to degrade PAHs. It is extensively reported that PAHs can be photocatalytically degraded in a pure solid phase such as: alumina, silica, Fe_2O_3 and TiO_2 and liquid phase. However, few studies have investigated the photo catalytic degradation of PAH compounds in the presence of nanometer anatase TiO_2 on soil surfaces [177].

TiO_2 is extensively used as a photocatalyst because of the strong oxidizing power of its holes, redox selectivity and high photo stability. The band gap of TiO_2 reported as a semiconductor material is about 3.2eV, which corresponds to a radiation of wavelength of around 380 nm. Therefore, UV light with a wavelength of less than 380 nm is needed to excite the electrons present in the valence band to the conduction band. The electron-hole pairs thus generated serve as the oxidizing and reducing agents. In the photo degradation of contaminants in water, hydroxyl radicals ($^{\cdot}OH$) formed either through the interaction of O_2 with hot electrons or through the interaction of water molecules with the hole to form a superoxide radical are the key active species [178].

The photo degradation of PAH compounds in water using a TiO_2 catalyst have proved a high efficiency [179].

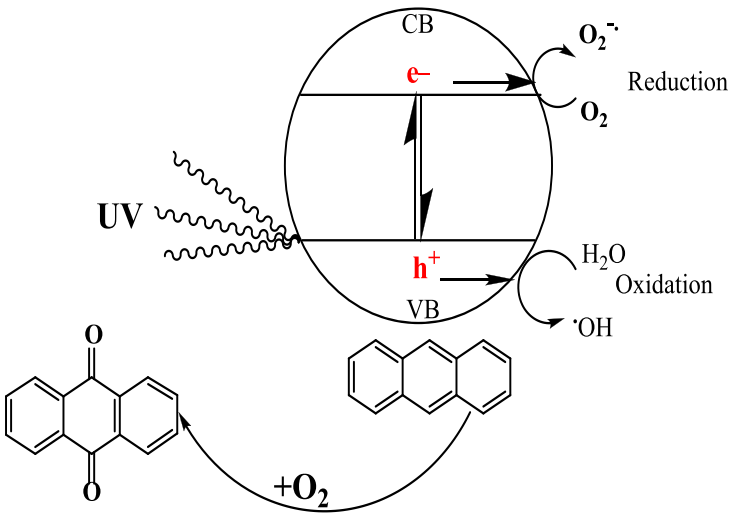

Scheme 1.1: Mechanism diagram of photocatalytic degradation for Anthracene.

1.4.5. Fenton's Methods

The oxidation process of organic substrates by ferrous iron ions and hydrogen peroxide is called "Fenton chemistry." It was H.J.H. Fenton [171] who first observed the oxidation of tartaric acid by hydrogen peroxide in the presence of ferrous iron ions. Frequently the terms "Fenton reagent" or "Fenton reaction" are often used. The Fenton reagent was known more than one century ago but its application as an oxidizing reagent for removing hazardous organic pollutants was not applied until the late 1960s [180]. After this time, investigations showed that the Fenton reagent is very effective for treating different industrial wastewater pollutants such as aromatic amines, a large variety of dyes, pesticides, and explosives. In general, Fenton reactions can be heterogeneously catalyzed (Fenton-like) or homogeneously catalyzed (conventional Fenton and modified Fenton). The Fenton and photo-Fenton processes mechanism can be summarized by the following reactions [181].

$$Fe_2 + H_2O_2 \rightarrow Fe_3 + OH^- + OH^{\bullet} \quad \text{.....(1)}$$

$$Fe^{+3} + H_2O_2 \rightarrow Fe^{+2} + HO_2^- + OH^+ \quad \text{.....(2)}$$

$$Fe^{+3} + H_2O_2 + h\nu \rightarrow Fe^{+2} + OH + H \quad \text{.....(3)}$$

Electro kinetics has also been applied to remove organic pollutants such as PAHs, pesticides, herbicides and chlorinated organic compounds from the soil. Kyoungphile

Nam et al., (2001) used biodegradation combined with a modified Fenton reaction to enhance the degradation of polycyclic aromatic hydrocarbons [182].

Laurent et al., (2012) [183] reported the ability to remove PAHs from the soil by a modified Fenton reaction.

Previous study researchers were used a modified Fenton treatment coupled with a chelating agent to remove polycyclic aromatic hydrocarbons from contaminated soil [184].

Flotron et al., (2005) [185] investigated the feasibility of employing Fenton's reagent to degrade sorbed polycyclic aromatic hydrocarbons in three different solid matrices: sewage sludge, an agricultural soil, and marine sediment.

Jonsson et al., (2007) [186] investigated the ability of chemical degradation for PAHs in older soil samples from different contaminated sites by Fenton's reagent.

Da Silva et al., (2009) [171] were reported the ability to oxidation the contaminated soils with both Phenanthrene and Pyrene by Fenton's reagent.

Hydroxyl radicals are considered one of the strongest oxidants and are the main oxidizing reagent in the Fenton process. Fenton (1984) first observed the Fenton reaction. The principle of these processes is based on an electron transfer between a metal ion and H_2O_2 such as ferrous iron (Fe^{2+}), which acts as a catalyst. It is an economical process having no energy requirements as needed by the devices (UV lamps, ozonizers and ultrasounds) in other AOPs. Fenton and its related processes are potentially convenient ways to generate oxidizing species for contaminant degradation. The Fenton method leads to multiple benefits such as both hydrogen peroxide and iron being relatively safe and cheap; there is no mass transfer limitation except during coagulation, where a huge dosage of activator-ferrous salt is used and the process is considered technologically simple. The mixture of Fe^{2+} and H_2O_2 produces hydroxyl radicals ($^{\cdot}OH$), which are highly oxidative with respect to organic compounds present in wastewater. The fate of organic pollutants and their degradation by-products is primarily dependent on their ability to react with hydroxyl radicals. Hydroxyl radicals attack the organic contaminants and lead to the complete destruction of these contaminants with water, CO_2 and inorganic salts as end products [187].

Advanced electrochemical oxidation processes (AEOPs), such as electro-Fenton, anodic oxidation, electro-Fenton coupled to anodic oxidation, and solar photo-electro-Fenton have been used for organic waste treatment during the last decade.

The electro-Fenton (EF) process is based on the in-situ electro generation of ·OH radicals, according to the electrochemically assisted Fenton's reaction.

$$H_2O_2 + Fe^{+2} \rightarrow Fe^{+3} + OH^- + \bullet OH \quad \ldots\ldots\ldots \quad (4)$$

Hydrogen peroxide (H_2O_2) and ferrous (Fe^{2+}) ions are simultaneously produced in an aqueous medium by the bi-electronic reduction of the dissolved molecular oxygen Eq.(5) and ferric ions (initially introduced at a catalytic concentration) Eq. (6).

$$O_2 + 2H^+ + 2e^- \rightarrow H_2O_2 \quad \ldots\ldots\ldots \quad (5)$$

$$Fe^{+3} + e^- \rightarrow Fe^{+2} \quad \ldots\ldots\ldots \quad (6)$$

The electro-generated Fe^{+3} ions are reduced through eq. (6) at the cathode to catalyze the reaction (4). Molecular oxygen, utilized in reaction (5), is yielded at the anode by the oxidation of water through the reaction (7) [188, and reference there in].

$$H_2O_2 \rightarrow O_2 + 4H^+ + 4e^- \quad \ldots\ldots\ldots (7)$$

1.4.6. Ozonation Methods

PAHs are by-products of the pyrolysis of petroleum derivatives at high temperatures, as well as in acetylene production from natural gas, refinery operations, etc. In various studies there has been detected the presence of PAHs in water, air and soil. In some cases there were found a concentration of these pollutants of more than 10 g/kg. PAH compounds are at a scale from a few fused aromatic rings to micrometer-scale graphene sheets. Small (six or less) PAHs are produced because of the combustion that is prevalent in an environment. PAH compounds, which consist of three or more fused rings, have relatively low vapor pressures and will partition to atmospheric aerosols and the environment, where they react with ozone and other oxidants present in the atmosphere. Small PAH compounds and their products after oxidation have well-documented adverse effects on human health. Understanding the mechanisms of oxidation of PAHs by ozone evaluates their environmental effects and human exposure to them [189].

Some results related to Anthracene degradation by ozonation have been reported, concerned with the 9, 10-anthraquinone formation as a main Anthracene by-product, or 9, 10-anthraquinone and the Anthrone production in silica as a solid phase. In each,

these processes have an influence on some operation variables: doses of oxidant, organic matter, etc. Some studies have shown that PAH oxidation by ozonation produce biodegradable by-products more than initial compounds; therefore it can mix treatments, in which it can combine the oxidative process and biodegradation. Many water pollutants were removed successfully from the aqueous solution by direct oxidation with ozone. To enhance the efficiency of degradation pollutants (especially those reacting slowly toward the oxidation by ozone alone), a second oxidant and /or UV light were used for this reason. Among the degradation of pollutants by AOP methods, the combination of ozone and UV light deserves special consideration. In this system, more than three pathways of pollutant removal can develop (direct ozonation, direct photolysis and radical oxidation). The radical of hydroxyl results from the decomposition of ozone because of photolysis and the reaction with a hydroxyl anion, which leads to hydroxyl radical production in subsequent reactions. The hydroxyl radicals can react without selectivity on numerous organic pollutants in water. The organic molecules exited by UV radiation can react with ozone and oxygen. In addition to the intermediates, they can decompose to giving radical species which can take part in the reaction. Oxygen with ozone usually delivered to the reaction mixture, is also suspected of participation in the oxidation processes. The O_3/UV system was applied in the degradation of various compounds such as chlorinated organic nitro-compounds, detergents aromatics and pesticides. PAH compounds were also the subject of study [190].

1.5. Aims of the Present Work

This work is composed of four main parts. The first one reports an investigation of the PAH sources which contribute to the contamination of the surface water of the Shatt Al-Hilla River with these compounds. This investigation was carried out by a boat trip.

The second part includes local measurements of some physicochemical properties of surface water. The third part reports the effect of spatial and weather on PAH concentrations in selected sites, this part aimed to compare between two extraction techniques: solid phase extraction and liquid liquid extraction.

The fourth studies the treatment methods for the Anthracene compound; these methods consist of the following methods:

1-Direct photolysis method.

2- Advanced oxidation processes.

3- Photocatalytic degradation studying the effects of different conditions on photocatalytic oxidation using two types of titanium dioxide. These conditions are summarized below:

a- Effect of anthracene concentration.

b- Effect of pH.

c- Effect of temperature.

d- Effect of hydrogen peroxide.

e- Effect of light intensity.

4- Fenton processes studying different factors such as:

a- Effect of initial concentration of anthracene.

b- Effect of ferric sulphate.
c- Effect of pH.

d- Effect of temperature.

e- Effect of hydrogen peroxide.

5- Ozonation methods.

CHAPTER TWO

EXPERIMENTAL

2.1. Chemicals

The chemicals used in this work are listed in Table 2.1. All chemicals are standard and used without further purifications.

Table 2.1. Applied chemicals and reagents.

No.	CHEMICAL	COMPANY
1	9,10- Anthraquinone	Sigma-Aldrich/Germany
2	Acetone	Sigma-Aldrich/Germany
3	Acetonitrile	Sigma-Aldrich/Germany
4	Anhydrous Na_2SO_4	Riedel-De – Germany

5	Anthracene	Sigma-Aldrich/Germany
6	Dichloromethane	Sigma-Aldrich/Germany
7	Ethyl Acetate	Sigma-Aldrich/Germany
8	Ferrous Sulfate	Sigma-Aldrich/Germany
9	Hydrogen Peroxide	Bemburg Plant-Germany
10	Methanol	Sigma-Aldrich/Germany
11	Sodium Hydroxide	Sigma-Aldrich/Germany
12	Sulfuric Acid	Sigma-Aldrich/Germany
13	Titanium Dioxide	Degussa/Germany
14	Titanium Dioxide (Hombikat UV100)	Sachtleben Chemie GMBH, Germany.
15	US EPA 610 PAH standard mixture.	Supelco- USA

2.2. Instruments

Different instruments were used in this study. Types of instrument and the suppliers companies are listed in Table 2.2.

Table 2.2. Applied Instruments.

No.	INSTRUMENTS	COMPANY	Location
1	Analytical Balance	Sartorius/Germany	Iraq, Germany
2	Chiller	JSR/Korea	Germany
4	Conductive Meter	Hanna- Rommania.	Iraq
5	FTIR	Bruker IFS 66/	Germany
6	GC	Shimadzu 2010/Japan	Germany
7	GC	Agelent 7890A/USA	Iraq
8	GC-MS	Shimadzu/Japan	Germany
9	HPLC LC-2010A	Shimadzu/Japan	Iraq
10	Magnetic Stirrer	Heidolph/Germany	Germany
11	Ozone Generator	Ozomax/Canada	Iraq
12	pH Meter	Hanna- Rommania.	Iraq
13	Rotary Evaporator	Buchi-Re121-Swizerland	Germany
14	Ultra Sonic Shaker	Falk/Italy	Iraq
15	UV Meter	Honel UV technology-Germany.	Germany
16	UV-Visible Double beam Spectrophotometer	UV-1800 Shimadzu/Japan	Iraq

2.3. The Study Area

Shatt Al-Hilla River is an important River for water supply and irrigation in the Babylon Governorate. The total length of this River is 97 km. Many pollution sources are present near this river such as draining sewage, agriculture pumps, textile factories treated wastewater and outlet pipes from water treatment stations of drinking water in addition to the pollution by atmospheric deposition of PAHs and other volatile compounds. The Shatt AL-Hilla River starts from Saddat Al-Hindya, and finishes at the southern borders of Al-Hilla city in Sadder Al-Dughara, passing through several villages and cities. These sites were selected during a boat trip to explore the sites contaminated with PAHs, which are illustrated by the following description and map in Figure 2.1:

1- S1 represents the site near the Saddat AL-Hindiya barrage, which is located beyond this barrage about 1km on the left bank of the Shatt Al-Hilla River. This site was selected to investigate the influence of pollutant in Shatt AL-Hilla that is located before entering the study area.

2- S2 represents the site near the municipal water purification station. This station is used for drinking water and is about 4 km from Saddat AL-Hindiya barrage on the left bank. This station has an out let pipe. This pipe is used to remove the slurry, sediments, and impurity precipitate from the crude water. This is purified in precipitation tanks and then the precipitants are drained into the river again via these pipes. The water content has a high percentage of PAHs, and for this reason site two was selected to indicate the pollution that was coming from this station in addition to that coming from the site located nearby. Samples were collected 3m from the pipe outlet.

3- S3 represents the site near the Al-Jebal treatment station, about 2 km from Saddat Al-Hindiya barrage on the right bank of the Shatt Al-Hilla River; in this station the sewage water is discharged into the river via a pipe. Sewage water may include PAHs, according to the assumption of which, this site was selected to indicate the total pollution for this site and others located nearby. Samples were taken by filling specified bottles at a distance of about 3m from the pollution source.

4- S4 represents the site near (Al-Sadda Al-Muaffa) about 6 km from the Saddat Al-Hindiya barrage on the left bank of the river. At this station pollution is produced from the agriculture water pumps which are used for plant irrigation; these pumps operate by means of oil derivatives, a type of fuels rich with PAH compounds, especially

when the fuel combustion is incomplete. This site was selected to investigate the effect of these pumps on the pollution levels.

5- S5 represents the site near the Al-Batta Bridge, about 2 km north of Al-Hilla city on the right bank of the Shatt Al-Hilla River. In this station many drivers are used to wash their cars and the washing water is drained directly to the river. It is often mixed with different types of oil derivatives such as gasoline, lubricating oil, gearbox oil, wax and so on, and for this reason site five was selected to indicate the effect of these pollutants in addition to those coming from nearby. The sampling site was about fifteen meters from the pollution source.

6- S6 represents the site near Sooq Al-wardiya in the middle of Al-Hilla city on the left bank of the river. In this station, the pollution source is the sewage drain pipe coming from the Al-wardiya region, which discharges its contents into the river. This site was selected to measure the pollution levels in production sources and others. Sample bottles were filled at distance of 3m from the pollution pipe.

7- S7 represents the site near the central small bridge in Al-Hilla city on the right bank of the river. The pollution source is a drainage pipe that discharges water mixed with different oil derivatives and a sewage drain. This pipe also carries out wastewater coming from the big market in Hilla city (Sooq Al-Hilla). This site was selected to investigate the pollution levels in pollution sources and others. Samples bottles were filled at 3m distance from the pollution pipe.

8- S8 represents the site near the Al-Farisy region 2km south of the city center on the right bank of the river. The pollution source at this site is the drain pipe constantly coming from the treatment complex for sewage water. This site was selected to indicate the total pollution for this site and others located nearby. Sample bottles were filled at 3m from the pollution pipe.

9- S9 represents the site near the Effar region about 4 km south of Hilla city center, on the right bank of the river. In this station pollution is produced from the agriculture water pumps, which are used for plant irrigation; these pumps also operate using oil derivatives, therefore it was been selected to indicate the effect of these pumps.

10- S10 represents the site of Dolab village, about 6km south of Al-Hilla city on the right bank. This site was selected to indicate the effect of fishing boats, which operate with hydrocarbon fuels, spread throughout this location and are used by anglers. The incomplete combustion of this fuel contributes to rising the contamination levels of PAH compounds, and for this reason, this site had selected.

11- S11 represents the site near Al-Dabla village, which is located about 12 km south of Al-Hilla city on the right bank of the river. This region was selected due to the pollution that is produced from the treatment plant for the sewage water from Al-Dabla village. This site was selected to indicate the total pollution for this site and others located nearby. Sample bottles were filled about 3m from the pollution pipe.

12- S12 represents the site near the Al-Ibrahimia Bridge, which is located about 20 km south of Al-Hilla city on the left bank. This site was selected to indicate the accumulative effects of the previous contamination sources.

13- S13 represents the region near the Al-Hashimiya water treatment station for drinking water, about 20 km south of Al-Hilla city on the right bank of the river. This station has a drainage pipe to remove slurry and sediments from precipitation tanks coming from this station. Sample bottles were filled about 3m from the pollution pipe.

14- S14 represents the last point of the study area about 45 km south of Al-Hilla city on the left bank of the river. This site was selected to evaluate the effect of all pollutant sources and before it from S_1 to S_{13} at this point.

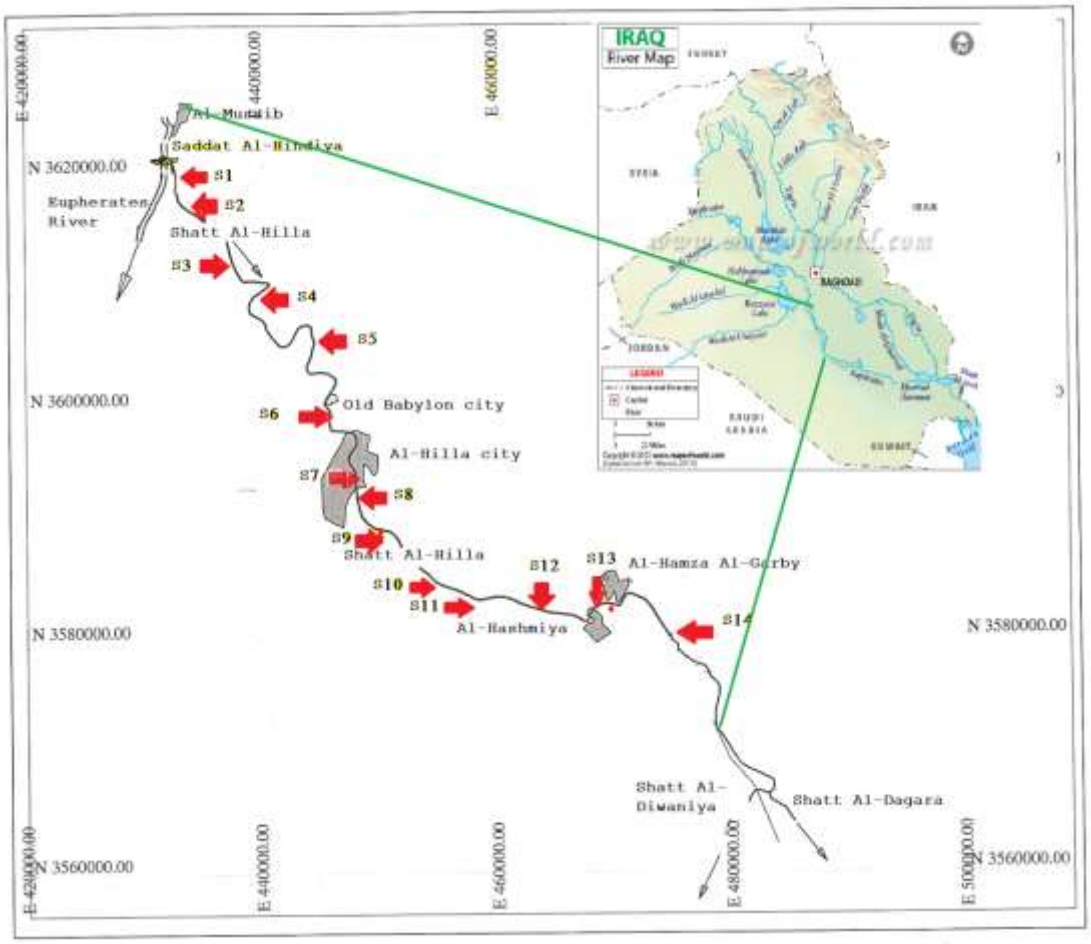

Figure 2.1. The map of sampling sites on the Shatt Al-Hilla River

2.4. Water analysis

2.4.1. Sample collections and field measurements:

Sample collections were carried out during the period from November 2011 to October 2012. Fourteen sites were selected on the Shatt Al-Hilla River, starting from site one beyond Saddat Al-Hindiya to site fourteen beyond Al-Hashmia city to assess the effects of pollution on the river properties. Samples were collected in replication.

Surface water samples from a depth of 30 cm from each site were taken monthly for the determination of physicochemical properties and PAH concentrations according to AS-EPA method [191].

1- At each site samples were taken using pre-cleaned amber glass bottles. The capacity of these bottles was 2.5 L, each supplied with a screw cap and lined with foil to prevent matching the PAH compounds with the plastic cap. Samples were kept in a cool box at 4°C and transported to the laboratory immediately, to ensure that no degradation would happen in terms of lower molecular weight of polycyclic

aromatic hydrocarbons when exposed to light or high temperatures through transferring samples to the lab.

2- Measurements of air and water temperatures were made in the field by mercury-filled celesium thermometers with a scale marked from 0 to 50.

3- Field electrical conductivity-meter was used to measure electrical conductivity of water samples.

4- Water pH was measured by pH–meters, which had been calibrated prior to use by standard pH buffers 4, 7 and 9.

2.4.2. Laboratory works

2.4.2.1. Extraction of PAHs

Extraction of PAHs from the surface water of the Shatt Al-Hilla River was achieved by two methods; solid phase extraction (SPE), and liquid-liquid extraction (LLE).

2.4.2.1.1. Solid Phase Extraction (SPE)

All the glassware was pre-cleaned with washing acids, solvents, detergents, hot water, rinsed with distilled water and then dried for 1 h at 120 ºC. SPE columns were conditioned with 5 mL of methanol, followed by 5 mL of deionized water. After the conditioning step, important for the SPE drying the SPE column, the PAHs were eluted with organic solvents [192]. Water samples were extracted by a Supelco, Supelclean™ ENVI-18 SPE tube bed wt. 500 mg, volume 6 mL. One liter of the water sample was passed through the extraction column with a flow rate of 5mL/min. Retained PAHs were eluted from the extraction column by 3x10 mL of dichloro methane. The passed solution was concentrated to near dryness by means of a rotary evaporator using water bath. The concentrated sample was collected in a small, dark, isolated glass container. Scheme 2.1. outlines the extraction procedure.

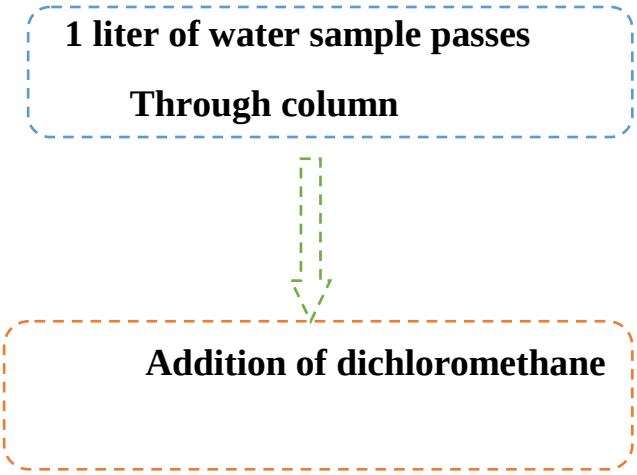

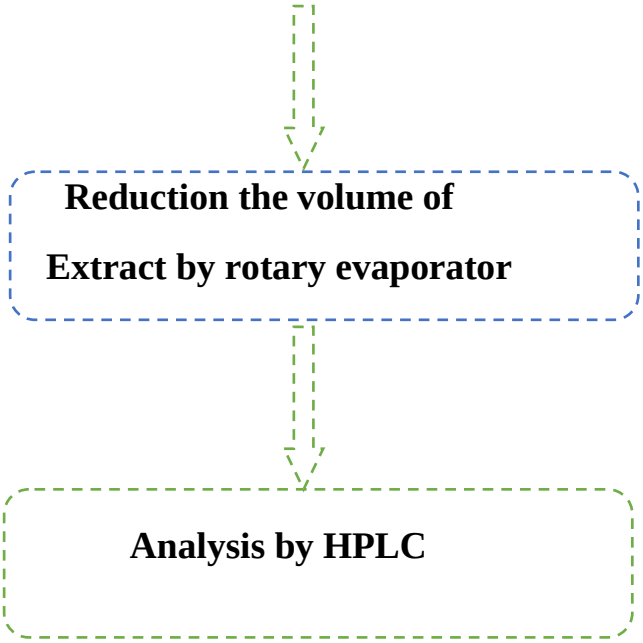

Scheme 2.1. Extraction procedure by SPE

Optimization of SPE Column

Several parameters for optimization columns for SPE were studied to select the optimum conditions for extraction process, these parameters are:

A- Effect of flow rate of water.

B- Effect of solvent type.

C- Effect of solvent volume used for elution.

A- Effect of flow rate of water

Several rates for dropping of water from SPE column were tested to compare between them and select the perfect for extraction. The efficiency for every flow rate was associated to the recovery percentage for standard solutions prepared for this purpose, n=3. Table2.3. illustrates that the flow rates of water with recovery for each one.

Table 2.3. Effect of flow rate of water in SPE

Flow rate mL/min	Recovery%
2.00	68.20

3.00	**76.63**
4.00	**90.71**
5.00	**92.21**
6.00	**85.89**

B- Effect of solvent type

Several solvents for elution the PAHs compound, which are suspended with cartridge of column, were tested at constant flow rate (5 mL/min). These solvents were dichloromethane, acetonitrile, n-hexane and benzene. The efficiency for every solvent depended on the recovery percentage for standard solutions prepared for this purpose, n=3. Table2.4. illustrates the solvent with recovery percentage for each.

Table 2.4. Effect of solvent type (eluant) in SPE

Solvent of elution	**Recovery%**
Dichloromethane	**92.15**
Acetonitrile	**87.73**
n-Hexane	**84.29**
Benzene	**84.33**

C- Effect of volume of solvent for elution

Several volumes of solvent used for elution suspended PAHs in cartridge of SPE column were tested to select the perfect. The solvent used in all experiments was dichloromethane with flow rate of water at 5 mL/min. The efficiency for every volume of solvent depended on the recovery percentage for standard solution prepared for this purpose, n=3. As shown in table 2.5, the perfect volume was 10 mL of dichloromethane.

Table 2.5. Effect of volume of solvent in SPE

Volume of solvent in mL	**Recovery%**

6.00	**77.92**
12.00	**80.53**
18.00	**87.07**
24.00	**88.84**
30.00	**92.19**

2.4.2.1.2. Liquid Liquid Extraction (LLE)

LLE was achieved according to US EPA method 3510[193], by adding 60mL of dichloromethane to one liter of water sample in two liters separator funnel. Shaking for two minutes with ventilation, the organic layer then was separated from aqueous layer. After separation, the organic layer was drained in to collection vessel. This operation was repeated twice to get quantitative recovery of all analytes. The organic solution was concentrated to near dryness using rotary evaporator. The comparison of the validation parameters between two methods (LLE and SPE) is shown in the table 2.6.

Table 2.6. Validation parameters of LLE and SPE

Validation parameters	LLE	SPE
Recovery%	89.72	92.21
Consuming of solvents per one L of sample/ mL	120.00	30.00
Consuming of time for one L of sample/min	4.00	220.00

2.4.2.2. HPLC Conditions

20 µL of the extracted sample was injected by micro syringe into a reversed-phase HPLC. The detailed experimental parameters for the HPLC Shimadzu LC-10 AVP were a PAH column of 250 x 4.6 mm; I.d with a guard column of 50 x 4.6mm; I.d, flow rate of 1.5 mL/min. Absorbance at 254 nm was detected by the UV detector. Polycyclic aromatic hydrocarbons compounds were eluted using water/acetonitrile gradient; as shown in Table 2.8, which illustrates the gradient program.

Optimization of HPLC Conditions

Effect of several parameters was studied for optimizing HPLC such as:

A- Effect of initial percentage of acetonitrile in gradient program:

Mobile phase consist of acetonitrile and water, in gradient program the mixing percentage of both components is important for peaks resolution. Figure 2.2 shows the measurements at different percentage of acetonitrile.

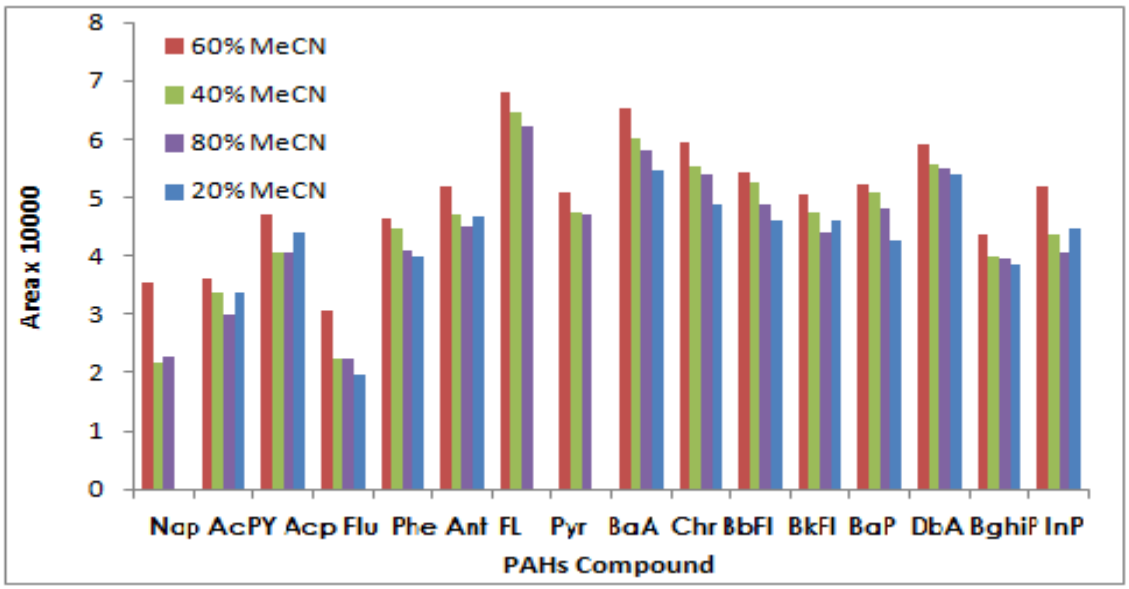

Figure 2.2. Effect of initial percentage of MeCN in mobile phase.

B- Effect of flow rate of mobile phase:

Figure 2.3 shows the measurements at different flow rate of mobile phase, it is clear that the perfect flow rate is 1.5 mL/min. All these experiments were achieved at same conditions of initial ratio of acetonitrile in gradient program(60%).

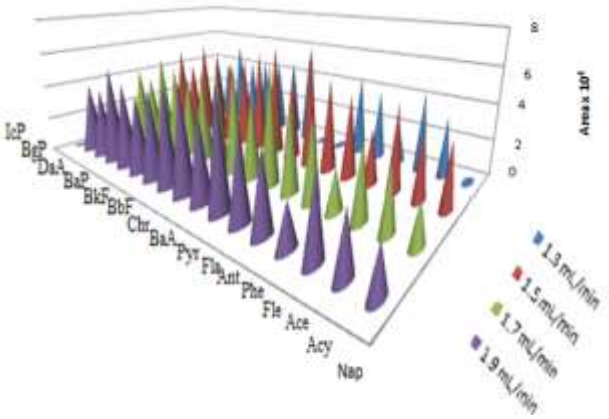

Figure 2.3. Effect of flow rate of mobile phase.

C- Effect of injection volume:

The correlation between the injection volume of sample and the number of detected PAH compounds was investigated. Table 2.7 illustrates the volume of

injection with number of compounds detected at same conditions such as: initial percentage of acetonitrile in gradient program (60%) and flow rate of mobile phase (1.5 mL/min).

Table 2.7. Effect of injection volume of PAHs on appearance of peaks.

Injection volume in µL	No. of detected compounds by HPLC
5.00	8
10.00	11
15.00	12
20.00	16
25.00	16

Mobile Phase: A: Deionized water, B: Acetonitrile.

Table 2.8. Gradient program for HPLC

Time (min)	Acetonitrile B (%)	Deionized water A(%)
0	60.00	40.00
1	60.00	40.00
15	100.00	0.00
17	100.00	0.00

Flow rate: 1.5 mL/min, Injuction. Volume: 20 µL, UV Detection: 254 nm.

Figure 2.4 illustrates the graphical abstract for the whole process of determination of PAHs from water samples.

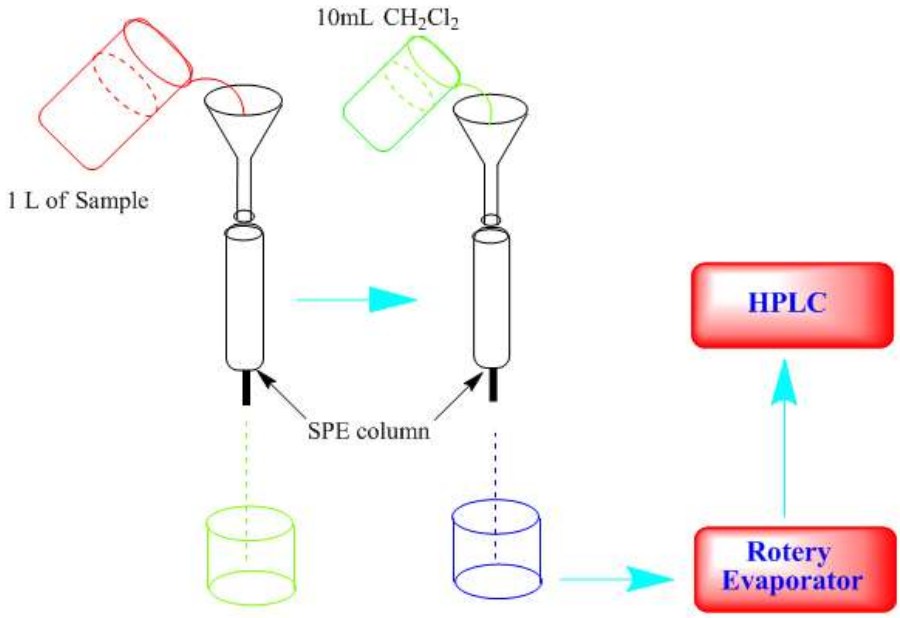

Figure 2.4. Graphical abstract for whole determination process of PAHs from water samples.

2.4.2.3. Calibration curves

A standard solution of sixteen US EPA 610 PAH Mix. Of the PAHs was obtained from the SUPELCO company as a PAH calibration individual in order to compare the retention times and the chromatograms of compounds in this standard with those in the samples. The standard calibration contained the following compounds: Naphthalene, Acenaphthylene, Acenaphthene, Fluorene, Phenanthrene, Anthracene, Fluoranthene, Pyrene, Benzo(a)anthracene, Chrycene, Benzo (b) Fluoranthene, Benzo(k) Fuoranthene, Benzo(a) pyrene, Dibenzo (a,h) anthracene, Benzo (ghi) Perylene and Indeno(1,2,3-cd) pyrene. Figures 2.5 to 2.20 are illustrating the calibration curves for each PAH individual compounds of the mixture.

2.4.2.3.1. Naphthalene

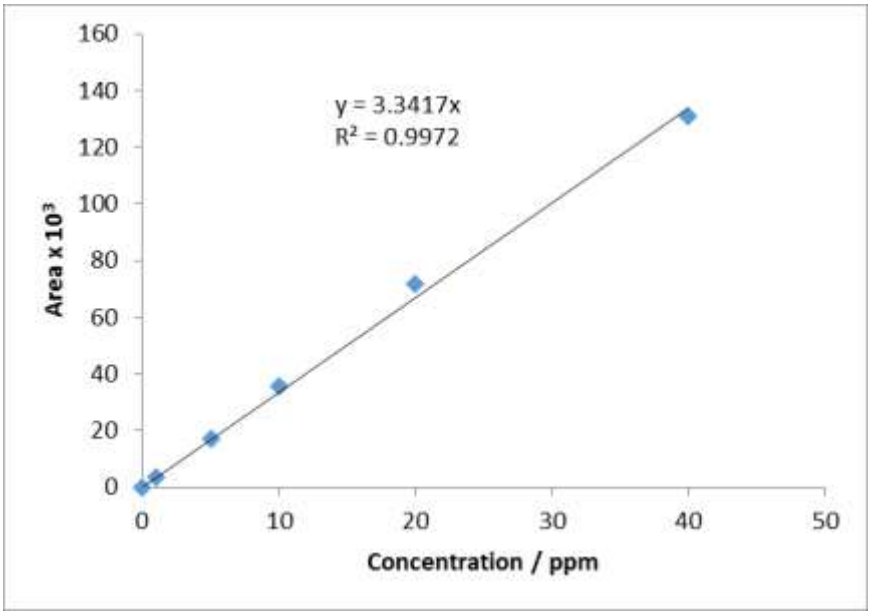

Figure 2.5. Calibration curve for Naphthalene.

2.4.2.3.2. Acenaphthylene

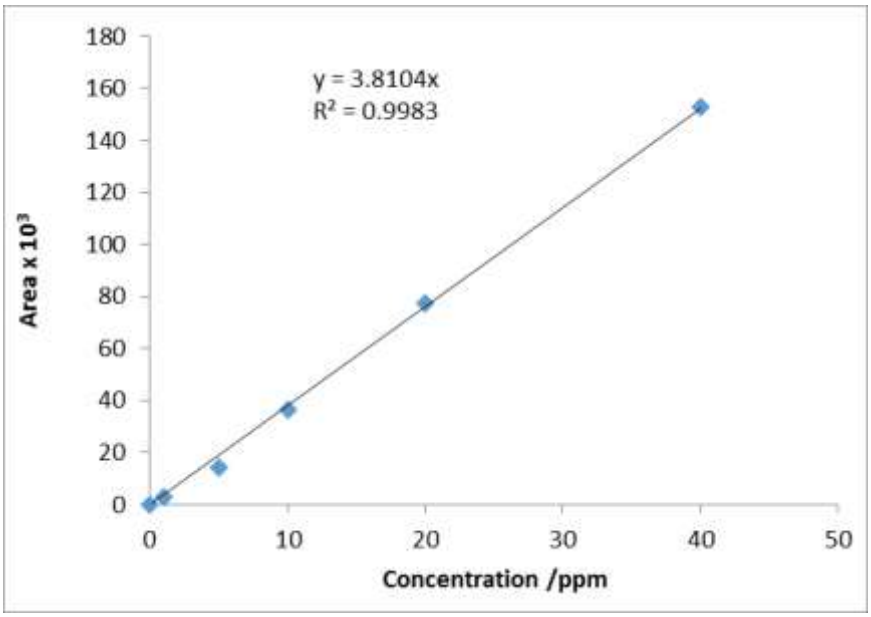

Figure 2.6. Calibration curve for Acenaphthylene.

2.4.2.3.3. Acenaphthene

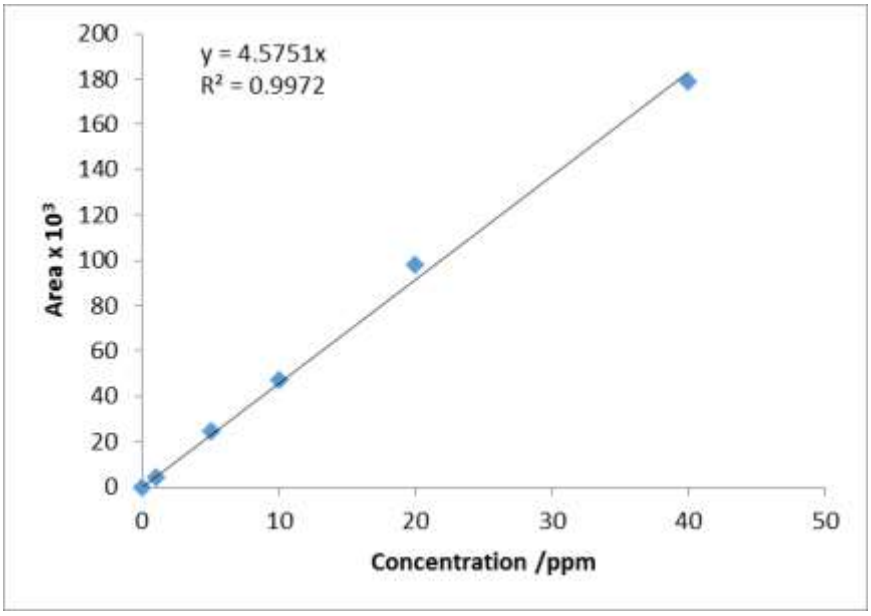

Figure 2.7. Calibration curve for Acenaphthene.

2.4.2.3.4. Fluorene

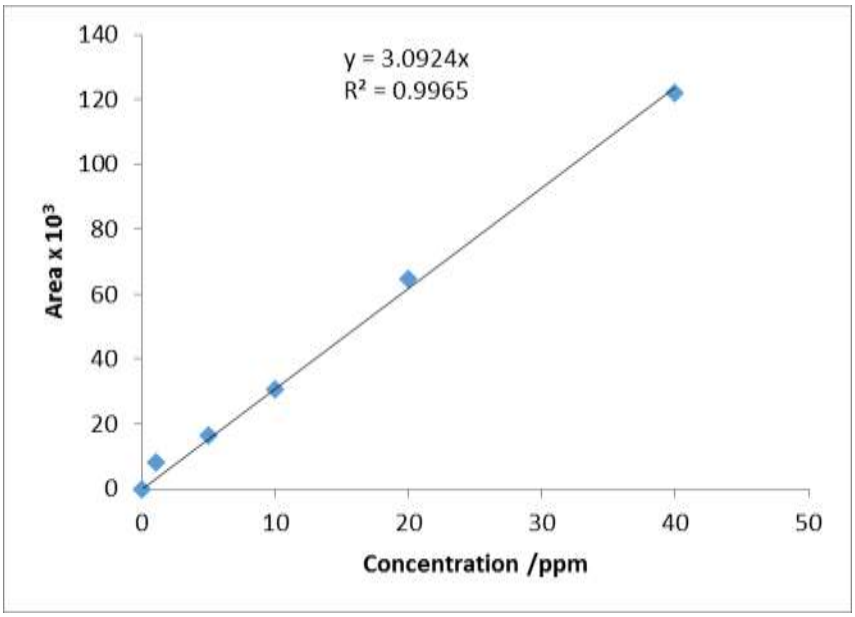

Figure 2.8. Calibration curve for Fluorene.

2.4.2.3.5. Phenanthrene

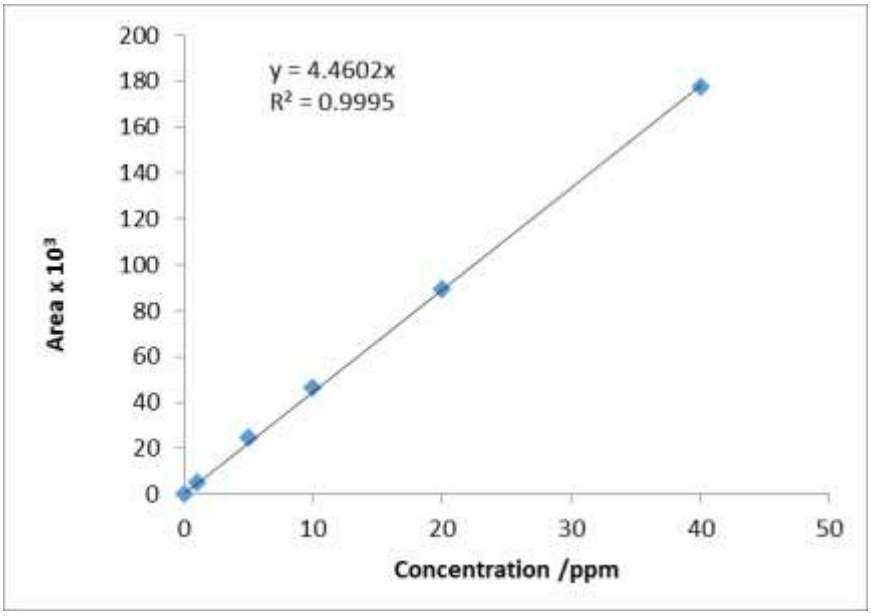

Figure 2.9. Calibration curve for Phenanthrene.

2.4.2.3.6. Anthracene

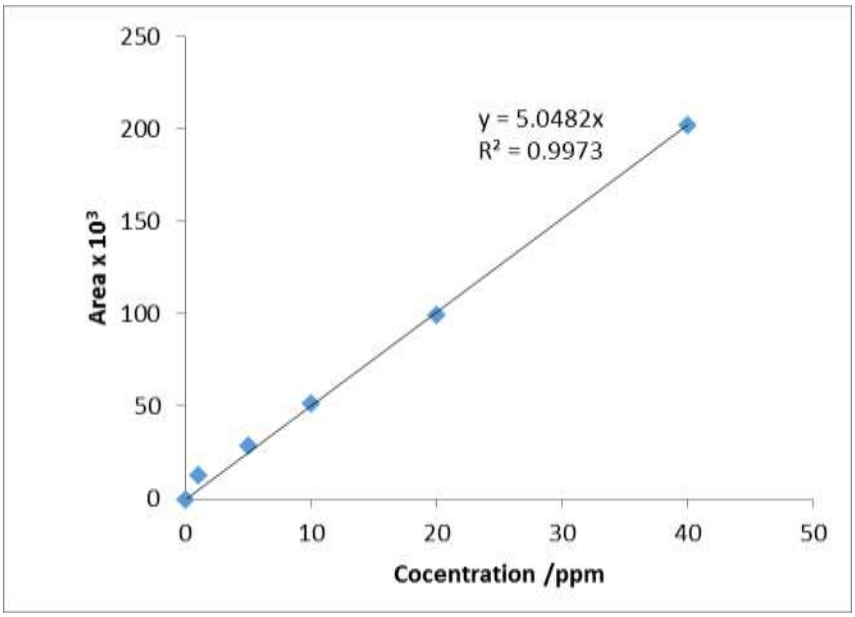

Figure 2.10. Calibration curve for Anthracene.

2.4.2.3.7. Fluoranthene

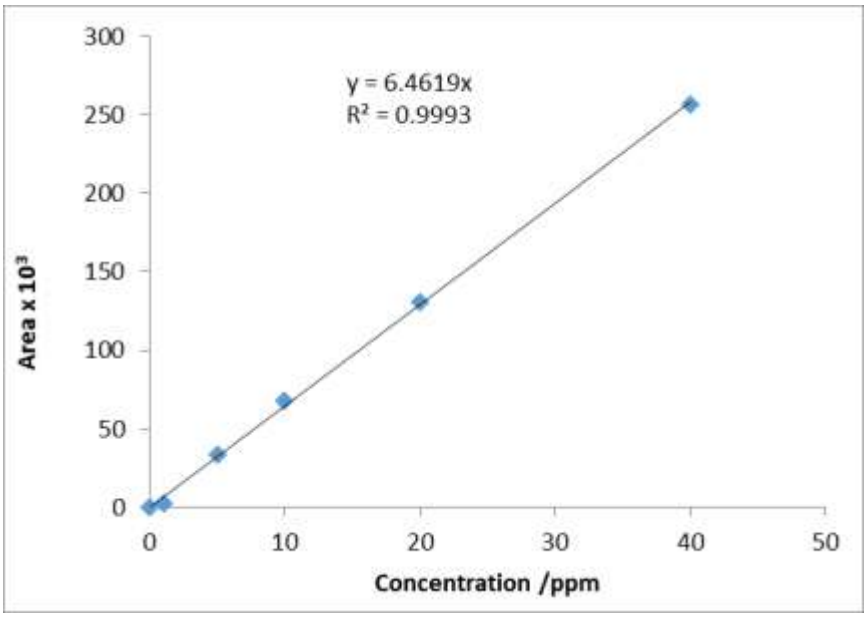

Figure 2.11. Calibration curve for Fluoranthene.

2.4.2.3.8. Pyrene

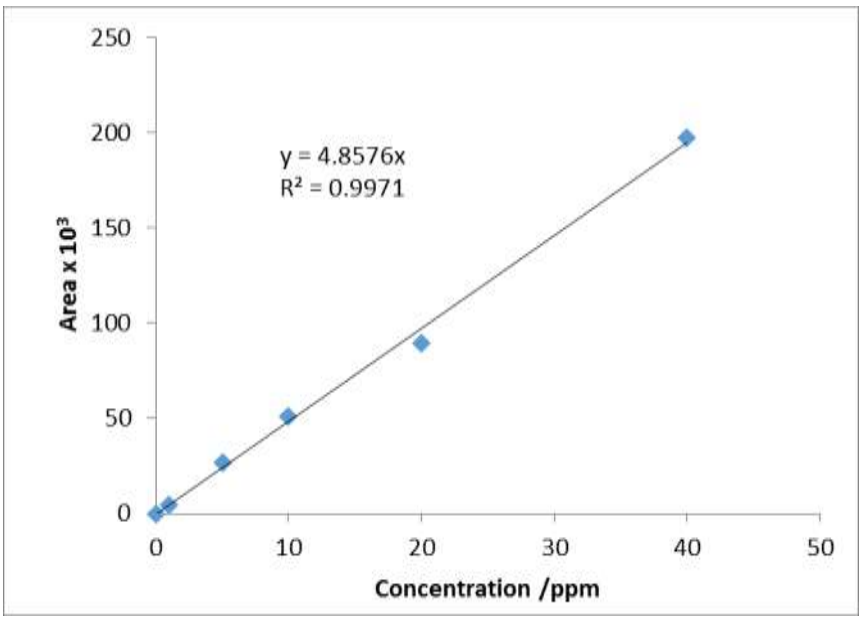

Figure 2.12. Calibration curve for Pyrene.

2.4.2.3.9. Benzo (a) Anthracene

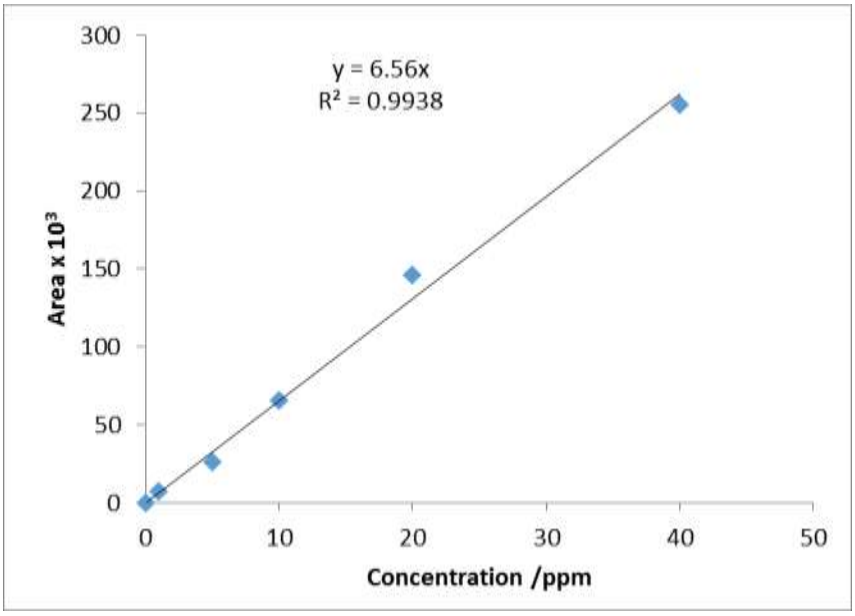

Figure 2.13. Calibration curve for Benzo (a) Anthracene.

2.4.2.3.10. Chrysene

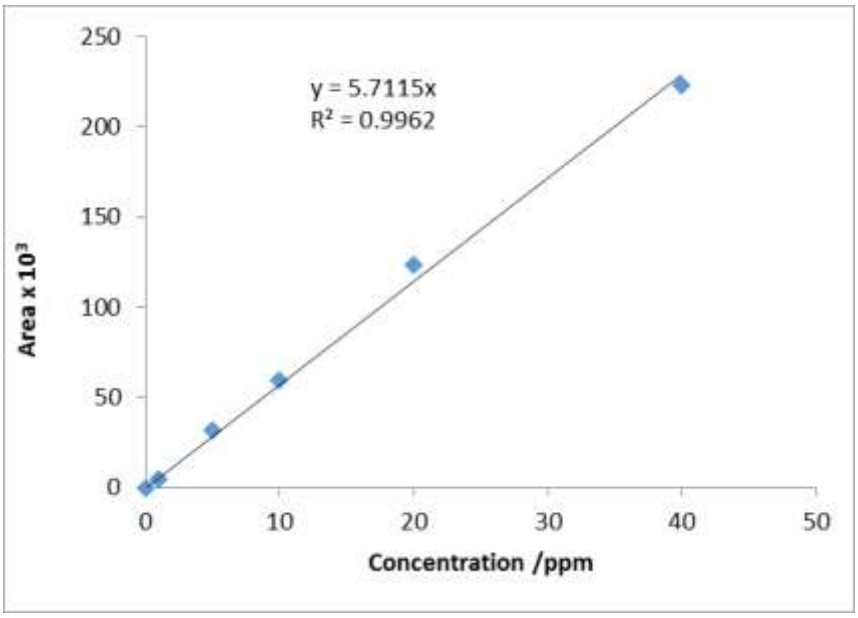

Figure 2.14. Calibration curve for Chrysene.

2.4.2.3.11. Benzo (b) Fluoranthene

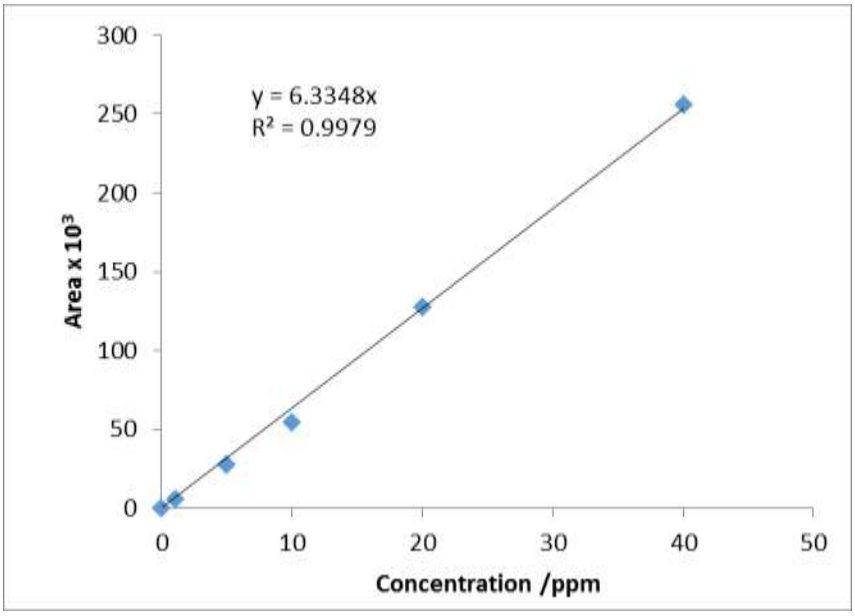

Figure 2.15. Calibration curve for Benzo (b) Fluoranthene.

2.4.2.3.12. Benzo (k) Fluoranthene

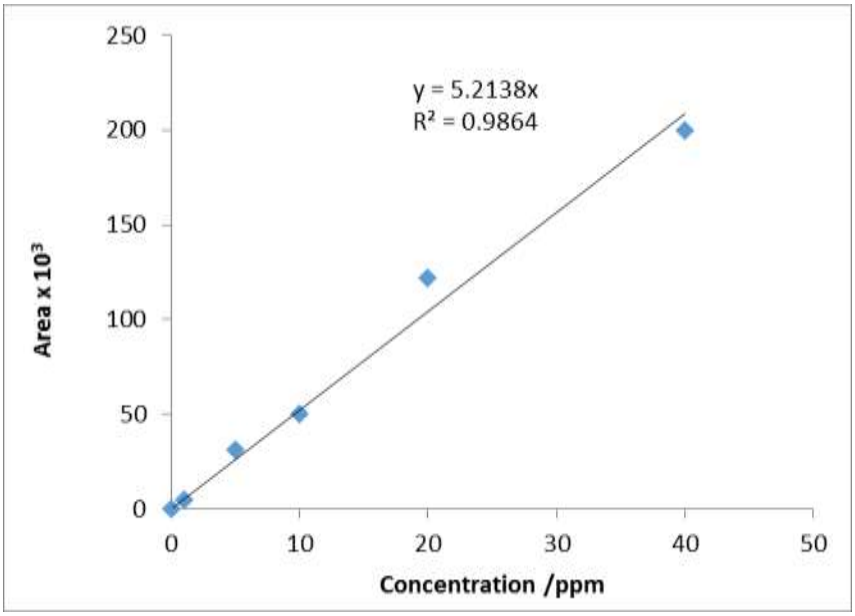

Figure 2.16. Calibration curve for Benzo (k) Fluoranthene.

2.4.2.3.13. Benzo (a) Pyrene.

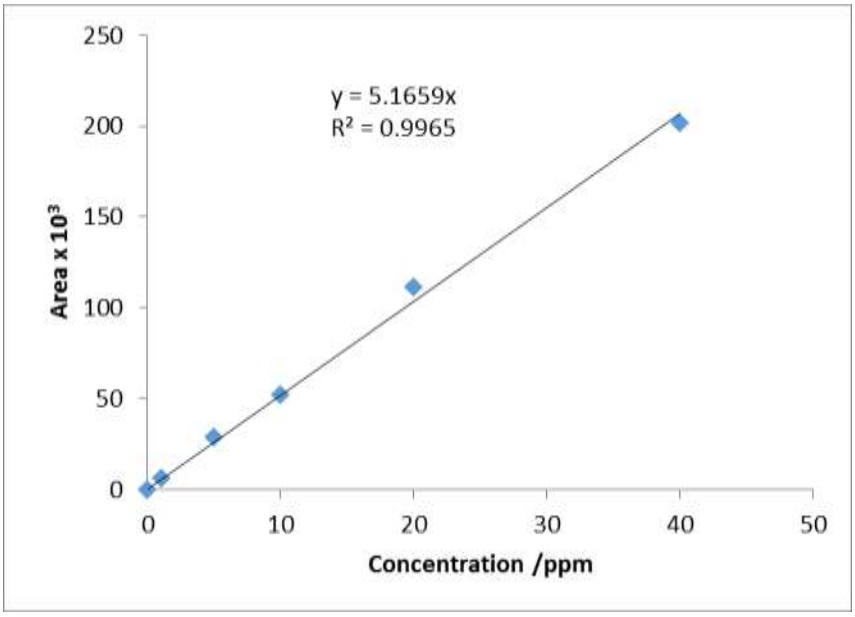

Figure 2.17. Calibration curve for Benzo (a)Pyrene.

2.4.2.3.14. Dibenzo (a,h)Anthracene

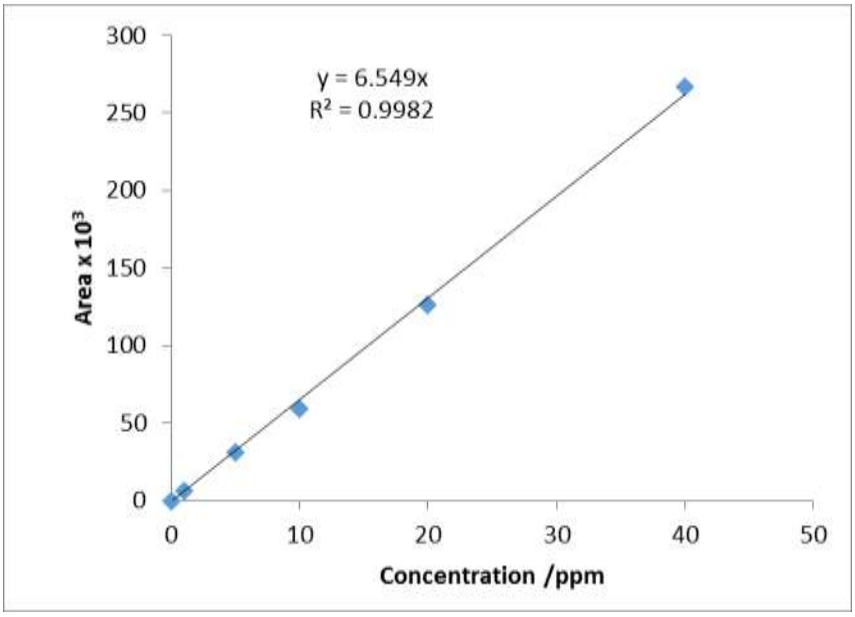

Figure 2.18. Calibration curve for Dibenzo (a,h)Anthracene.

2.4.2.3.15. Benzo (g,h,i)Perylene

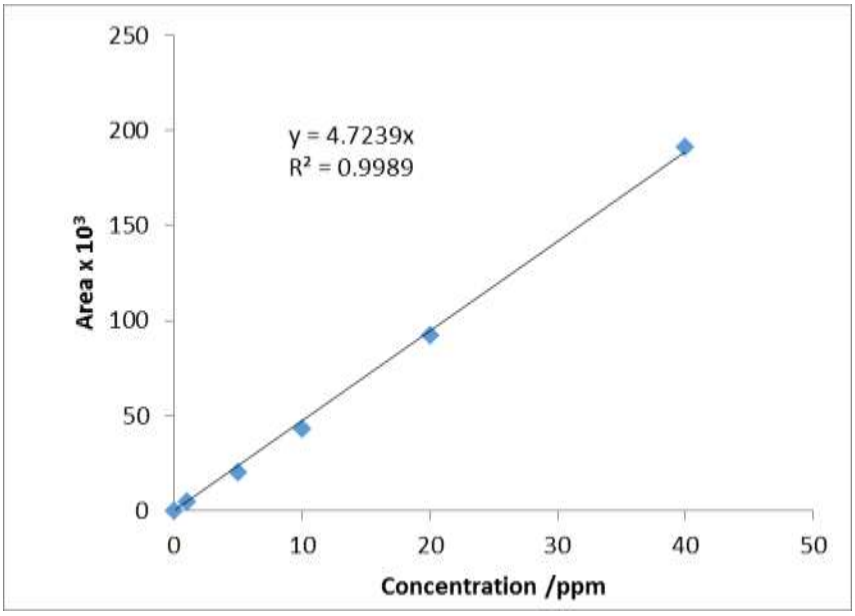

Figure 2.19. Calibration curve for Benzo (g,h,i)Perylene.

2.4.2.3.16. Indeno (1,2,3-cd)Pyrene

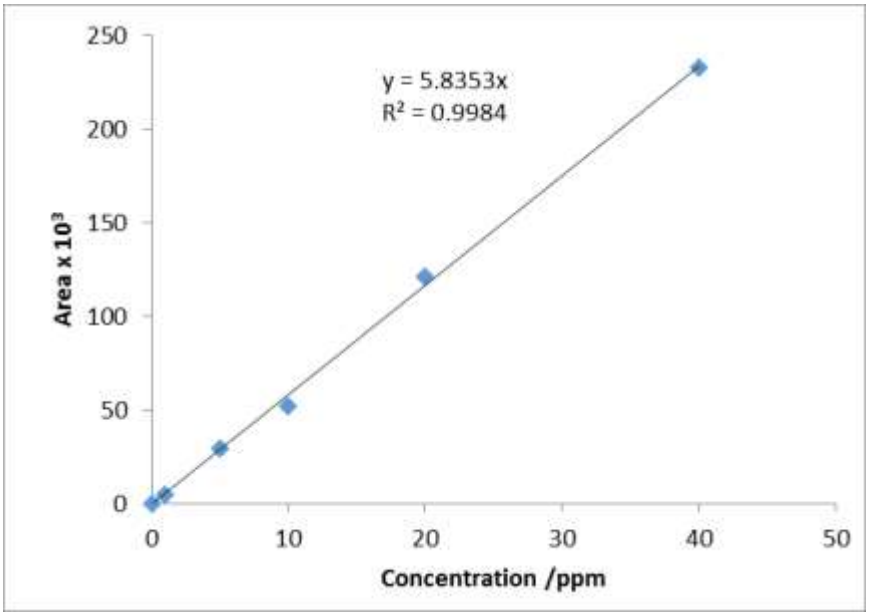

Figure 2.20. Calibration curve for Indeno (1,2,3-cd)Pyrene.

Table 2.9 illustrates the validation parameters for HPLC, these parameters include limit of detection(LOD), limit of quantification(LOQ) and recovery percentage got according to the following equations:

LOD = 3 x S.D./ m …….2-1

LOQ= 10 x S.D./ m ……2-2

%E rel. = (Taken value – Found value / Taken value) x100 …..2-3

% Recovery= 100 ± E-rel. ……2-4

Where: S.D. is the standard deviation for 5 reading

m is the slope from calibration curve for every compound.

Table 2.9. Validation parameters for HPLC

Compound	**LOD µg/L**	**LOQ µg/L**	**Recovery%**
Naphthalene	0.11	0.36	98.77
Acenaphthylene	0.09	0.29	97.83
Acenaphthene	0.31	1.03	98.22
Fluoranthene	0.18	0.59	99.40
Phenanthrene	0.22	0.73	97.17
Anthracene	0.15	0.49	97.22
Fluorine	0.53	1.76	97.82
Pyrene	0.14	0.46	98.26
Benzo(a)Anthracene	0.21	0.69	98.38
Chrysene	0.17	0.56	98.69
Benzo(b)Flourenthene	0.21	0.69	98.93
Benzo(k)Flouranthene	0.30	0.99	97.24
Benzo(a)Pyrene	0.28	0.93	97.62
Dibenzo(a,h)Anthrecene	0.20	0.66	98.39
Benzo(g,h,i)Perylene	0.12	0.39	98.62
In(12,3-cd)Pyrene	0.26	0.86	98.72

Figure 2.21, shows the HPLC chromatogram for standard sixteen PAHs and retention time for every compound.

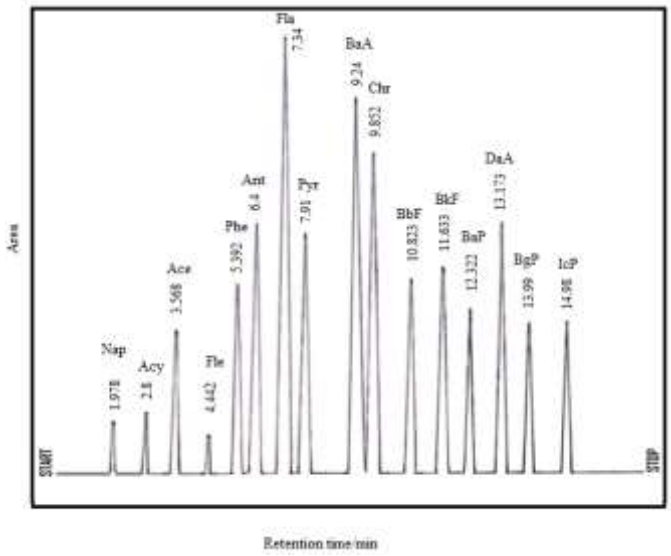

Figure 2.21. Chromatogram of HPLC for standard 16 PAHs .

Calculation for other factors such as, separation factor (α) and resolution factor (R) are present in table 2.10.

Table 2.10 resolution factors and separation factor for HPLC chromatogram

Successive pair of compounds	Separation factor (α)	Resolution factor (R)
Naphthalene & Acenaphthelyne	1.415	0.411
Acenaphthelyne & Acanaphthene	1.274	0.307

Acanaphthene & Fluoranthene	1.244	0.437
Fluoranthene & Phenanthrene	1.213	0.475
Phenanthrene & Anthracene	1.186	0.336
Anthracene & Fluorene	1.146	0.268
Fluorene & Pyrene	1.077	0.162
Pyrene & Benzo(a)Anthracene	1.168	0.380
Benzo(a)Anthracene & Chrysene	1.066	0.163
Chrysene & Benzo(b)Fluoranthene	1.098	0.298
Benzo(b)Fluoranthene& Benzo(k)Fluoranthene	1.074	0.270
Benzo(k)Fluoranthene& Benzo(a)Pyrene	1.059	0.229
Benzo(a)Pyrene& Dibenzo(a,h)Anthracene	1.069	0.283
Dibenzo(a,h)Anthracene& Benzo(g,h,i)Perylene	1.062	0.272
Benzo(g,h,i)Perylene& Indeno(1,2,3-cd)Pyrene	1.070	0.330

2.5. Treatment of Anthracene

2.5.1. Selection of the proper solvent

Several solvents have been used for dissolving anthracene in previous works. Generally, the method included dissolving anthracene crystals in different organic solvents to choose the perfect dissolution for Aanthracene; these solvents were methanol, dichloromethane, acetonitrile, ethyl acetate and acetone. According to the analysis data (recovery % and relative standard deviation), acetonitrile was the perfect solvent out of the others, as shown in Table 2.11.

Table 2.11. The average recovery% of Anthracene and relatively standard deviations RSD% with different organic solvents (n = 3).

Organic solvents	Recovery%	RSD %
Methanol	91.01	0.3
Dichloromethane	88.29	0.5
Acetonitrile	92.18	0.2
Ethyl acetate	81.72	0.4
Acetone	79.50	3.4

2.5.2. Preparation of aqueous solution for calibration curve

Several concentrations of aqueous solutions of anthracene dissolved in acetonitrile were prepared for calibration curve using GC instrument in order to compare the retention times and spectra of anthracene in the standard with those in the samples. Analytical standard of Anthracene was purchased from Sigma Aldrich. Samples were prepared from stock solution 100 ppm in aqueous solution [50% water and 50% Acetonitrile]. Then several concentrations were prepared and measured to build the calibration curve, Figure 2.22 shows the calibration curve for anthracene. The GC chromatogram for anthracene presents in Figure 2.23.

2.5.3. Optimization of GC parameters

All the extracted samples were analyzed for photocatalytic, direct photolysis and Fenton process using Shimadzu 2010 GC while analysis of anthracene ozonation was carried out by Agilent 7890A/ GC equipped with a flame ionization detector, HP-5 column, nitrogen gas 1 mL/min. The GC oven temperature was programmed to increase from 50 °C (2 min) to 200 °C (2 min) at a speed of 20 °C/min, to 240 °C (2 min) at 5 °C/min, and to 290 °C at 3 °C/min and then held for 15 min. The injector and detector temperatures were 275 °C and 300 °C, respectively. The analysis conditions are maintained in table 2.12. Several concentrations of standard anthracene were prepared for calibration curve as shown in Table 2.13.

Table 2.12. Chromatographic conditions used for determination Anthracene by GC:

Parameters	Details
Column	Type: Hp5(30m x Internal Diameter 0.28mm x Film thickness 0.25µm), temp.=130°C
Injection volume	1 µL
Injector mode	Split less, temp. =275°C
Carrier gas	Nitrogen
Detector	Type: FID

Table 2.13. Range of concentrations used for calibration curve.

Area	Conc./ppm
9.733	0.50
16.764	1.00
93.325	5.00
204.25	10.00
405.743	20.00
766.098	40.00

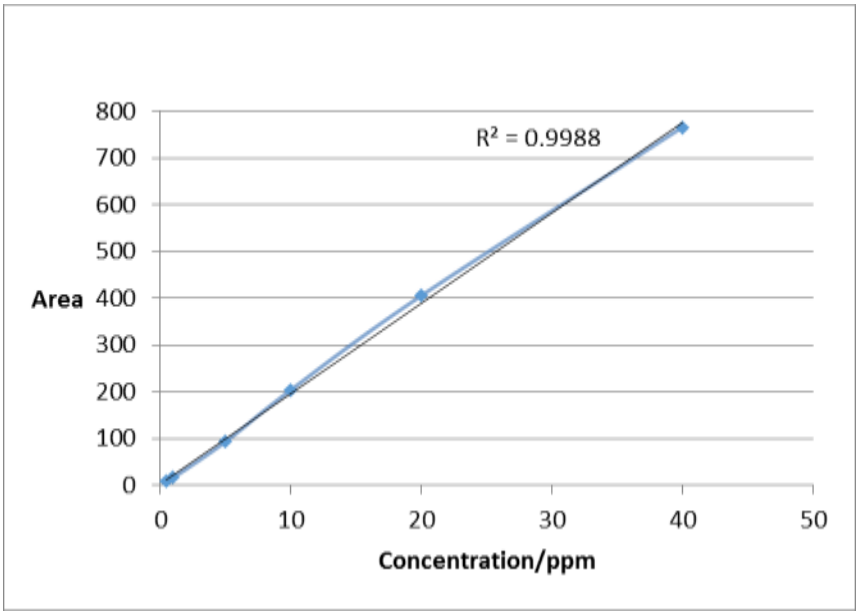

Figure 2.22. Calibration curve of Anthracene for GC.

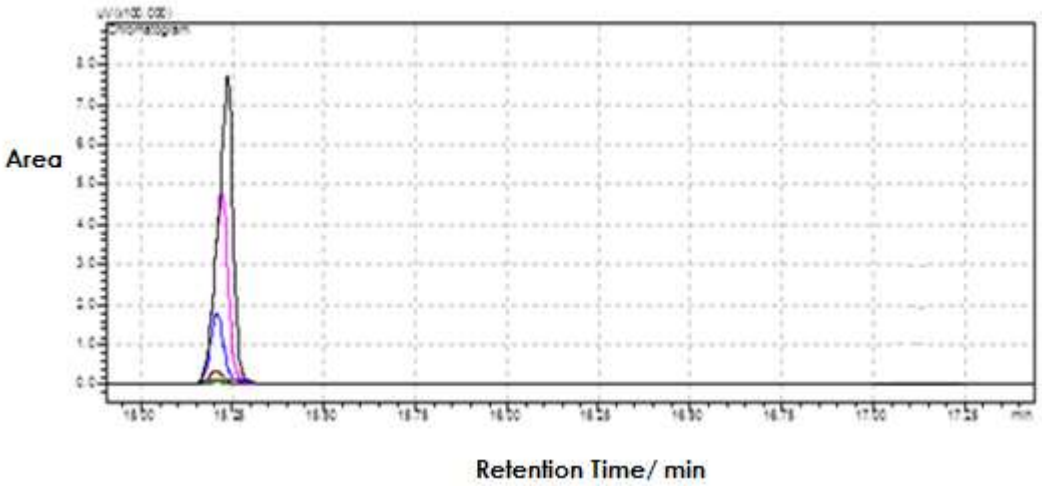

Figure 2.23. Chromatogram of GC for the Anthracene calibration curve.

2.5.4. Photocatalytic reactor units

The experiments were carried out in glass dual wall reactor, to keep the temperature constant using chiller as a thermostatic temperature controller. Agitation of the reaction mixture was provided by a magnetic stirrer (Heidolph-Mr3001). The photo reactor was operated in a batch mode. The study was carried out for the selected compound Anthracene (Sigma Aldrich) without additional purification. The pH of the reaction solution was adjusted by adding an exact volume of sodium hydroxide or sulfuric acid. A general diagram of the experimental set-up is shown in Scheme 2.2.

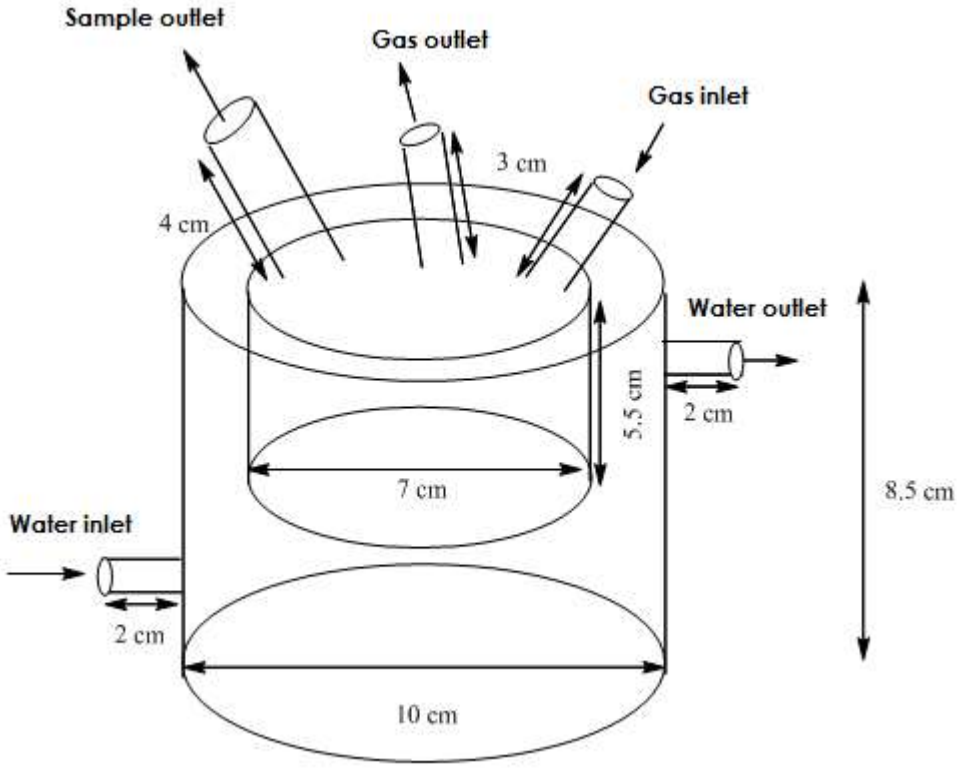

Scheme 2.2. Schematic Diagram of the Photocatalytic Vessel.

2.5.5. Direct Photolysis experiments

Water samples were extracted using solid phase extraction using dichloromethane. After the water was removed from the extract by using anhydrous Na_2SO_4 as a drying agent, the extracts were concentrated in a rotary evaporator at temperatures of below 35 ◦C to near dryness. The experiments were carried out in glass reactor, connected to a thermostatic bath to keep the temperature constant. Agitation of the reaction mixture was provided by a magnetic stirrer. The photo reactor was operated in a batch mode. The study was carried out for the selected compound anthracene without additional purification. Stock solutions were prepared in acetonitrile. The reaction solutions were prepared by mixing a proper volume of acetonitrile solution with distilled water treated in a Millipore Milli-Q Plus System. The pH of the reaction solution was adjusted by adding an exact volume of sodium hydroxide or sulfuric acid. The samples were measured by GC instruments from a Shimadzu Model 2010 equipped with a flame ionization detector and an HP-5 column.

2.5.6. Photocatalytic Activity Experiments

Samples were extracted by solid phase extraction method using dichloromethane. After removing the water from the extract by anhydrous Na_2SO_4, the extracts were

concentrated in a rotary evaporator at temperatures below 35 ◦C in a water bath to near dryness. The experiments were carried out in glass dual wall reactor, to keep the temperature constant using a chiller as a temperature controller. Agitation of the reaction mixture was provided by a magnetic stirrer. The photo reactor was operated in a batch mode. The study was carried out for the selected compound anthracene (Sigma Aldrich) without additional purification. The pH of the reaction solution was adjusted by adding an exact volume of sodium hydroxide or sulfuric acid. The samples were measured by a GC instrument from the Shimadzu Model 2010 equipped with a flame ionization detector and an HP-5 column. Suspension solutions were prepared by adding 0.175 g of catalysts per100 mL of anthracene aqueous solution. Prior to irradiation, suspensions were stirred in darkness for 60 min using a magnetic stirrer to ensure adsorption equilibrium. During adsorption and irradiation, suspensions were sampled at regular intervals. 5 mL of the reaction mixture was extracted by SPE and concentrated to 1 mL by a rotary evaporator.

2.5.7. Fenton process

The experiments were conducted in a 150mL dual wall reactor, which was connected with a temperature controller (chiller unit) to maintain the required temperature. The outside of the reactor was covered with aluminum foil to protect it from light. Homogeneous mixing was provided using a magnetic stirring bar. In each experiment, 100mL of anthracene solution at the desired initial concentration was inserted into the reactor. An aliquot was withdrawn for further analysis. After that, the pH was adjusted with a sulfuric acid solution and another aliquot was collected. Then, the required amount of iron (II) salt was added. When the salt was totally dissolved, a certain quantity of H_2O_2 solution was introduced in order to start the reaction. Aliquots were taken from the reactor at selected time intervals and immediately analyzed. The arrest of Fenton's reaction was achieved with the addition of some drops of concentrated sulfuric acid in order to decrease the pH to less than 1.0 [194]. GC analysis was made on an instrument from the Shimadzu Model 2010 equipped with a flame ionization detector and an HP-5 column. More details on the analytical conditions are illustrated in Table 2.11.

2.5.8. Ozonation method

Anthracene was dissolved in acetonitrile. The solution concentration was 25ppm. The radiolysis was conducted at a room temperature in a 100 ml volumetric flask tightly closed with a screw cap. Each flask was filled with approximately 50 ml of the anthracene dissolved in acetonitrile. A mercury lamp was used as a radiation source at a light intensity of 3.0mW/cm^2. GC analysis was made on an instrument from the Agilent Technologies Model 6789 equipped with a flame ionization detector and an HP-5 column. More details on the analytical conditions are illustrated in Table 2.12.

The radiolyzed sample was treated with O_3. The experimental methodology was followed by introducing ozone gas to the aqueous solution of anthracene; the ozone concentration in the reaction medium was constant during the whole time of irradiation. Several experiments were conducted in this part to compare the efficiency for every one; these experiments included using Ozone alone; UV alone; UV and Ozone; Ozone and TiO_2; UV, Ozone and H_2O_2; and UV, Ozone and TiO_2. The flow rate of Ozone was 2ml/min, the feeding gas was oxygen into the ozone generator.

2.6. Degradation of 9,10- Anthraquinone. The produced anthraquinone from the degraded anthracene was compared with the standard by GC-MS. Where 25 ppm of prepared anthraquinone was exposed to light and then several samples were measured at different of exposure times to follow the extent time of degradation and identify the required time for the complete degradation of this compound.

CHAPTER THREE

RESULTS

3.1. Physicochemical Properties

Several physicochemical properties such as temperature of the air, temperature of the water, electrical conductivity and pH of the surface water of the Shatt Al-Hilla samples were studied. Tables 3.1 and 3.2, show the spatial variation in the range, mean and standard deviation for these properties.

3.1.1. Air and water temperature

The maximum air temperature was 40ºC, recorded during July 2012 at site 10, while the minimum air temperature was 12 ºC during December 2011 at site 1. The lowest surface water temperature was 14 ºC, recorded in January 2012 at site 1 and site 4, whereas the highest temperature was 28 ºC, recorded during July 2012 at sites 6-14.

3.1.2. Electrical conductivity (EC)

The lowest EC value recorded was 835 µs/cm in November 2011 at site 10, and the highest value was1250 µs/cm, recorded during June 2012 at site 7.

3.1.3. Water pH

The minimum pH values measured were 6.4 once during November 2011 at site 1 and twice during December 2011 at sites 3 and 5, while the maximum pH value was measured during October 2012 at site 11.

Table 3.1. Statistical parameters of the air temperature and water temperature of water samples

Properties	**Air temperature**			**Water temperature**		
Site No.	Rang	Mean	S.D.	Rang	Mean	S.D.
S1	12-30	23.71	7.42	14-27	19.66	6.36
S2	13-31	23.93	6.36	15-27	20.25	4.94
S3	13-31	24.30	7.77	15-27	20.62	3.88
S4	13-30	24.16	6.36	14-27	20.50	4.94
S5	14-31	25.45	9.89	16-27	20.41	5.65
S6	14-37	28.50	14.14	16-28	21.41	6.36
S7	14-38	28.49	14.84	16-28	21.08	5.65
S8	16-37	29.69	13.43	18-28	21.41	4.94

S9	16-38	29.79	14.14	18-28	21.16	4.94
S10	15-40	29.70	13.43	18-28	21.25	4.94
S11	17-37	29.20	12.02	19-28	21.41	5.65
S12	16-37	29.21	11.31	19-28	21.16	5.65
S13	17-37	28.90	12.02	18-28	21.16	4.94
S14	17-37	28.44	12.37	17-28	21.04	5.30

Table 3.2. The statistical parameters of the electrical conductivity and pH of water samples

Properties	**EC- µS/cm**			**pH**		
Site No.	Rang	Mean	S.D.	Rang	Mean	S.D.
S1	844-1071	971.91	94.04	6.4-8.3	7.34	1.32
S2	847-1096	994.75	139.30	6.5-8.4	7.49	1.30
S3	930-1099	1014.00	38.18	6.4-8.5	7.69	1.32
S4	848-1079	973.83	119.50	6.6-8.5	7.60	1.35
S5	836-1090	995.58	74.95	6.4-8.5	7.58	1.19
S6	993-1075	1026.00	12.72	6.6-8.7	7.78	1.37
S7	870-1250	1046.33	96.16	6.6-8.8	7.86	1.25
S8	855-1186	1008.16	112.43	6.6-8.8	7.89	1.17
S9	859-1090	998.25	111.72	6.6-8.8	7.89	1.13
S10	835-1127	995.33	121.62	6.9-8.8	7.99	1.05
S11	910-1081	1010.50	68.58	6.9-8.9	8.10	1.08
S12	819-1074	982.41	132.93	6.9-8.7	8.03	0.91
S13	848-1074	1002.50	76.36	7.0-8.6	8.09	0.79
S14	837-1093	981.91	142.12	7.1-8.5	8.01	0.65

3.2 PAHs concentrations in the surface water samples

The concentrations of PAHs in the water were measured. These concentrations varied from site to site and from month to month. Concentration details were separated according to every single compound starting with naphthalene and finishing with Indeno(1,2,3-cd)pyrene. These Tables include some statistical calculations such as totals, averages and standard deviations.

33.2.1. Naphthalene

The highest concentration of naphthalene was 89.26 ppb, measured at site five in October 2012, while no concentrations were detected at any of the sites during the months of November, January, February, March, April and May. The most common appearance of this compound was in June at 7 sites out of 14 (S2, S4, S5, S7, S8, S10 and S11). Site five was the most polluted with naphthalene out of the 14 sites; the average at this site was 7.73 ppb. The total amount of naphthalene at all the sites over twelve months was 375.52 ppb. All these data are shown in Table 3.3.

Table 3.3. Concentrations of Naphthalene /(ppb) in the studied fourteen sites

Site No.	Nov. 2011	Dec. 2011	Jan. 2012	Feb. 2012	Mar. 2012	Apr. 2012	May 2012	Jun. 2012	Jul. 2012	Aug. 2012	Sept. 2012	Oct. 2012	Summation	Average	STDEV
S1	0.00	2.33	0.00	0.00	0.00	0.00	0.00	0.00	9.69	1.13	0.00	1.36	14.51	1.20	2.91
S2	0.00	0.00	0.00	0.00	0.00	0.00	0.00	19.02	1.76	0.00	0.00	2.93	23.71	1.97	6.01

S3	0.00	0.00	0.00	0.00	0.00	0.00	0.00	0.00	0.00	0.00	0.00	46.68	46.68	3.89	0.00
S4	0.00	0.00	0.00	0.00	0.00	0.00	0.00	1.40	0.00	0.00	0.00	0.00	1.40	0.11	0.31
S5	0.00	0.00	0.00	0.00	0.00	0.00	0.00	3.61	0.00	0.00	0.00	89.26	92.87	7.73	1.08
S6	0.00	0.00	0.00	0.00	0.00	0.00	0.00	0.00	0.00	0.00	0.00	0.00	0.00	0.00	0.00
S7	0.00	0.00	0.00	0.00	0.00	0.00	0.00	12.63	0.00	0.00	0.00	0.00	12.63	1.05	3.80
S8	0.00	0.00	0.00	0.00	0.00	0.00	0.00	76.78	0.00	0.00	0.00	0.00	76.78	6.39	23.15
S9	0.00	0.00	0.00	0.00	0.00	0.00	0.00	0.00	0.00	2.61	0.00	1.76	4.37	0.36	1.08
S10	0.00	0.00	0.00	0.00	0.00	0.00	0.00	0.98	0.00	0.00	0.00	0.00	0.98	0.16	0.08
S11	0.00	0.00	0.00	0.00	0.00	0.00	0.00	0.94	0.00	0.92	0.00	0.00	1.86	0.15	0.37
S12	0.00	0.00	0.00	0.00	0.00	0.00	0.00	0.00	0.00	85.60	0.00	0.00	85.60	7.13	25.77
S13	0.00	1.72	0.00	0.00	0.00	0.00	0.00	0.00	0.97	0.00	4.94	0.00	7.63	0.63	1.77
S14	0.00	0.00	0.00	0.00	0.00	0.00	0.00	0.00	0.00	6.51	0.00	0.00	6.51	0.54	1.96
Annual summation													375.52		

3.2.2. Acenaphthylene

The highest concentration of acenaphthylene was 118.11 ppb, measured at site eight in August 2012. The most common appearance of this compound was in August 2012, at ten sites out of the fourteen sites (S2, S3, S4, S5, S7, S8, S10, S11, S12 and S14). Site three was the most contaminated site with acenaphthylene out of the fourteen, the average at this site was 11.22 ppb over one year. The total amount of acenaphthylene at all the sites over twelve months was 636.74 ppb. Table 3.4 illustrates the concentrations of acenaphthylene for the fourteen sites over twelve months.

Table 3.4. Concentrations of Acenaphthylene /(ppb) in the studied fourteen sites

Site	**Nov.**	**Dec.**	**Jan.**	**Feb.**	**Mar.**	**Apr.**	**May**	**Jun.**	**Jul. 201**	**Aug.**	**Sept.**	**Oct.**	**Summa**	**Avera**	**STDEV**

No.	2011	2011	2012	2012	2012	2012	2012	2012	2	2012	2012	2012	tion	ge	
S1	0.00	2.71	1.29	0.00	0.00	0.00	0.00	0.00	0.00	0.00	0.00	1.68	5.68	0.47	1.055
S2	0.00	11.76	4.74	11.42	0.00	0.00	3.39	1.26	1.02	1.28	0.00	0.00	34.87	2.90	4.55
S3	0.00	0.00	6.81	9.02	0.00	1.58	51.71	2.85	0.00	1.69	15.93	45.07	134.66	11.22	18.28
S4	0.00	0.00	0.00	0.00	0.00	0.00	9.43	3.94	44.07	1.79	1.27	1.14	61.64	5.13	13.18
S5	0.00	0.00	0.00	1.51	0.00	0.00	0.00	0.00	0.00	1.11	1.19	63.12	66.93	5.57	18.75
S6	10.54	0.00	0.00	1.71	0.00	0.00	1.23	20.13	1.57	0.00	1.19	0.00	36.37	3.03	6.99
S7	0.00	0.00	0.00	1.46	0.00	0.00	7.71	0.00	2.83	1.28	1.33	0.00	14.61	1.21	3.09
S8	0.00	0.00	1.55	0.00	0.00	0.00	0.97	10.19	0.00	118.11	0.00	0.00	130.82	10.90	33.91
S9	0.00	0.00	1.16	0.00	0.00	0.00	1.46	11.43	0.00	0.00	1.79	1.02	16.86	1.40	3.82
S10	0.00	0.96	1.48	0.00	1.20	0.00	0.00	0.00	1.11	1.38	0.00	0.00	6.13	0.51	0.99
S11	17.85	0.00	0.00	4.91	3.76	0.00	0.00	1.03	0.00	1.47	1.21	0.00	30.23	2.51	5.23
S12	0.00	0.00	0.00	0.00	24.04	0.00	0.00	9.05	1.36	11.81	0.00	0.00	46.26	3.85	7.80
S13	8.52	1.96	0.00	1.87	0.00	0.00	0.00	0.00	1.36	0.00	0.00	0.00	13.71	1.14	3.01
S14	24.88	0.00	0.00	2.73	0.00	0.00	0.00	3.81	0.00	5.51	0.00	1.04	37.97	3.16	7.15
Annual summation													636.74		

3.2.3. Acenaphthene

The maximum concentration of acenaphthene was 107.18 ppb regarded in site nine in December 2011. The most appearance for this compound was in December 2011 and

May 2012, 9 sites of 14 (S3, S4, S6, S7, S8, S9, S12, S13 and S14) in December 2011 and 9 sites (S1, S2, S3, S4, S6, S8, S9, S10 and S12) in May 2012. Site nine was the most contaminated site with acenaphthene out of the fourteen; the average at this site was 10.86 ppb over one year. The total amount of acenaphthene at all the sites over twelve months was 300.10 ppb. Table 3.5 illustrates the concentrations of acenaphthene for the fourteen sites over twelve months.

Table 3.5. Concentrations of Acenaphthene/(ppb) in the studied fourteen sites

Site No.	Nov. 2011	Dec. 2011	Jan. 2012	Feb. 2012	Mar. 2012	Apr. 2012	May 2012	Jun. 2012	Jul. 2012	Aug. 2012	Sept. 2012	Oct. 2012	Summation	Average	STDEV
S1	0.00	0.00	1.65	0.00	0.00	1.96	2.09	0.00	28.54	1.23	0.00	0.00	35.47	2.95	8.71
S2	0.00	0.00	0.00	0.00	0.00	0.00	4.54	0.00	0.00	0.00	0.00	0.00	4.54	0.37	1.31
S3	0.00	2.034	0.00	0.00	0.00	6.85	8.62	0.00	1.27	0.00	0.00	4.93	23.70	1.97	3.08
S4	12.13	2.03	0.00	0.00	0.00	3.77	3.71	0.00	0.00	0.00	0.00	0.00	21.64	1.80	3.50
S5	0.00	0.00	0.00	0.00	0.00	0.00	0.00	1.06	0.00	0.00	0.00	0.00	1.06	0.08	0.22
S6	0.00	11.06	0.00	2.27	0.00	0.00	4.56	0.00	0.00	0.00	0.00	0.00	17.89	1.49	3.29
S7	0.00	6.22	0.00	2.35	0.00	0.00	0.00	0.00	0.00	0.00	0.08	0.00	8.65	0.72	1.85
S8	26.21	5.15	0.00	1.07	1.18	0.00	2.27	0.00	0.00	0.00	0.00	0.00	35.88	2.99	7.47
S9	14.95	107.18	0.00	0.00	4.01	0.00	2.35	0.00	0.00	1.88	0.00	0.00	130.37	10.86	30.64
S10	0.00	0.00	5.75	1.79	0.00	0.00	1.10	0.00	0.00	0.00	0.00	0.00	8.64	0.72	1.93
S11	0.00	0.00	0.00	0.56	0.00	0.00	0.00	0.00	0.00	0.00	0.00	0.00	0.56	0.04	0.15
S12	0.00	5.11	0.00	0.00	0.00	0.00	1.79	0.00	0.00	0.00	0.00	0.00	6.90	0.57	1.75
S13	0.00	1.67	0.00	0.00	0.00	0.00	0.00	0.00	0.00	0.00	0.00	0.00	1.67	0.13	0.43
S14	0.00	2.06	0.00	0.00	0.00	0.00	0.00	0.00	0.00	1.06	0.00	0.00	3.12	0.26	0.65

Annual summation	300.10

3.2.4. Fluorene

The maximum concentration of fluorene was 96.63 ppb, measured at site six in February 2012. The most common appearance of this compound was in February 2012; this compound was detected at all fourteen sites during this month. Site six was the most contaminated site with fluorene out of the fourteen; the average at this site was 18.99 ppb over one year. The total amount of fluorene at all the sites over twelve months was 1690.60 ppb. Table 3.6 illustrates the concentrations of fluorene for the fourteen sites over twelve months.

Table 3.6. Concentrations of Fluorene/(ppb) in the studied fourteen sites

Site No.	Nov. 2011	Dec. 2011	Jan. 2012	Feb. 2012	Mar. 2012	Apr. 2012	May 2012	Jun. 2012	Jul. 2012	Aug. 2012	Sept. 2012	Oct. 2012	Summation	Average	STDEV
S1	14.11	0.00	1.49	21.32	0.00	7.29	2.59	0.00	0.00	0.00	0.00	0.00	46.8	3.9	6.95
S2	0.00	23.02	2.83	1.15	42.01	2.54	7.61	0.00	0.00	0.00	0.00	0.00	79.16	6.59	13.26
S3	0.00	1.29	17.11	86.38	64.38	0.00	6.12	0.00	0.00	0.00	0.00	2.37	177.65	14.80	29.09
S4	10.08	1.29	10.82	86.32	19.77	0.00	0.00	0.00	2.38	0.00	0.00	0.00	130.66	10.88	24.57
S5	0.00	0.00	1.11	51.56	16.78	2.73	0.00	0.00	0.00	0.00	0.00	0.00	72.18	6.01	15.11
S6	52.5	0.00	3.36	96.6	51.6	15.8	7.84	0.00	0.00	0.00	0.00	0.00	227.	18.9	31.28

	7			3	4	9							93	9	
S7	0.00	0.00	14.67	46.39	0.00	19.69	46.17	0.00	0.00	0.00	0.00	0.00	126.92	10.57	17.94
S8	14.95	0.00	13.57	10.81	32.63	9.43	96.64	0.00	0.03	0.00	0.00	0.00	178.06	14.83	27.59
S9	0.00	2.81	2.97	84.51	0.00	28.83	46.39	0.00	0.00	0.00	0.00	0.00	165.51	13.79	26.74
S10	23.74	0.00	0.00	77.38	1.18	0.00	10.81	0.00	0.00	0.00	0.00	0.00	113.11	9.42	22.56
S11	0.00	0.00	0.00	34.32	0.00	27.45	84..51	0.00	0.00	0.00	0.00	0.00	61.77	5.61	12.58
S12	0.00	0.00	2.11	33.18	12.45	0.00	77.38	12.05	0.00	0.00	0.00	0.00	137.17	11.43	23.01
S13	43.72	2.81	0.01	7.83	2.32	0.00	4.97	0.00	0.00	0.00	0.00	0.00	61.66	5.13	12.40
S14	65.04	0.00	33.84	1.82	2.95	0.00	0.00	0.00	0.00	1.51	6.86	0.00	112.02	9.33	20.04
Annual summation													1690.60		

3.2.5. Phenanthrene

The highest concentration of phenanthrene was 205.22 ppb, measured at site fourteen in November 2011. The most common appearance for this compound was in November 2011 at nine sites (S1, S4, S5, S6, S7, S9, S10, S13 and S14), where this compound was detected during this month. Site fourteen was the most contaminated site with phenanthrene out of the fourteen; the average at this site was 17.14 ppb over one year. The total amount of phenanthrene at all the sites over twelve months was 620.71 ppb. Table 3.7 illustrates the concentrations of phenanthrene for the fourteen sites over twelve months.

Table 3.7. Concentrations of Phenanthrene/(ppb) in the studied fourteen sites

Site No.	Nov. 2011	Dec. 2011	Jan. 2012	Feb. 2012	Mar. 2012	Apr. 2012	May 2012	Jun. 2012	Jul. 2012	Aug. 2012	Sept. 2012	Oct. 2012	Summation	Average	STDEV
S1	18.39	0.00	3.34	0.00	0.00	0.00	58.75	0.00	0.00	0.00	0.00	0.00	80.48	6.70	17.21
S2	0.00	12.15	0.00	0.00	0.00	0.00	0.00	0.00	0.00	0.00	0.00	0.00	12.15	1.01	3.50
S3	0.00	0.00	0.00	0.00	1.22	4.45	0.00	0.00	1.46	0.00	0.00	3.35	10.48	0.87	1.99
S4	10.46	0.00	0.00	2.31	0.00	0.00	2.92	0.00	0.00	0.00	0.00	0.00	15.69	1.30	4.15
S5	16.05	12.31	0.00	0.00	0.00	0.00	0.00	0.00	0.00	0.00	0.00	0.00	28.36	2.36	5.54
S6	43.02	0.00	0.00	0.00	0.00	0.00	0.00	0.00	0.00	0.00	0.00	0.00	43.02	3.58	12.41
S7	33.56	0.00	0.00	5.69	0.00	0.00	0.00	0.00	0.00	0.00	0.00	0.00	39.25	3.27	9.67
S8	0.00	0.00	0.00	4.84	0.00	0.00	0.00	0.00	0.00	0.00	0.00	0.00	4.84	0.40	1.39
S9	26.15	0.00	0.00	0.00	2.84	0.00	5.65	0.00	0.00	0.00	0.00	0.00	34.64	2.88	7.53
S10	83.67	0.00	0.00	0.00	0.00	0.00	4.84	0.00	0.00	0.00	0.00	0.00	88.51	7.37	24.06
S11	0.00	0.00	3.48	0.00	0.00	0.00	0.00	0.00	0.00	0.00	0.00	0.00	3.48	0.29	1.00
S12	0.00	0.00	0.00	2.94	0.00	0.00	0.00	0.00	0.00	0.00	0.00	0.00	2.94	0.24	0.84
S13	48.46	0.00	0.00	1.38	0.00	0.00	0.00	0.00	0.00	0.00	1.24	0.00	51.08	4.25	14.24
S14	205.22	0.00	0.00	0.00	0.00	0.00	0.00	0.00	0.00	0.00	0.00	0.00	205.22	17.14	59.22
Annual summation													620.71		

3.2.6. Anthracene

The highest concentration of anthracene was 94.60 ppb, measured at site eleven in November 2011. The most common appearance of this compound was in November 2011 at eight sites (S1, S2, S5, S6, S7, S10, S11and S13), where this compound was detected during this month. Site eleven was the most contaminated site with anthracene out of the fourteen; the average at this site was 10.26 ppb over one year. The total amount of anthracene at all the sites over twelve months was 610.02 ppb. Table 3.8 illustrates the concentrations of anthracene for the fourteen sites over twelve months.

Table 3.8. Concentrations of Anthracene/(ppb) in the studied the fourteen sites

Site No.	Nov. 2011	Dec. 2011	Jan. 2012	Feb. 2012	Mar. 2012	Apr. 2012	May 2012	Jun. 2012	Jul. 2012	Aug. 2012	Sept. 2012	Oct. 2012	Summation	Average	STDEV
S1	18.04	1.56	0.00	0.00	47.06	2.36	8.73	0.00	1.94	0.00	0.00	0.00	79.69	6.64	14.11
S2	65.55	0.00	0.00	2.08	0.00	5.85	0.00	0.00	0.00	1.27	1.14	0.00	75.89	6.32	18.78
S3	0.00	0.00	0.00	0.00	1.01	0.00	0.00	0.00	0.00	0.00	1.19	3.52	5.72	0.47	1.04
S4	0.00	0.00	0.00	1.79	0.00	17.73	0.00	0.00	0.00	0.00	0.00	0.00	19.52	1.62	5.39
S5	18.56	0.00	0.00	1.04	0.00	0.00	66.32	0.00	1.21	2.01	0.00	5.45	94.59	7.88	20.39
S6	2.06	0.00	0.00	4.34	0.00	0.00	6.35	0.00	0.00	0.00	0.00	0.00	12.75	1.06	2.12
S7	21.90	0.00	0.00	0.00	0.00	0.00	6.48	7.12	1.14	0.00	0.00	0.00	36.64	3.05	6.56
S8	0.00	0.00	0.00	0.00	0.00	2.11	4.34	0.00	0.00	11.75	0.00	0.00	18.2	1.51	4.04
S9	0.00	0.00	0.00	0.00	0.00	0.00	0.00	0.00	0.00	1.03	0.00	0.00	1.03	0.08	0.27
S10	62.43	0.00	0.00	1.11	0.00	1.24	0.00	0.00	0.00	0.00	0.00	0.00	64.78	5.39	18.27
S11	94.60	0.00	10.19	12.75	5.68	0.00	0.00	0.00	0.00	0.00	0.00	0.00	123.22	10.26	26.93
S12	0.00	0.00	0.00	0.00	0.00	0.00	0.00	0.00	0.00	13.97	0.00	0.00	13.97	1.16	4.03

S13	45.46	3.58	0.00	0.00	0.00	0.00	0.00	0.00	0.00	0.00	1.32	0.00	50.36	4.19	13.34
S14	0.00	10.05	0.00	1.74	0.00	0.00	0.00	0.00	0.00	1.87	0.00	0.00	13.66	1.13	3.45
Annual summation													610.02		

3.2.7. Fluoranthene

The highest concentration of fluoranthene was 107.74 ppb, measured at site fourteen in November 2011. The most common appearance for this compound was in February 2012 at eleven sites (S2, S3, S4, S5, S6, S8, S9, S10, S11, S13 and S14), and in May 2012 at eleven sites S1, S3, S4, S5, S6, S7, S8, S9, S10, S11 and S12), where this compound was detected during these months. Site twelve was the most contaminated site with fluoranthene out of the fourteen; the average at this site was 17.46 ppb over one year. The total sum of fluoranthene at all the sites over twelve months was 1146.18 ppb. Table 3.9 illustrates the concentrations of fluoranthene at the fourteen sites over twelve months.

Table 3.9. Concentrations of Fluoranthene/(ppb) in the studied fourteen sites

Site No.	Nov. 2011	Dec. 2011	Jan. 2012	Feb. 2012	Mar. 2012	Apr. 2012	May 2012	Jun. 2012	Jul. 2012	Aug. 2012	Sept. 2012	Oct. 2012	Summation	Average	STDEV
S1	14.03	0.00	3.81	0.00	0.00	1.71	18.09	0.00	1.54	0.00	0.00	0.00	39.18	3.26	6.65
S2	50.64	0.00	4.33	7.73	3.22	3.38	0.00	0.00	0.00	0.00	0.00	0.00	69.3	5.77	14.34
S3	74.41	0.00	5.61	19.58	0.00	2.33	3.04	0.00	1.16	0.00	4.75	1.34	112.22	9.35	21.19
S4	0.00	0.00	0.00	17.64	0.00	4.97	15.01	0.00	0.00	0.00	0.00	0.00	37.62	3.13	6.34
S5	14.67	0.00	15.45	35.85	0.00	6.23	11.85	0.00	0.00	0.00	0.00	5.01	89.06	7.42	10.79
S6	24.52	0.00	0.00	9.37	0.00	6.53	5.38	0.00	0.00	0.00	0.00	0.00	45.8	3.81	7.29

S7	0.00	1.63	0.00	0.00	0.00	1.47	11.55	1.16	0.00	0.00	0.00	0.00	15.81	1.31	3.56
S8	0.00	0.00	4.82	38.12	0.00	7.01	9.37	0.00	0.00	9.48	0.00	0.00	68.8	5.73	10.90
S9	0.00	0.00	1.11	16.99	3.01	0.00	5.69	0.00	0.00	1.36	0.00	1.84	30.00	2.50	5.47
S10	0.00	0.00	10.65	41.45	29.53	0.00	38.27	0.00	0.00	0.00	0.00	0.00	119.9	9.99	16.40
S11	0.00	0.00	0.00	17.11	1.76	1.62	18.99	0.00	0.00	0.00	0.00	0.00	39.48	3.29	7.14
S12	73.96	0.00	0.00	0.00	6.08	0.00	41.45	0.00	0.00	88.13	0.00	0.00	209.62	17.46	32.09
S13	0.00	0.00	0.00	78.47	6.89	0.00	0.00	0.00	0.00	0.00	1.55	0.00	86.91	7.24	22.54
S14	107.74	0.00	3.94	2.68	32.36	0.00	0.00	0.00	17.29	1.18	17.29	0.00	182.48	15.20	31.08
Annual summation													1146.18		

3.2.8. Pyrene

The highest concentration of pyrene was 270.15 ppb, measured at regarded in site three in November 2011. The most common appearance of this compound was in November 2011 at eight sites (S2, S3, S4, S5, S6, S12, S13 and S14), where this compound was detected during this month. Site three was the most contaminated site with pyrene out of the fourteen; the average at this site was 30.11 ppb over one year. The total amount of pyrene at all the sites over twelve months was 729.84 ppb. Table 3.10 illustrates the concentrations of pyrene at the fourteen sites over twelve months.

Table 3.10. Concentrations of Pyrene/(ppb) in the studied fourteen sites

Site No.	**Nov. 201**	**Dec. 201**	**Jan. 201**	**Feb. 201**	**Mar. 201**	**Apr. 201**	**May 201**	**Jun. 201**	**Jul. 2012**	**Aug. 201**	**Sept. 201**	**Oct. 201**	**Summatio**	**Average**	**STDEV**

	1	1	2	2	2	2	2	2		2	2	2	n		
S1	0.00	0.00	0.00	0.00	0.00	2.95	0.00	0.00	0.00	0.00	0.00	0.00	2.95	0.24	0.85
S2	96.89	0.00	0.00	0.00	0.00	1.80	3.76	0.00	0.00	0.00	0.00	0.00	102.45	8.53	27.85
S3	270.15	1.47	0.00	1.91	0.00	0.00	7.86	0.00	0.00	80.01	0.00	0.00	361.4	30.11	79.04
S4	1.13	1.47	0.00	0.00	0.00	1.87	0.00	0.00	0.00	0.00	0.00	0.00	4.47	0.37	0.71
S5	2.00	0.00	0.00	0.00	0.00	0.00	15.52	0.00	0.00	0.00	0.00	1.34	18.86	1.57	4.44
S6	38.88	0.00	14.22	0.00	0.00	0.00	0.00	0.00	0.00	0.00	0.00	0.00	53.1	4.42	11.57
S7	0.00	0.00	0.00	0.00	0.00	0.00	0.00	0.00	0.00	0.00	0.00	0.00	0.00	0.00	0.00
S8	0.00	0.00	0.00	0.00	1.14	1.15	0.00	0.00	0.00	0.00	1.01	0.00	3.3	0.27	0.65
S9	0.00	2.01	0.00	0.00	0.00	2.79	0.00	0.00	0.00	0.00	0.00	0.00	4.8	0.40	0.91
S10	0.00	3.48	0.00	1.58	0.00	0.00	1.53	0.00	0.00	0.00	0.00	0.00	6.59	0.54	1.09
S11	0.00	0.00	0.00	0.00	0.00	0.00	0.00	0.00	0.00	0.00	0.00	0.00	0.00	0.00	0.00
S12	54.57	0.00	0.00	0.00	3.71	0.00	0.00	0.00	0.00	7.04	0.00	0.00	65.32	5.44	15.62
S13	26.27	5.73	0.00	0.00	0.00	0.00	0.00	0.00	0.00	0.00	0.00	0.00	32	2.66	7.61
S14	58.64	5.35	0.00	1.45	0.00	0.00	0.00	0.00	0.00	1.94	7.16	0.00	74.54	6.21	16.70
Annual summation													729.84		

3.2.9. Benzo(a)anthracene

The highest concentration of benzo(a)anthracene was 151.11 ppb, measured at site five in November 2011. The most common appearance of this compound was in February 2012 at ten sites (S2, S3, S5, S6, S7, S8, S9, S10, S11and S14), where this

compound was detected during this month. Site five was the most contaminated site with benzo(a)anthracene out of the fourteen; the average at this site was 18.16 ppb over one year. The total sum of benzo(a)anthracene at all the sites over twelve months was 1280.11 ppb. Table 3.11 illustrates the concentrations of benzo(a)anthracene at the fourteen sites over twelve months.

Table 3.11. Concentrations of Benzo(a)anthracene/(ppb) in the studied fourteen sites

Site No.	Nov. 2011	Dec. 2011	Jan. 2012	Feb. 2012	Mar. 2012	Apr. 2012	May 2012	Jun. 2012	Jul. 2012	Aug. 2012	Sept. 2012	Oct. 2012	Summation	Average	STDEV
S1	15.92	0.00	9.14	0.00	0.00	1.75	0.00	0.00	0.00	0.00	0.00	0.00	26.81	2.23	5.19
S2	0.00	21.95	19.20	40.63	0.00	0.00	0.00	0.00	0.00	0.00	0.00	0.00	81.78	6.81	13.28
S3	103.82	0.00	8.18	8.87	1.41	18.75	9.54	0.00	0.00	0.00	0.00	0.00	150.57	12.54	29.35
S4	0.00	0.00	0.00	0.00	0.00	19.09	0.00	0.00	0.00	0.00	0.00	0.00	19.09	1.59	5.51
S5	151.11	3.09	4.46	24.01	0.00	0.00	33.36	0.00	0.00	0.00	0.00	1.99	218.02	18.16	43.27
S6	0.00	3.04	12.66	14.27	3.06	0.00	0.00	0.00	0.00	0.00	0.00	0.00	33.03	2.75	5.14
S7	63.77	1.15	0.00	32.96	0.00	0.00	0.00	1.56	0.00	0.00	0.00	0.00	99.44	8.28	19.84
S8	0.00	1.45	47.91	43.41	0.00	0.00	14.26	0.00	0.00	2.42	0.00	0.00	109.45	9.12	17.56
S9	42.07	0.00	40.22	58.57	33.59	0.00	32.96	0.00	0.00	1.58	0.00	0.00	208.99	17.41	22.14
S10	66.12	0.00	0.00	18.61	17.56	0.00	43.67	0.00	0.00	0.00	0.00	0.00	145.96	12.16	21.60
S11	0.00	0.00	0.00	20.89	0.00	0.00	73.95	0.00	0.00	0.00	0.00	0.00	94.84	7.90	21.61
S12	0.00	0.00	0.00	0.00	0.00	0.00	18.61	0.00	0.00	2.42	0.00	0.00	21.03	1.75	5.35

S13	0.00	0.00	2.82	0.00	0.00	0.00	38.21	0.00	0.00	0.00	0.00	0.00	41.03	3.41	11.58
S14	0.00	0.00	0.00	1.16	0.00	0.00	0.00	0.00	15.57	0.00	13.34	0.00	30.07	2.50	5.58
Annual summation													1280.11		

3.2.10. Chrysene

The highest concentration of chrysene was 158.96 ppb, measured at site two in November 2011. The most common appearance of this compound was in December 2011 at seven sites (S1, S2, S3, S4, S6, S7 and S8), where this compound was detected during this month. Site two was the most contaminated site with chrysene out of the fourteen; the average at this site was 15.43 ppb over one year. The total amount of chrysene at all the sites over twelve months was 398.5 ppb. Table 3.12 illustrates the concentrations of chrysene at the fourteen sites over twelve months.

Table 3.12. Concentrations of Chrysene/(ppb) in the studied fourteen sites

Site No.	**Nov. 2011**	**Dec. 2011**	**Jan. 2012**	**Feb. 2012**	**Mar. 2012**	**Apr. 2012**	**May 2012**	**Jun. 2012**	**Jul. 2012**	**Aug. 2012**	**Sept. 2012**	**Oct. 2012**	**Summation**	**Average**	**STDEV**
S1	0.00	7.81	0.00	8.46	0.00	1.49	0.00	0.00	0.00	0.00	0.00	0.00	17.76	1.48	3.12
S2	158.96	1.74	0.00	0.00	1.96	0.00	22.59	0.00	0.00	0.00	0.00	0.00	185.25	15.43	45.64
S3	0.00	7.88	4.39	0.00	0.00	0.00	0.00	0.00	1.54	0.00	2.11	2.02	17.94	1.49	2.48
S4	0.00	7.88	0.00	0.00	0.00	0.00	0.00	0.00	2.02	0.00	0.00	0.00	9.9	0.82	2.29
S5	0.00	0.00	0.00	0.00	1.01	0.00	0.00	0.00	0.00	0.00	0.00	1.53	2.54	0.21	0.46
S6	32.6	3.24	1.81	0.00	0.00	0.00	0.00	0.00	0.00	0.00	0.00	0.00	37.21	3.10	9.20
S7	0.00	11.05	0.00	0.00	0.00	0.00	0.00	1.75	0.00	0.00	0.00	0.00	12.8	1.06	3.18

S8	29.48	9.44	0.00	0.00	0.00	0.00	0.00	0.00	0.00	2.43	4.58	0.00	45.93	3.82	8.57
S9	0.00	0.00	0.00	0.00	1.19	0.00	0.00	0.00	0.00	0.00	0.00	0.00	1.19	0.09	0.34
S10	0.00	0.00	0.00	0.00	0.00	0.00	0.00	0.00	0.00	0.00	0.00	0.00	0.00	0.00	0.00
S11	0.00	0.00	0.00	0.00	0.00	18.50	0.00	0.00	0.00	0.00	0.00	0.00	18.50	1.54	5.29
S12	0.00	0.00	0.00	0.00	0.00	0.00	0.00	0.00	0.00	2.44	0.00	0.00	2.44	0.20	0.70
S13	0.00	0.00	0.00	0.00	0.00	0.00	0.00	0.00	0.00	0.00	0.00	0.00	0.00	0.00	0.00
S14	44.66	0.00	0.00	0.00	0.00	0.00	0.00	0.00	0.00	2.25	0.00	0.00	46.91	3.90	13.46
Annual summation													398.5		

3.2.11. Benzo(b)fluoranthene

The highest concentration of benzo(b)fluoranthene was 124.52 ppb, measured at site three in November 2011. The most common appearance of this compound was in February 2012 at eleven sites (S2, S3, S4, S5, S6, S7, S9, S10, S11, S12 and S14), where this compound was detected during this month. Site ten was the most contaminated site with benzo(b)fluoranthene out of the fourteen; the average at this site was 15.30 ppb over one year. The total amount of benzo(b)fluoranthene at all the sites over twelve months was 1003.74 ppb. Table 3.13 illustrates the concentrations of benzo(b)fluoranthene at the fourteen sites over twelve months.

Table 3.13. Concentrations of Benzo(b)fluoranthene/(ppb) in the studied fourteen sites

Site No.	**Nov. 2011**	**Dec. 2011**	**Jan. 2012**	**Feb. 2012**	**Mar. 2012**	**Apr. 2012**	**May 2012**	**Jun. 2012**	**Jul. 2012**	**Aug. 2012**	**Sept. 2012**	**Oct. 2012**	**Summation**	**Average**	**STDEV**
S1	14.14	0.00	0.00	0.00	0.00	44.87	0.00	0.00	0.00	0.00	0.00	0.00	59.01	4.91	13.21

S2	0.00	25.82	6.75	4.06	2.70	4.83	0.00	0.00	0.00	0.00	0.00	0.00	44.16	3.68	7.35
S3	124.52	1.46	0.00	30.90	0.00	0.00	2.52	0.00	0.00	0.00	0.00	2.05	161.45	13.45	35.99
S4	20.83	1.46	0.00	10.08	35.02	6.98	0.00	0.00	0.00	0.00	0.00	0.00	74.37	6.19	11.08
S5	0.00	4.12	6.61	21.64	31.66	0.00	16.95	0.00	0.00	0.00	0.00	0.00	80.98	6.74	10.65
S6	0.00	2.37	0.00	13.79	0.00	0.00	18.38	0.00	0.00	0.00	0.00	0.00	34.54	2.87	6.27
S7	0.00	0.00	0.00	10.82	1.00	6.92	0.00	0.00	0.00	0.00	0.00	0.00	18.74	1.56	3.52
S8	0.00	1.01	0.00	0.00	0.00	4.58	13.79	0.00	0.00	0.00	4.38	0.00	23.76	1.98	4.09
S9	8.95	6.24	0.00	23.95	4.06	0.00	10.85	0.00	0.00	0.00	0.00	0.00	54.05	4.50	7.27
S10	11.77	8.29	25.97	122.25	15.39	0.00	0.00	0.00	0.00	0.00	0.00	0.00	183.67	15.30	34.70
S11	0.00	0.00	0.00	19.10	0.00	0.00	23.95	0.00	0.00	0.00	0.00	0.00	43.05	3.58	8.40
S12	0.00	3.42	0.00	6.97	1.46	0.00	122.21	0.00	0.00	6.84	0.00	0.00	140.9	11.74	34.88
S13	24.79	0.00	29.48	0.00	0.00	0.00	0.00	0.00	0.00	0.00	0.00	0.00	54.27	4.52	10.53
S14	0.00	15.06	0.00	9.71	0.00	0.00	0.00	0.00	0.00	0.00	6.02	0.00	30.79	2.56	5.03
Annual summation													1003.74		

3.2.12. Benzo(k)fluoranthene

The highest concentration of benzo(k)fluoranthene was 194.79 ppb, measured at site thirteen in November 2011. The most common appearance of this compound was in February 2012 at thirteen sites (S1, S2, S3, S5, S6, S7, S8, S9, S10, S11, S12, S13 and S14), where this compound was detected during this month. Site thirteen was the most

contaminated site with benzo(k)fluoranthene out of the fourteen; the average at this site was 17.25 ppb over one year. The total amount of benzo(k)fluoranthene at all the sites over twelve months was 1059.75 ppb. Table 3.14 illustrates the concentrations of benzo(k)fluoranthene at the fourteen sites over twelve months.

Table 3.14. Concentrations of Benzo(k)fluoranthene/(ppb) in the studied fourteen sites

Site No.	Nov. 2011	Dec. 2011	Jan. 2012	Feb. 2012	Mar. 2012	Apr. 2012	May 2012	Jun. 2012	Jul. 2012	Aug. 2012	Sept. 2012	Oct. 2012	Summation	Average	STDEV
S1	16.83	0.00	0.00	1.34	5.67	1.05	5.14	0.00	1.51	0.00	0.00	0.00	31.54	2.62	5.57
S2	0.00	1.81	0.00	1.09	1.75	0.00	0.00	0.00	0.00	0.00	0.00	0.00	4.65	0.38	0.59
S3	0.00	0.00	0.00	5.06	11.61	2.67	0.00	0.00	0.00	0.00	0.00	1.29	20.63	1.71	3.48
S4	2.98	0.00	1.04	0.00	0.00	5.01	0.00	0.00	0.00	0.00	0.00	0.00	9.03	0.75	1.64
S5	43.85	0.00	32.53	20.34	0.00	10.48	0.00	0.00	0.00	0.00	0.00	0.97	108.17	9.01	15.16
S6	24.66	0.00	17.11	12.86	22.45	3.56	0.00	0.00	0.00	0.00	0.00	0.00	80.64	6.72	9.72
S7	0.00	0.00	0.00	4.22	0.00	0.00	0.00	0.00	0.00	0.00	0.00	0.00	4.22	0.35	1.20
S8	0.00	0.00	0.00	96.88	6.36	0.00	12.86	0.00	0.00	0.00	0.00	0.00	116.1	9.67	27.74
S9	0.00	0.00	34.27	53.94	0.00	8.38	4.19	0.00	0.00	0.00	0.00	0.00	100.78	8.39	17.37
S10	0.00	0.97	0.00	21.24	0.00	0.00	96.70	0.00	0.00	0.00	0.00	0.00	118.91	9.90	28.05
S11	0.00	0.00	0.00	17.46	0.00	6.22	53.94	0.00	0.00	0.00	0.00	0.00	77.62	6.46	15.81
S12	0.00	0.00	19.22	30.44	0.00	0.00	21.24	0.00	0.00	1.55	0.00	0.00	72.45	6.03	10.92
S13	194.79	0.00	0.00	4.49	7.75	0.00	0.00	0.00	0.00	0.00	0.00	0.00	207.03	17.25	55.96

S14	29.47	0.00	70.69	1.79	4.19	0.00	0.00	0.00	0.00	1.84	0.00	0.00	107.98	8.99	21.39
Annual summation													1059.75		

3.2.13. Benzo(a)pyrene

The highest concentration of benzo(a)pyrene was 601.81ppb, measured at site six in November 2011. The most common appearance of this compound was in May 2012 at eight sites (S3, S6, S7, S8, S10, S11, S12, and S13), where this compound was detected during this month. Site six was the most contaminated site with benzo(a)pyrene out of the fourteen; the average at this site was 50.17 ppb over one year. The total amount of benzo(a)pyrene at all the sites over twelve months was 871.69 ppb. Table 3.15 illustrates the concentrations of benzo(a)pyrene at the fourteen sites over twelve months.

Table 3.15. Concentrations of Benzo(a)pyrene/(ppb) in the studied fourteen sites

Site No.	Nov. 2011	Dec. 2011	Jan. 2012	Feb. 2012	Mar. 2012	Apr. 2012	May 2012	Jun. 2012	Jul. 2012	Aug. 2012	Sept. 2012	Oct. 2012	Summation	Average	STDEV
S1	0.00	0.00	0.00	0.00	0.00	0.00	0.00	0.00	0.00	0.00	0.00	0.00	0	0	0
S2	54.79	0.00	0.00	0.00	0.00	0.00	0.00	0.00	0.00	0.00	0.00	0.00	54.79	4.56	15.78
S3	65.47	0.00	0.00	0.00	0.00	0.00	2.97	0.00	0.00	0.00	0.00	0.00	68.44	5.70	18.83
S4	4.17	0.00	0.00	4.10	0.00	0.00	0.00	0.00	0.00	0.00	0.00	0.00	8.27	0.68	1.58
S5	0.00	0.00	0.00	0.00	1.04	0.00	0.00	0.00	0.00	0.00	0.00	0.00	1.04	0.08	0.21
S6	601.81	0.00	0.00	0.00	0.00	0.00	0.24	0.00	0.00	0.00	0.00	0.00	602.05	50.17	173.72
S7	26.28	0.00	0.00	0.00	0.00	1.09	1.01	0.00	0.00	0.00	0.00	1.01	29.39	2.44	8.44
S8	0.00	0.00	2.46	0.00	0.00	0.00	1.60	0.00	0.00	0.00	0.00	0.00	4.06	0.33	0.99

S9	27.76	0.00	0.00	0.00	0.00	0.00	0.00	0.00	0.00	0.00	0.00	0.00	27.76	2.31	8.01
S10	0.00	0.00	0.00	0.00	3.37	0.00	4.36	0.00	1.22	1.25	0.00	0.00	10.2	0.85	1.98
S11	0.00	0.00	0.00	0.00	0.00	0.00	4.26	0.00	0.00	0.00	0.00	0.00	4.26	0.35	1.22
S12	0.00	0.00	1.63	0.00	13.25	0.00	1.44	0.00	0.00	0.00	0.00	0.00	16.32	1.36	4.08
S13	0.00	0.00	0.00	0.00	3.46	0.00	32.13	0.00	0.00	0.00	1.21	0.00	36.8	3.06	9.51
S14	0.00	5.98	0.00	0.00	2.33	0.00	0.00	0.00	0.00	0.00	0.00	0.00	8.31	0.69	2.29
Annual summation													871.69		

3.2.14. Dibenzo(a,h)anthracene

The highest concentration of dibenzo(a,h)anthracene was 292.04ppb, measured at site one in November 2011. The most common appearance of this compound were in December 2011, May 2012 and September 2011 at five sites, where this compound was detected during this month. Site one was the most contaminated site with dibenzo(a,h)anthracene out of the fourteen; the average at this site was 24.34 ppb over one year. The total amount of dibenzo(a,h)anthracene at all the sites over twelve months was 803.63 ppb. Table 3.16 illustrates the concentrations of dibenzo(a,h)anthracene at the fourteen sites over twelve months.

Table 3.16. Concentrations of Dibenzo(a,h)anthracene/(ppb) in the studied fourteen sites

Site No.	**Nov. 2011**	**Dec. 2011**	**Jan. 2012**	**Feb. 2012**	**Mar. 2012**	**Apr. 2012**	**May 2012**	**Jun. 2012**	**Jul. 2012**	**Aug. 2012**	**Sept. 2012**	**Oct. 2012**	**Summation**	**Average**	**STDEV**
S1	292.04	0.00	0.00	0.00	0.00	0.00	0.00	0.00	0.00	0.00	0.00	0.00	292.04	24.34	84.30

S2	16.22	0.00	0.00	9.78	0.00	0.00	0.00	0.00	1.39	1.14	0.00	0.00	28.53	2.37	5.72
S3	0.00	5.04	0.00	0.00	0.00	33.39	4.16	0.00	0.00	0.00	1.19	1.04	44.82	3.73	9.49
S4	0.00	5.03	0.00	0.00	0.00	0.00	6.27	1.48	1.83	0.00	1.21	0.00	15.82	1.31	2.88
S5	0.00	0.00	7.82	0.00	0.00	3.06	30.73	0.00	0.00	0.00	0.00	1.60	43.21	3.60	9.15
S6	159.96	3.65	0.00	1.63	0.00	0.00	18.09	0.00	0.00	0.00	0.00	0.00	183.33	15.27	45.86
S7	0.00	0.00	5.15	0.00	1.55	0.00	0.00	0.00	0.00	0.00	1.69	0.00	8.39	0.69	1.77
S8	0.00	3.75	1.59	0.00	0.00	0.00	0.00	0.00	0.00	0.00	0.00	0.00	5.34	0.44	1.09
S9	0.00	0.00	73.45	3.26	0.00	0.00	0.00	0.00	0.00	0.00	1.39	0.00	78.1	6.50	21.11
S10	21.93	0.00	0.00	0.00	0.00	0.00	0.00	0.00	0.00	0.00	0.00	0.00	21.93	1.82	6.28
S11	0.00	0.00	0.00	0.00	0.00	0.00	0.00	0.42	0.00	0.00	0.00	0.00	0.42	0.03	0.08
S12	0.00	0.00	0.00	0.00	0.00	0.00	0.00	0.00	0.00	0.00	0.00	0.00	0.00	0.00	0.00
S13	0.00	7.28	0.00	0.00	0.00	0.00	72.44	0.00	0.00	0.00	1.83	0.00	81.55	6.79	21.09
S14	0.00	0.00	0.00	0.00	0.00	0.00	0.00	0.00	0.00	0.00	0.00	0.00	0.00	0.00	0.00
Annual summation													803.63		

3.2.15. Benzo(g,h,i)Pyrelene

The highest concentration of Benzo(g,h,i)Pyrelene was 270.56 ppb, measured at site one in November 2011. The most common appearance of this compound was in February 2012 at nine sites (S2, S3, S4, S5, S8, S10, S11, S12 and S13), where this compound was detected during this month. Site one was the most contaminated site with Benzo(g,h,i)Pyrelene out of the fourteen; the average at this site was 25.02 ppb over one year. The total amount of Benzo(g,h,i)Pyrelene at all the sites over twelve months was 850.87 ppb. Table 3.17 illustrates the concentrations of Benzo(g,h,i)Pyrelene at the fourteen sites over twelve months.

Table 3.17. Concentrations of Benzo(g,h,i)Pyrelene/(ppb) in the studied fourteen sites

Site No.	Nov. 2011	Dec. 2011	Jan. 2012	Feb. 2012	Mar. 2012	Apr. 2012	May 2012	Jun. 2012	Jul. 2012	Aug. 2012	Sept. 2012	Oct. 2012	Summation	Average	STDEV
S1	270.56	0.00	24.56	0.00	3.83	1.39	0.00	0.00	0.00	0.00	0.00	0.00	300.34	25.02	77.63
S2	39.29	5.04	1.76	2.73	5.21	12.69	0.00	0.00	0.00	0.00	0.00	0.00	66.72	5.56	11.36
S3	0.00	3.87	1.85	1.66	0.00	8.58	0.00	0.00	1.74	0.00	0.00	0.00	17.7	1.47	3.08
S4	14.87	3.86	0.00	3.99	4.96	0.00	8.92	0.97	0.00	0.00	0.00	0.00	37.57	3.13	4.65
S5	0.00	0.00	0.00	11.64	5.81	0.00	0.00	0.00	0.00	0.00	0.00	0.95	18.4	1.53	3.59
S6	102.21	0.00	32.52	0.00	0.00	16.51	19.11	0.00	0.00	1.24	0.00	0.00	171.59	14.29	29.68
S7	0.00	4.06	11.98	0.00	0.00	10.43	0.00	0.00	0.00	0.00	148	0.00	27.95	2.32	4.52
S8	0.00	1.55	0.00	2.82	0.00	0.00	0.00	0.00	0.00	1.35	0.99	0.00	6.71	0.55	1.11
S9	0.00	0.00	0.00	0.00	55.87	4.87	0.00	0.00	0.00	0.00	1.32	0.00	62.06	5.17	16.05
S10	0.00	0.00	0.00	6.35	0.00	5.71	3.84	0.00	0.00	0.00	0.00	0.00	15.9	1.32	2.45
S11	0.00	0.00	2.08	24.22	0.00	4.99	0.00	0.00	0.00	0.00	0.00	0.00	31.29	2.60	6.96
S12	0.00	0.00	9.07	0.96	11.51	0.00	6.35	0.00	0.00	1.37	0.00	0.00	29.26	2.43	4.11
S13	0.00	0.00	0.00	40.49	0.00	0.00	0.00	0.00	0.00	0.00	0.00	0.00	40.49	3.37	11.68
S14	0.00	0.00	18.86	0.00	6.03	0.00	0.00	0.00	0.00	0.00	0.00	0.00	24.89	2.07	5.56
Annual summation													850.87		

3.2.16. Indeno (1,2,3-cd)Pyrene

The highest concentration of Indeno (1,2,3-cd)Pyrene was 141.01 ppb, measured at site one in November 2011. The most common appearance of this compound was in November 2011 at six sites (S1, S2, S4, S5, S6 and S13), where this compound detected during this month. Site one was the most contaminated site with Indeno (1,2,3-cd)Pyrene out of the fourteen, the average at this site was 11.88 ppb over one year. The total amount of Indeno (1,2,3-cd)Pyrene at all sites over twelve months was 738.20 ppb. Table 3.18 illustrates the concentration of Indeno (1,2,3-cd)Pyrene at the fourteen sites over twelve months.

Table3.18. Concentrations of Indeno (1,2,3-cd)Pyrene/(ppb) in the studied fourteen sites

Site No.	Nov. 2011	Dec. 2011	Jan. 2012	Feb. 2012	Mar. 2012	Apr. 2012	May 2012	Jun. 2012	Jul. 2012	Aug. 2012	Sept. 2012	Oct. 2012	Summation	Average	STDEV
S1	141.01	0.00	0.00	1.61	0.00	0.00	0.00	0.00	0.00	0.00	0.00	0.00	142.62	11.88	40.66
S2	104.95	0.00	0.00	0.00	0.00	0.00	0.00	0.00	0.00	0.95	0.00	0.00	105.90	8.82	30.27
S3	0.00	0.00	0.00	0.00	0.00	0.00	0.00	0.00	1.71	0.00	1.13	1.55	4.39	0.36	0.74
S4	13.24	0.00	0.00	0.00	0.00	0.00	0.00	0.00	2.75	0.00	0.00	0.00	15.99	1.33	3.82
S5	2.87	1.31	0.00	0.00	1.66	0.00	0.00	1.86	0.00	0.00	0.00	1.07	8.77	0.73	1.41
S6	86.41	0.00	0.00	0.00	0.00	0.00	0.00	1.52	0.00	0.00	0.00	0.00	87.93	7.32	24.90
S7	0.00	0.00	66.32	0.00	2.99	3.46	0.00	0.00	0.00	0.00	0.00	0.00	72.77	6.06	19.00
S8	0.00	0.00	0.00	0.00	0.00	6.37	0.00	0.00	0.00	2.65	2.57	0.00	11.59	0.96	2.45
S9	0.00	0.00	0.00	0.00	0.00	0.00	7.11	3.12	0.00	0.00	0.00	1.82	12.05	1.00	2.40
S10	0.00	0.00	0.00	0.00	0.00	0.00	0.00	0.00	0.00	0.76	0.00	0.00	0.76	0.06	0.14
S11	0.00	0.00	0.00	0.00	0.00	0.00	0.00	0.00	0.00	0.00	0.00	0.00	0.00	0.00	0.00

S12	0.00	0.00	4.51	32.16	0.00	0.00	0.00	0.00	0.00	21.31	0.00	0.00	57.98	4.83	10.53
S13	17.00	0.00	0.00	32.98	85.54	1.47	0.00	0.00	0.00	0.00	0.00	0.00	136.99	11.41	25.57
S14	0.00	0.00	0.00	5.85	74.56	0.00	0.00	0.00	0.00	0.00	0.00	0.00	80.41	6.70	21.43
Annual summation													738.20		

3.3. Treatment of Anthracene

3.3.1. Direct photolysis

A photolysis reaction was carried out in the absence of a catalyst. Table 3.19 shows the results of the photolysis for 100 mL of aqueous solution of anthracene. Figure 3.1 shows the results of the photolysis of the anthracene with the presence of UV (A) light and the absence of a catalyst at 298.15 K with pH value 6.8. It was found that the anthracene was degraded after 360 minutes of irradiation. The final concentration of anthracene after exposure to the light was 2.9 ppm.

Table 3.19. Concentrations of Anthracene after exposure to irradiation

Irradiation time/min	Concentration of Anthracene / ppm
0	25
30	14.6
60	10.5
90	8.7
120	7.3
180	5.5
210	4.3
300	3.5
360	2.9

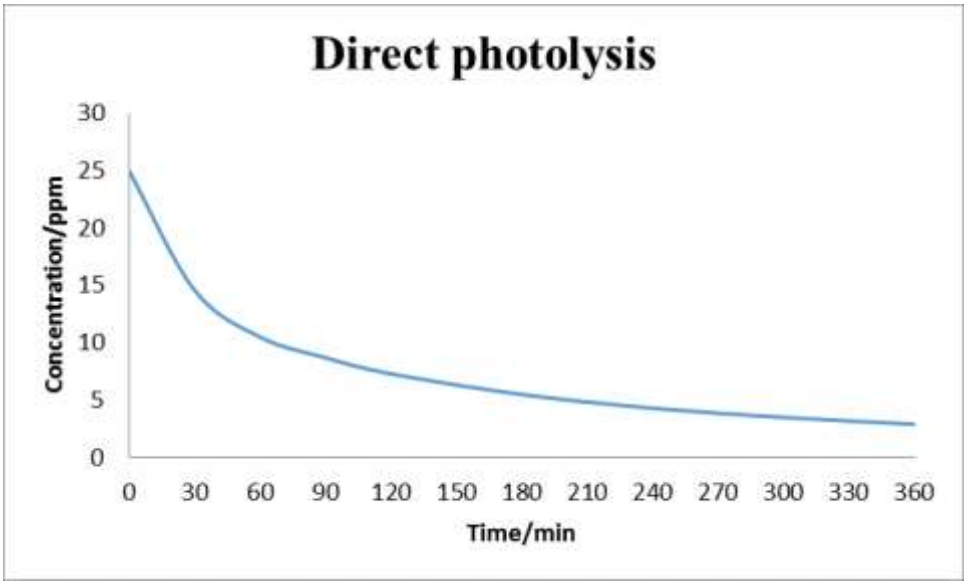

Figure 3.1. Direct photolysis of Anthracene

3.3.2. Treatment of Anthracene by Advanced Oxidation Processes

3.3.2.1. Treatment of Anthracene by photocatalysis using UV +TiO_2

These experiments were carried out in the presence of catalysts (titanium dioxide) and UV-A light.

3.3.2.1.1. Comparison between Degussa P25 and Hombikat UV100 Titanium dioxide

Two types of titanium dioxide (Degussa P25 and Hombikat UV100) were used as catalyst; firstly to compare between them, and then to select the most suitable to use for anthracene degradation in the same conditions. The results are listed in Table 3.20. Figure 3.2 shows the comparative study of the photocatalysts Degussa P25 and Hombikat UV100 with anthracene. From this Figure it is evident that Degussa P25 gives the highest degradation rate compared to Hombikat UV100 after 180 minutes under the following experimental conditions: an initial anthracene concentration of 25 ppm, solution pH equal to 6.8, light intensity equal to 2.5 $mW.cm^{-2}$, a TiO_2 concentration 175 mg/100 mL, and a temperature equal to 298.15 K.

Table 3.20. Concentrations of Anthracene residual after exposure to irradiation with two types of titanium dioxide

Irradiation time/min	Concentration of Anthracene / ppm	
	TiO_2- P25	TiO_2- UV100
0	24.890	24.890

30	8.258	9.107
60	1.471	3.805
90	0.169	0.749
120	0.065	0.447
180	0.009	0.069

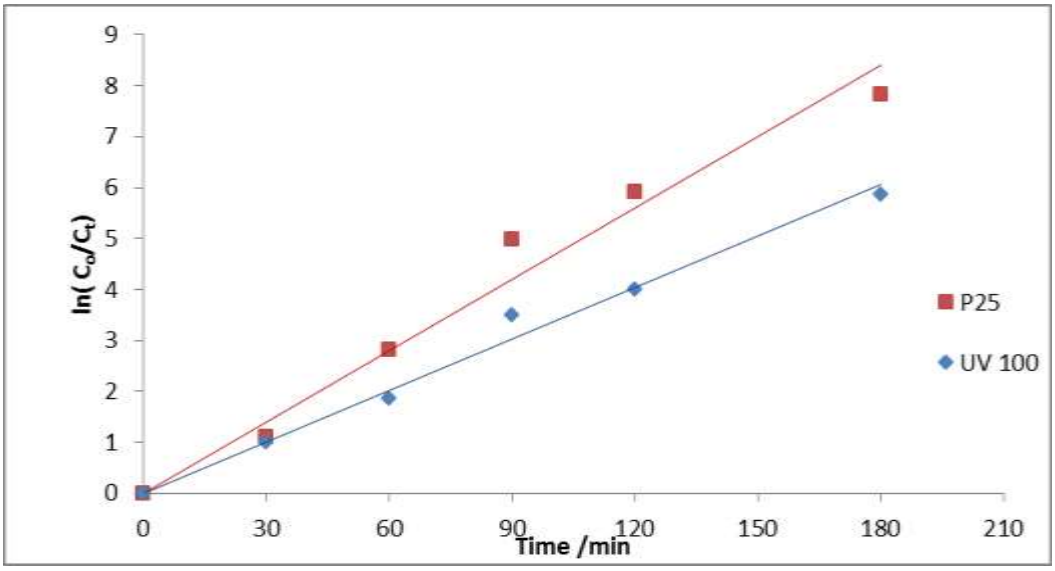

Figure 3.2. Comparison between the efficiency of Degussa P25 and Hombikat UV100 for the degradation of anthracene

3.3.2.1.2. Effect of Anthracene concentration

In these experiments a series of different concentrations of anthracene within a range of 1, 5, 10 and 25 ppm were used. These results are shown in Figure 3.3 with the primarily experimental condition's light intensity equal to 2.5 $mWcm^{-2}$, solution pH equal to 6.8, a temperature equal to 298.15K and TiO_2 (P25) concentration of 175 mg/100ml. The results listed in table 3.21 are showing the concentrations for every time of irradiation. The results shown in figure 3.4, illustrate the relationship between the initial anthracene concentration and the rate constant of the reaction. It is found that the rate constant of the reaction rises with increases in the initial anthracene concentration.

Table 3.21. Concentrations of Anthracene after exposure to irradiation at different initial concentrations by TiO_2 Degussa

Irradiation time/min	Concentration of Anthracene / ppm			
	1	5	10	25
0	0.896	4.878	9.921	24.910
30	0.728	3.271	5.409	8.263
60	0.503	2.174	1.627	1.473
90	0.406	1.796	1.290	0.168
120	0.443	1.320	0.727	0.065
180	0.327	0.787	0.275	0.020

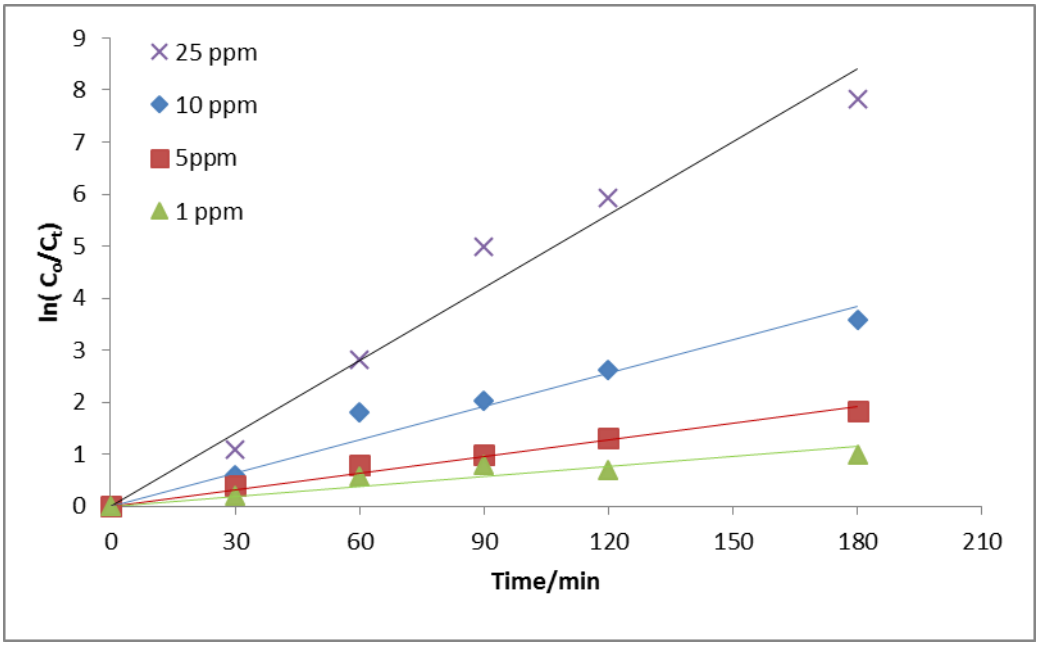

Figure 3.3. The changes of $\ln(C_o/C_t)$ with irradiation times on different Anthracene concentrations by TiO_2 (Degussa P25)

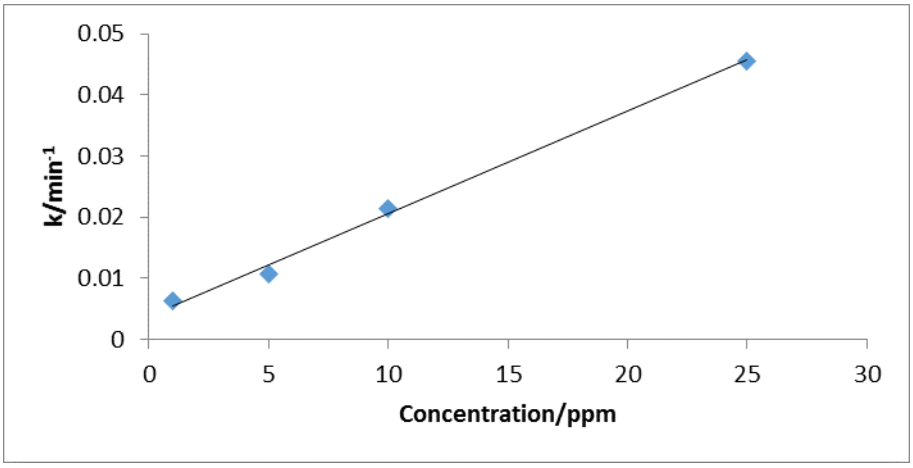

Figure 3.4. Effects of initial Anthracene concentrations at a rate constant by TiO_2 (Degussa P25)

3.3.2.1.3. Effects of Light Intensity

The results listed in Table 3.22. Figure 3.5 shows the effect of light intensity on the photocatalytic degradation of anthracene using TiO_2 Degussa P25. In these experiments different light intensities were used within the range (1-2.5) $mWcm^{-2}$. Under these predetermined experimental conditions: the initial anthracene concentration was 25 ppm, the solution pH was equal to 6.8, the TiO_2 (Degussa P25) concentration was 175 mg/100ml and temperature was equal to 298.15K. Figure 3.6, shows the relationship between the light intensity for TiO_2 (Degussa P25) and the rate constant of the reaction. It is found that the rate constant of the reaction rises with the increase in light intensity, and the highest value of light intensity was equal to 2.5 mW. cm^{-2}.

Table 3.22. Concentrations of Anthracene after exposure to irradiation with different light intensities constant by TiO_2 (Degussa P25)

Irradiation time/min	Concentration of Anthracene / ppm			
	1.0 mW/cm^2	1.5 mW/cm^2	2.0 mW/cm^2	2.5 mW/cm^2
0	24.780	24.780	24.780	24.780
30	16.367	15.966	8.224	6.502
60	13.438	7.738	2.669	1.259
90	7.886	3.111	0.458	0.248

120	4.944	1.866	0.178	0.028
180	3.261	0.278	0.027	0.015

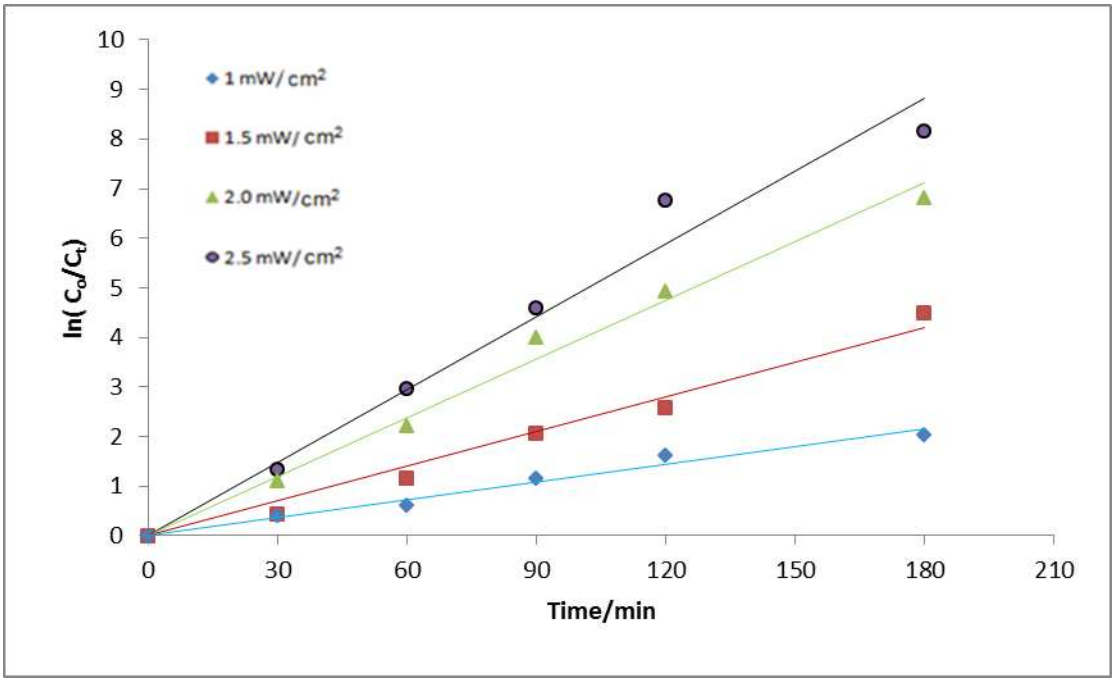

Figure 3.5. The change of ln (C_o/C_t) irradiation times at different light intensities by TiO_2 (Degussa P25)

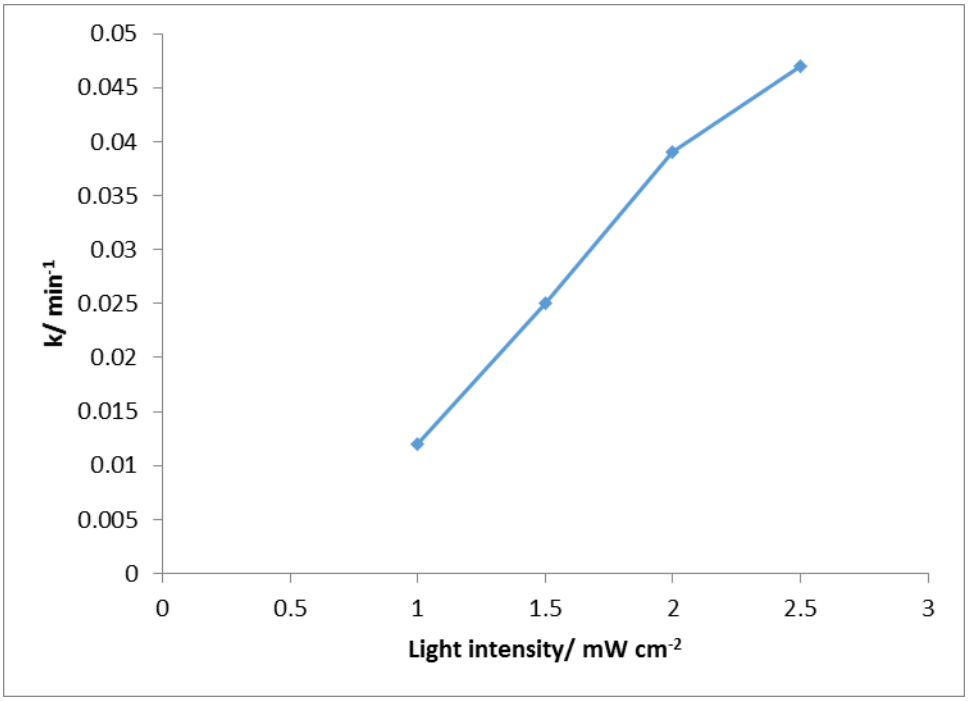

Figure 3.6. The effect of initial light intensity on the rate constant by TiO_2 (Degussa P25)

3.3.2.1.4. Effects of pH

The results listed in Table 3.23 show the effect of pH on the photocatalytic degradation of anthracene by using TiO_2 Degussa P25 in the same conditions. pH plays an important role in the production of hydroxyl radicals. In these experiments TiO_2 Degussa P25 was used as a photocatalyst to degrade the anthracene in the aqueous suspensions under these predetermined experimental conditions: the light intensity was equal to 2.5mWcm^{-2}, the temperature was equal to 298.15K, the TiO_2 (Degussa P25) concentration was 175 mg/100ml and the initial anthracene concentration was 25 ppm. A pH range between 3 to 11 was used, as shown in Figure 3.7. which shows a pseudo first order reaction. The results shown in Figure 3.8 demonstrate the rate constant of the reaction rises with an increase in the solution pH up to the maximum level of pH 6.8, and then decreased. The degradation rate of anthracene rises with an increase in pH; it was found that the ideal pH of TiO_2 (Degussa P25) was at pH 6.8.

Table 3.23. Concentrations of Anthracene after exposure to irradiation in different pH values by TiO_2 (Degussa P25)

Irradiation time/min	Concentration of Anthracene / ppm				
	pH 3	pH 5	pH 6.8	pH 9	pH 11
0	24.626	24.626	24.626	24.626	24.626
30	9.205	12.077	8.173	10.197	15.990
60	3.417	5.430	1.467	9.706	11.693
90	1.775	3.585	0.166	6.409	3.574
120	0.788	1.946	0.065	3.702	6.000
180	0.393	1.157	0.003	2.674	4.562

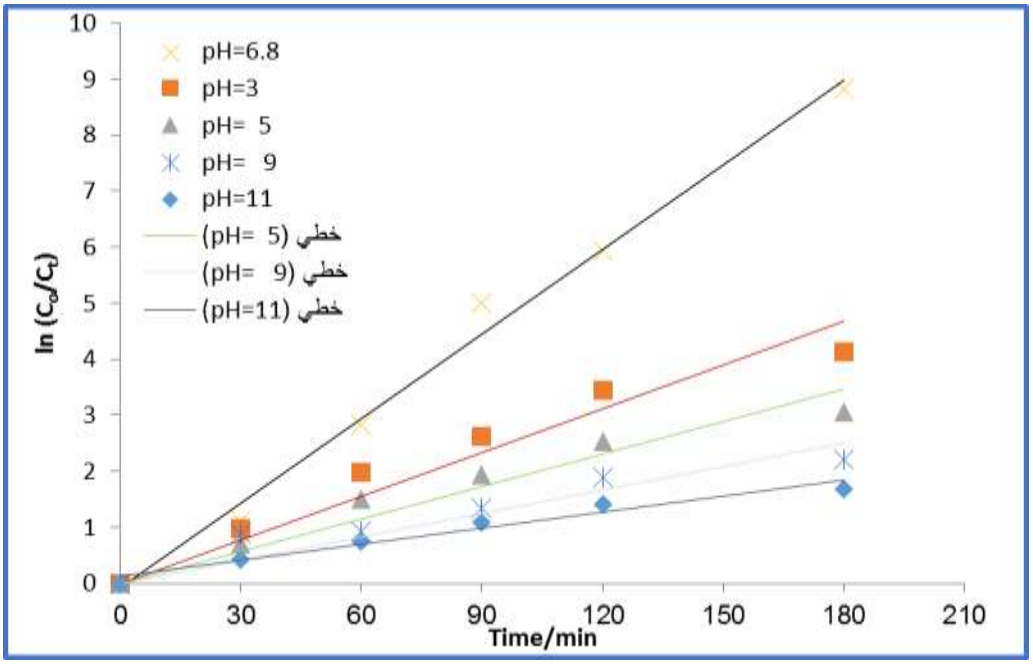

Figure 3.7. The change of $\ln(C_o/C_t)$ according to irradiation time at different values of pH by TiO_2 (Degussa P25)

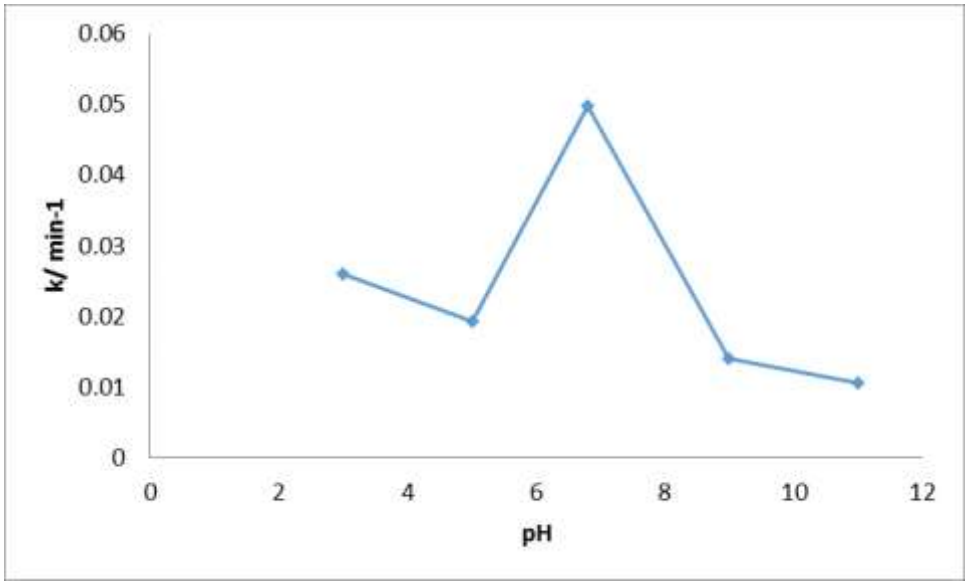

Figure 3.8. The effect of the initial pH of a solution on the rate by TiO_2 (Degussa P25)

3.3.2.1.5. Effects of temperature

The results are listed in Table 3.24. These results show that higher temperatures will lead to faster degradation rates of anthracene under these experimental conditions: a light intensity equal to 2.5 mW cm^{-2}, an initial anthracene concentration of 25 ppm, a solution pH equal to 6.8 and a TiO_2 (Degussa P25) concentration of 175 mg/100ml. In these experiments different temperatures were used for TiO_2 Degussa P25 within the range of 278.15-308.15 K as shown in figure 3.9. It was found that the degradation rate of anthracene rises with increases in temperature. Figure 3.10 indicates the Arrhenius relationship, which gives an activation energy of 12.76 $kJ.mol^{-1}$ for the photocatalytic degradation efficiency of anthracene by using TiO_2 (Degussa P25).

Table 3.24. Concentrations of Anthracene after exposure to irradiation at different temperatures by TiO_2 (Degussa P25)

Irradiation time/min	Concentration of Anthracene / ppm		
	278.15K	288.15K	308.15K
0	24.890	24.890	24.890
30	16.806	14.321	7.496
60	10.788	7.604	3.890
90	8.497	6.156	1.839
120	5.532	4.218	1.185
180	2.719	1.588	0.381

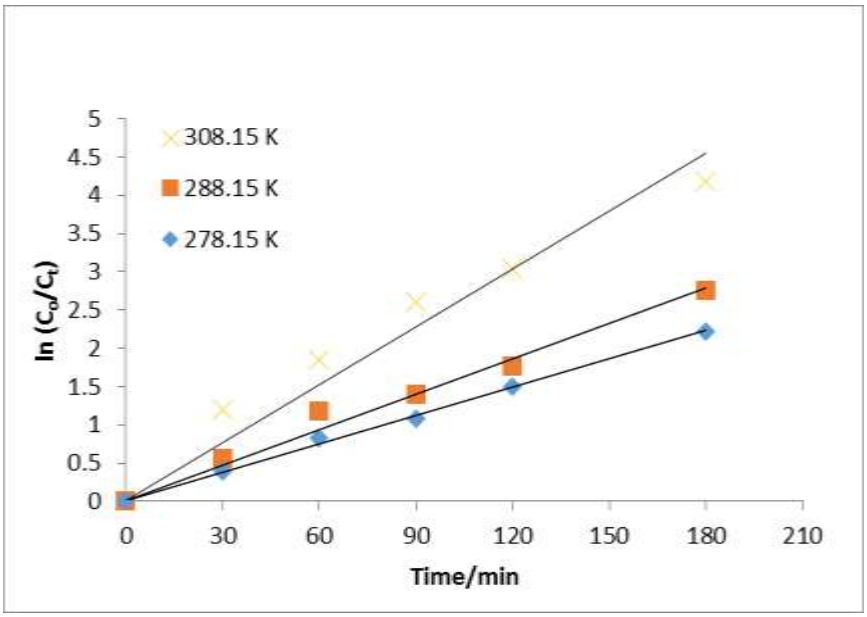

Figure 3.9. The changes of $\ln(C_o/C_t)$ with irradiation times at different temperatures of TiO_2 (Degussa P25)

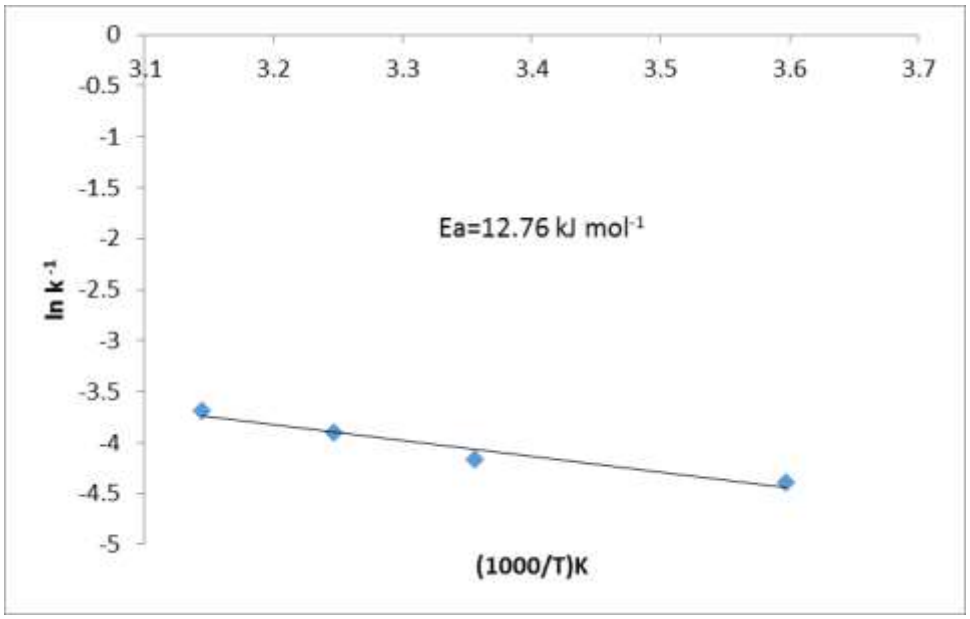

Figure 3.10. Arrhenius plot for photocatalytic degradation of anthracene

on TiO_2(Degussa P25) at (278.15-308.15) K

3.3.2.2. Treatment of Anthracene using UV, TiO_2 and H_2O_2

Hydrogen peroxide (H_2O_2) plays an important role in the production of hydroxyl radicals. In these experiments TiO_2 (DegussaP25) was used as a photocatalyst to degrade the anthracene in the aqueous suspensions under these predetermined experimental conditions: a light intensity equal to 2.5 mW cm^{-2}, a solution pH equal to 6.8, a temperature equal to 298.15K, a TiO_2 (DegussaP25) concentration of 175 (mg/100ml) and an initial anthracene concentration of 25 ppm. The results are listed in Table 3.24. These results show the effects of using different concentrations of hydrogen peroxide (H_2O_2) within a range of (5-100) mmol/ L. Also, Figure 3.11. shows a pseudo first order reaction. Figure 3.12 shows that the rate constant of the reaction decreased with increases in the hydrogen peroxide concentration.

Table 3.25. Concentrations of Anthracene after exposure to irradiation at different concentrations of H_2O_2

Irradiation time/min	Concentration of Anthracene / ppm				
	Without H_2O_2	5 mmol. of H_2O_2	10mmol. of H_2O_2	50 mmol. of H_2O_2	100 mmol. of H_2O_2
0	24.920	24.920	24.920	24.920	24.920
30	8.268	13.076	16.525	18.150	18.979
60	1.472	7.169	9.319	11.650	13.528
90	0.168	2.499	5.299	7.111	9.533
120	0.065	1.043	3.107	4.820	6.697
180	0.003	0.329	1.681	2.758	5.274

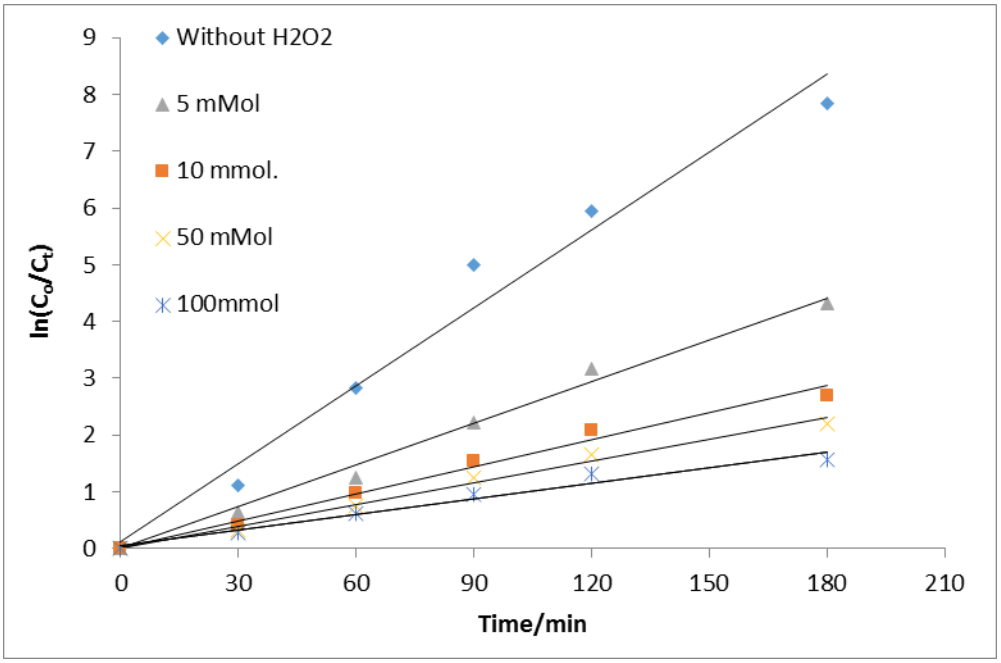

Figure 3.11. The changes of $\ln(C_o/C_t)$ with irradiation times at different concentrations of H_2O_2 by TiO_2 (DegussaP25)

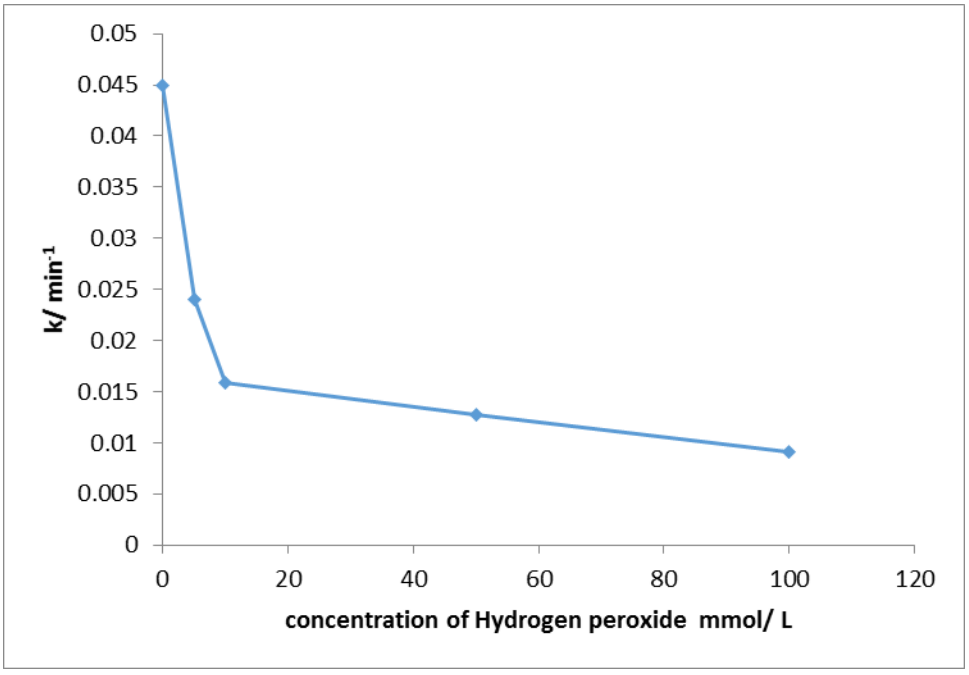

Figure 3.12. The effect of the addition of $[H_2O_2]$ on the rate constant by TiO_2 (DegussaP25)

3.2.2.3. Treatment of Anthracene by chemical Fenton method

Several parameters were studied using this method to get the optimum conditions for the degradation of anthracene. These conditions are as follows:

1- Effects of the initial concentration of anthracene.
2- Effects of $FeSO_4$ mass.
3- Effects of H_2O_2.
4- Effects of pH.
5- Effect of temperature.

3.2.2.3.1. Effects of the initial concentration of Anthracene

In these experiments two concentrations for anthracene within the range of (4 and 16) ppm were used. These results are listed in Table 3.26. The results shown in Figure 3.13 demonstrate that the changes of ln (C_o/C_t) with reaction times at Anthracene concentrations 4 and 16ppm. The reaction was achieved in the following conditions: room temperature, at pH=5, $FeSo_4$ mass= 80 mg and 100 mmol of hydrogen peroxide.

Table 3.26. Concentrations of Anthracene after exposure to chemical Fenton with different initial concentrations

Irradiation time/min	Concentration of Anthracene / ppm	
	4.000	16.000
0	3.930	15.940
15	3.126	-
30	2.740	-
45	2.653	1.606
60	2.550	1.224
75	2.411	0.901
90	2.386	0.885

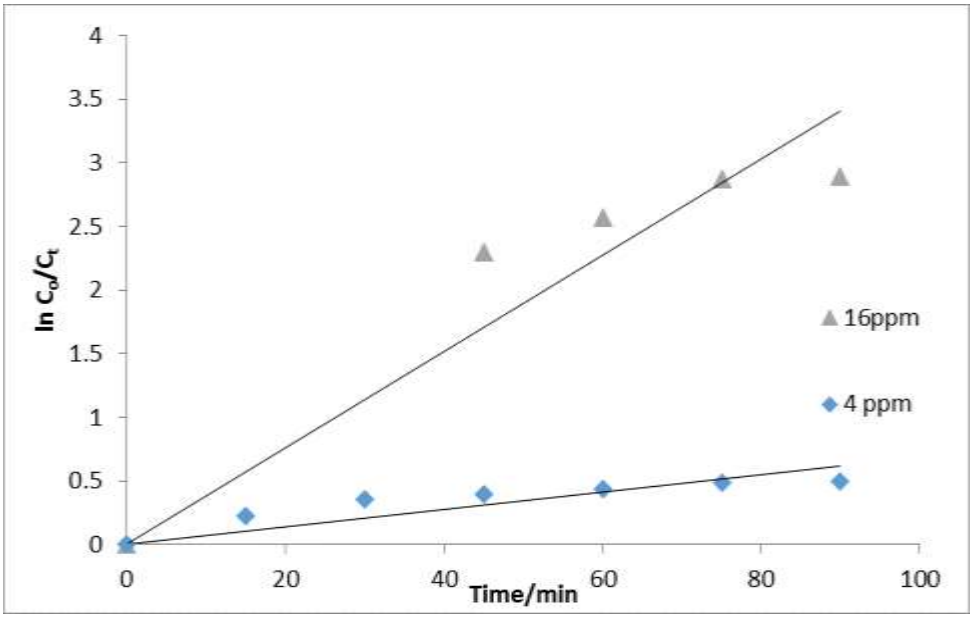

Figure 3.13. The changes of ln(C_0/C_t) with reaction times at different Anthracene concentrations

3.2.2.3.2. Effects of $FeSO_4$ mass

These experiments were carried out by using different masses of $FeSO_4$ with anthracene. The results are shown in Figure 3.14. Other factors were kept constant for all these experiments (an initial anthracene concentration of 16 ppm), pH=5, at room temperature and 100 mmol of hydrogen peroxide. From these experiments, it was found that 120 mg of $FeSO_4$ /100ml of anthracene yielded the optimum activity. The reaction rate constants expressed in min^{-1} were calculated from the slopes of such linear reaction plots. These reaction results are listed in table 3.27. Figure 3.15, showing that a $FeSO_4$ mass of 120 mg is sufficient to achieve the maximum reaction rate.

Table 3.27. Concentrations of Anthracene after treatment by chemical Fenton with different amounts of $FeSO_4$

Irradiation time/min	Concentration of Anthracene / ppm			
	30mg of	60mg of	90mg of	120mg of

	$FeSO_4$	$FeSO_4$	$FeSO_4$	$FeSO_4$
0	15.110	15.110	15.110	15.110
15	-	6.314	1.656	1.015
30	3.103	2.299	-	0.694
45	3.033	1.868	-	0.597
60	2.993	-	0.780	0.451

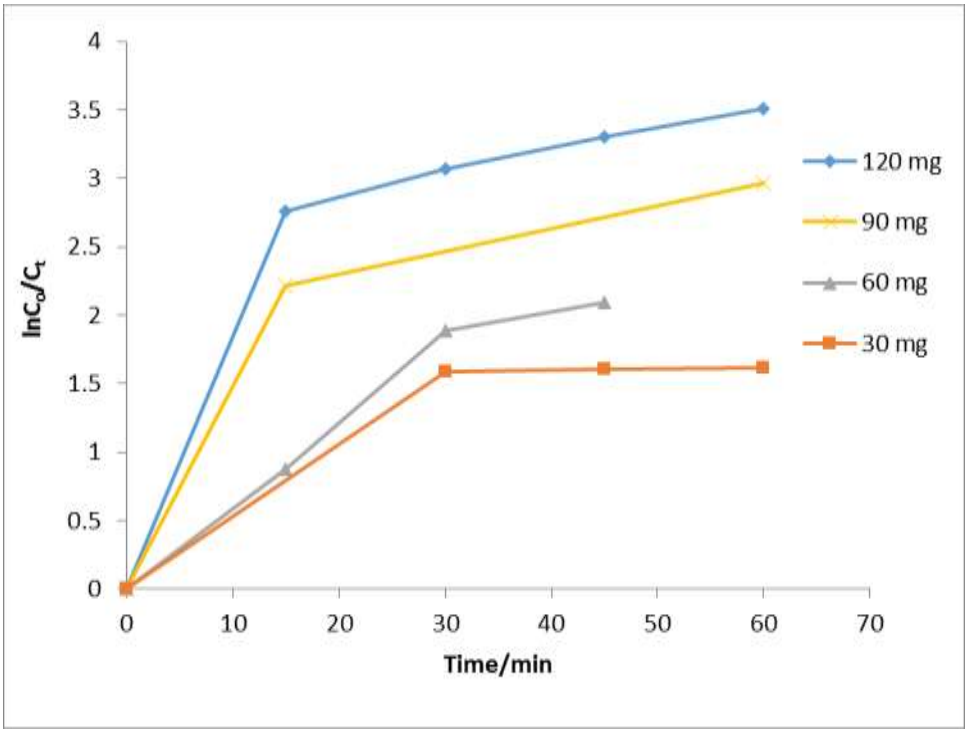

Figure 3.14. The changes of $\ln(C_o / C_t)$ with reaction times at different masses of $FeSO_4$

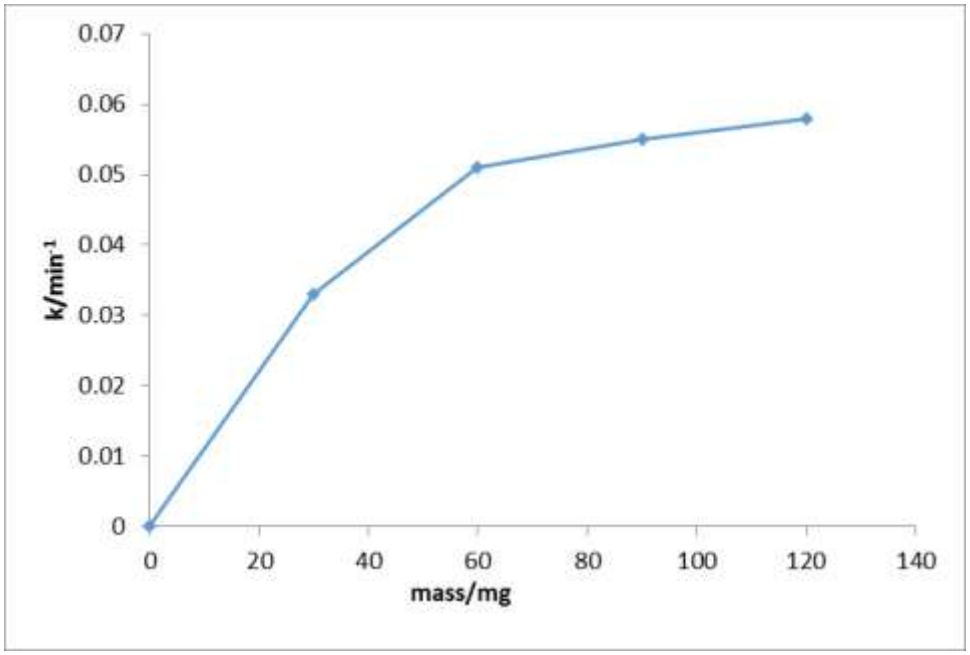

Figure 3.15. The effect of $FeSO_4$ masses on the rate constant

3.2.2.3.3. Effects of H_2O_2

Hydrogen peroxide (H_2O_2) plays an important role in the production of hydroxyl radicals. In these experiments, $FeSO_4$ was used to degrade the anthracene in the aqueous suspensions under these predetermined experimental conditions: $FeSO_4$ concentration of 120 (mg/100ml), pH=5 at room temperature and an initial anthracene concentration of 16 ppm. The effects of using different concentrations of hydrogen peroxide (H_2O_2) within the range of (50-200) mmol L^{-1} are shown in Figure 3.16. These reaction results are listed in table 3.28.

Figure 3.17 shows that the rate constant of reaction increases with increase of the hydrogen peroxide concentration.

Table 3.28. Concentrations of Anthracene after treatment by chemical Fenton with different concentrations of H_2O_2

Irradiation time/min	Concentration of Anthracene / ppm				
	Without H_2O_2	50 mmol. Of H_2O_2	100mmol. Of H_2O_2	150 mmol. Of H_2O_2	200 mmol. Of H_2O_2
0	15.31	15.31	15.31	15.31	15.31
15	15.31	-	-	0.574	0.385
30	15.31	3.101	1.040	0.570	0.347
45	15.31	3.032	0.846	-	-
60	15.31	2.993	-	0.504	-
75	15.31	2.569	0.748	0.441	0.154

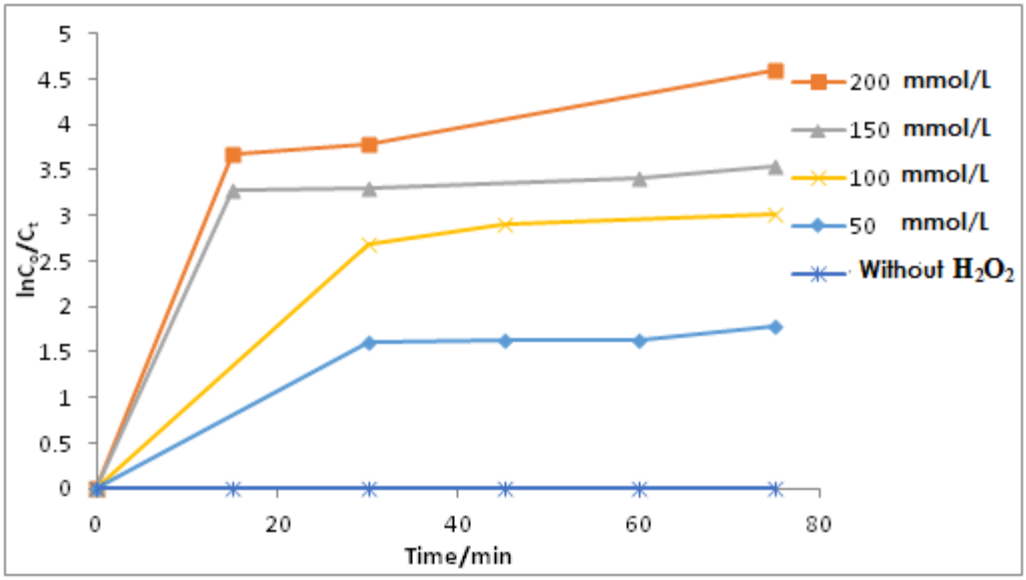

Figure 3.16. The changes of $\ln(C_o/C_t)$ with reaction times at different concentrations of H_2O_2 mmol./L

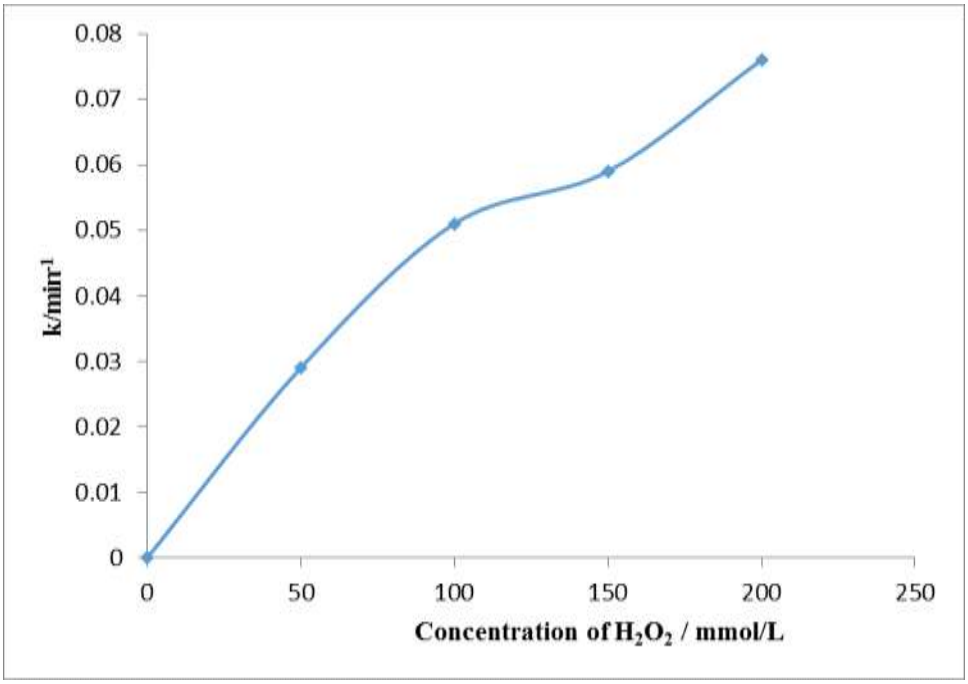

Figure 3.17. The effects of the addition of H_2O_2 on the rate constant by chemical Fenton

3.2.2.3.4. Effects of pH

pH plays an important role in the production of hydroxyl radicals. In these experiments $FeSO_4$ was used to degrade the anthracene in the aqueous suspensions under these predetermined experimental conditions: 200 mmol of hydrogen peroxide, at room temperature, $FeSO_4$ concentration of 120 mg/100ml and an initial anthracene concentration of 16 ppm using a pH range of between (2-5) as shown in Figure 3.18. The results are listed in Table 3.29. Figure 3.19 show the rate constant of the reaction rose with increases in the solution pH up to a maximum level of pH 4, and then decreased. The degradation rate of anthracene increases with rises in pH values

Table 3.29. Concentrations of Anthracene after treatment by chemical Fenton with different pH values

Irradiation	Concentration of Anthracene / ppm

time/min	pH 2	pH 3	pH 4	pH 5
0	15.930	15.930	15.930	15.930
15	7.247	12.543	0.916	9.202
30	5.750	9.202	0.339	6.009
45	3.570	7.280	0.104	4.217

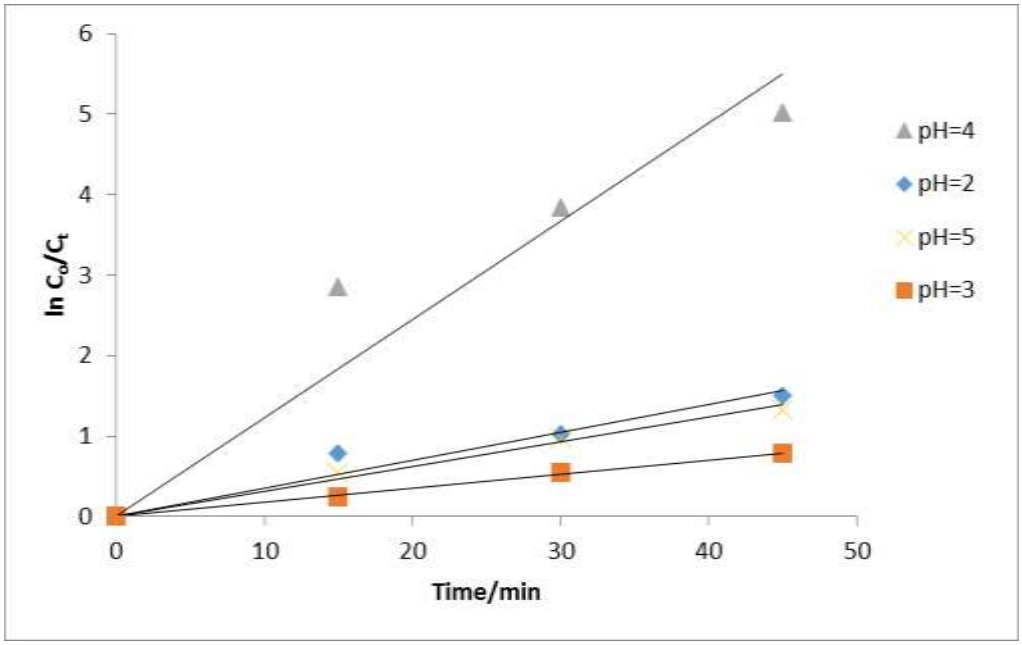

Figure 3.18. The changes of ln(C_0/C_t) with reaction times at different pH values

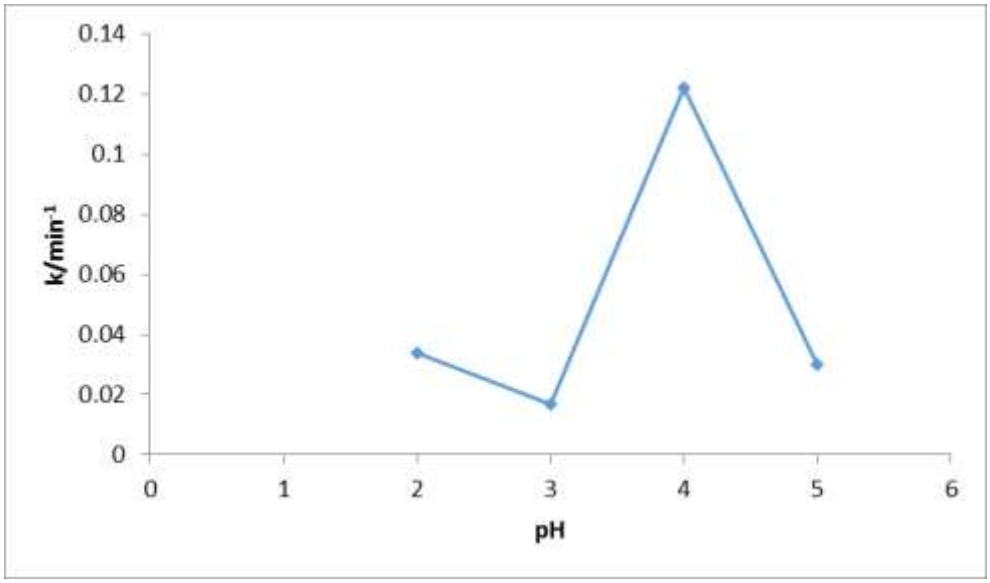

Figure 3.19. The effect of the initial pH of the solution on the rate constant

3.2.2.3.5. Effects of temperature.

The results listed in Table 3.30 show that higher temperatures will lead to faster degradation rates of anthracene under these experimental conditions: an initial anthracene concentration of 16 ppm, solution pH equal to 4, and a $FeSO_4$ concentration of 120 mg/100ml, 200 mmol of hydrogen peroxide. In these experiments different temperatures were used for $FeSO_4$ within a range of 293.15-323.15 K. It is found that the degradation rate of anthracene rises with increases in temperature as shown in Figure 3.20. The results in Figure 3.21 indicate an Arrhenius relationship, which gives activation energy of 17.78 $kJ.mol^{-1}$ for the degradation efficiency of anthracene by using $FeSO_4$.

Table 3.30. Concentrations of Anthracene after treatment by chemical Fenton at different temperatures

Irradiation time/min	Concentration of Anthracene / ppm			
	293.15K	303.15K	313.15K	323.15K
0	15.931	15.931	15.931	15.931
15	12.553	-	-	1.201
30	9.203	4.587	2.999	0.566
45	7.281	-	2.155	0.311
60	5.920	4.546	2.022	0.192

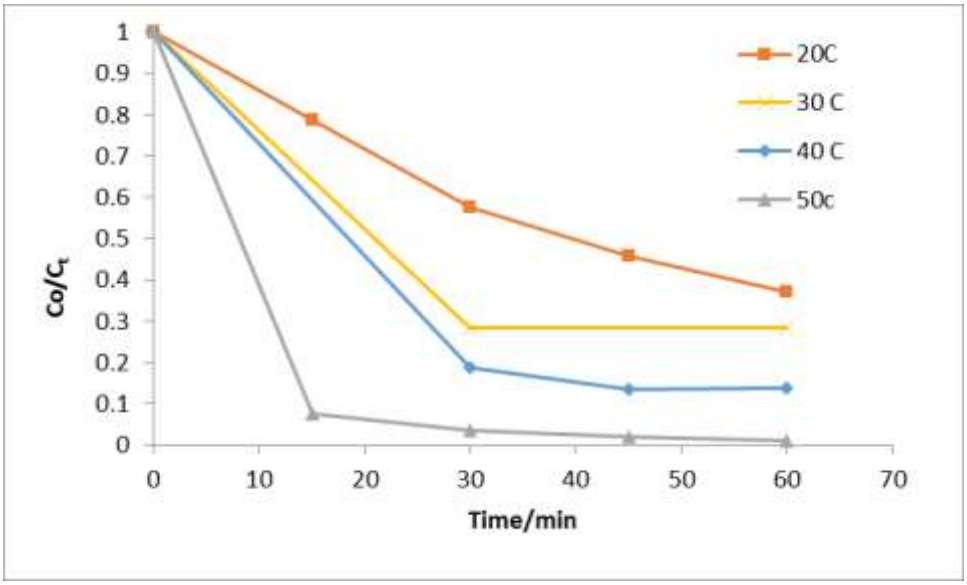

Figure 3.20. The changes of C_o/C_t with reaction times at different temperatures

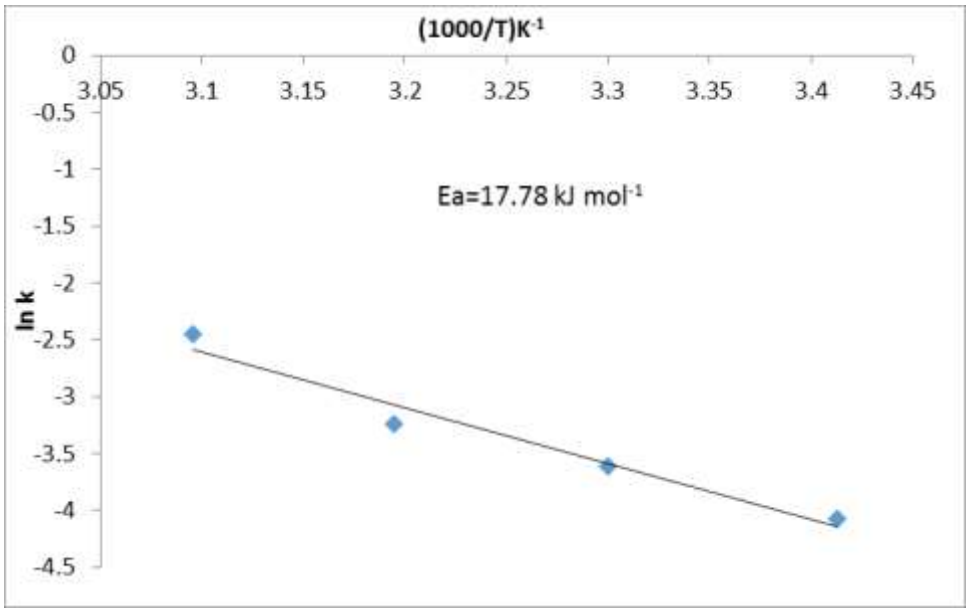

Figure 3.21. The Arrhenius plot by $FeSO_4$ of anthracene degradation at (293.15-323.15) K

3.2.2.4. The treatment of Anthracene by Photo-Fenton

The results listed in Table 3.31 show the effect of light intensity on the degradation of anthracene by using $FeSO_4$. In these experiments different light intensities were used

within the range of (1-3) $mWcm^{-2}$ under these predetermined experimental conditions: an initial anthracene concentration of 16 ppm, solution pH equal to 4, a $FeSO_4$ concentration of 120 mg/100ml, and temperature equal to 323.15K as shown in Figure 3.22. Figure 3.23. Shows the relationship between the light intensity for $FeSO_4$ and the rate constant of the reaction. It is found that the rate constant of the reaction rises with increases in light intensity, and the highest value of light intensity was equal to 3 mW cm^{-2}.

Table 3.31. Concentrations of Anthracene after treatment by chemical Fenton with different light intensities

Irradiation time/min	Concentration of Anthracene / ppm			
	1.0 mW/cm^2	1.5 mW/cm^2	2.0 mW/cm^2	3.0 mW/cm^2
0	15.930	15.930	15.930	15.930
15	15.635	11.932	9.128	3.560
30	-	8.781	4.961	2.670
45	8.086	6.785	2.569	1.598
60	7.008	6.341	1.584	0.979

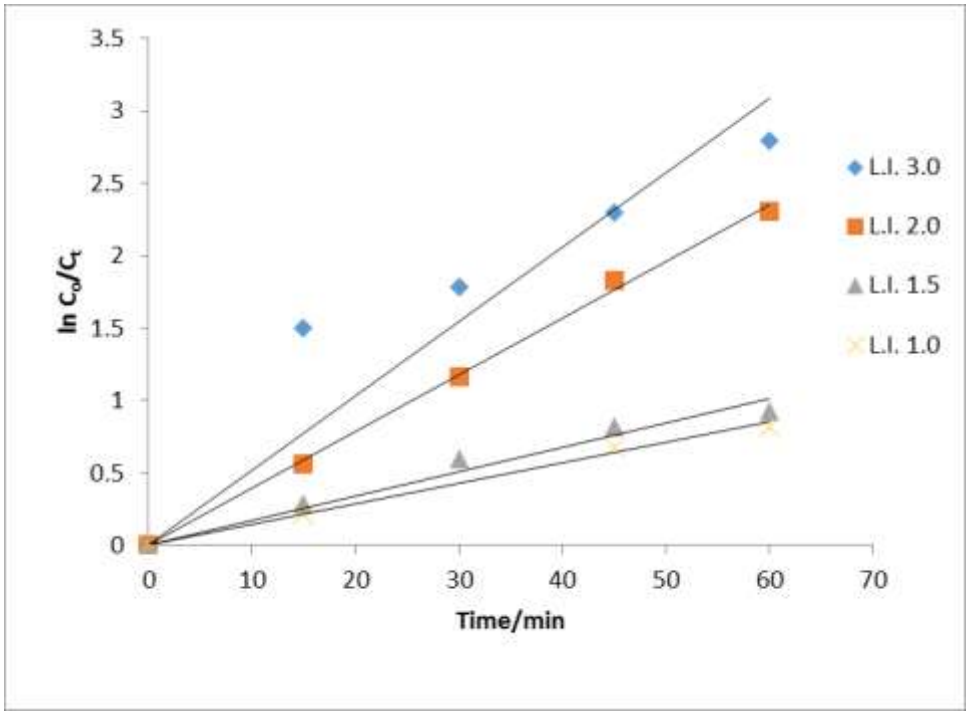

Figure 3.22. The changes of $\ln(C_o/C_t)$ with irradiation times at different light intensities

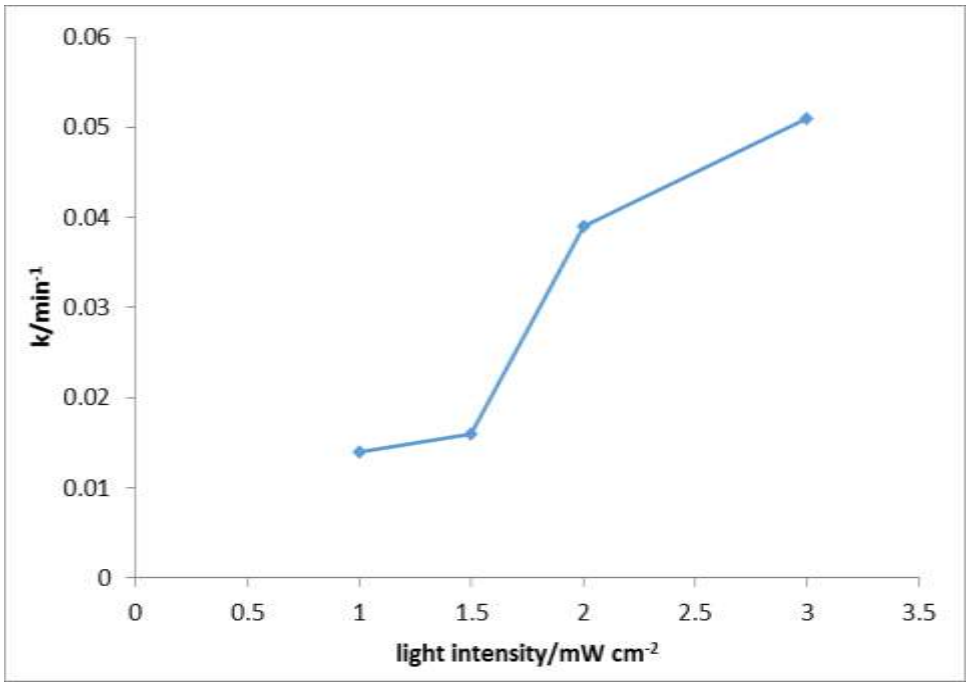

Figure 3.23. The effects of initial light intensity on the rate constant

3.2.2.5. Treatment of Anthracene by Ozone

Several experiments were done in this part of work in the same conditions (as mentioned in paragraph 2.5.8.), such as; initial concentrations of anthracene, temperature of the reactor, pH of the solution and light intensity when UV light was used; these experiments are listed below. Figure 3.24 illustrates these experiments.

1- Study of the effects of UV alone (direct photolysis).
2- Ozone alone.
3- UV and ozone.
4- UV and titanium dioxide (P25).
5- UV, ozone and hydrogen peroxide.
6- UV, ozone and titanium dioxide.

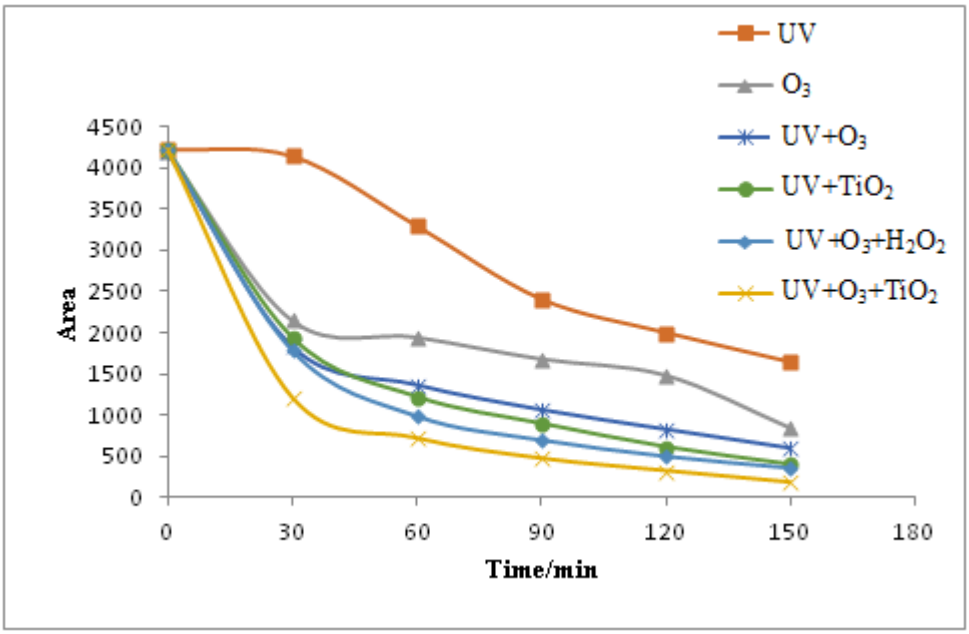

Figure 3.24. Comparison between different degradation methods

3.4. Investigation of 9,10-Anthraquinone

Following the main production of anthracene degradation, 9,10-anthraquinone was studied by comparing this standard compound with those produced by the degradation of anthracene. These investigations were compared by using the FTIR charts and GC-MS chromatograms for both compounds. Figure 3.25 shows the FTIR chart for both compounds.

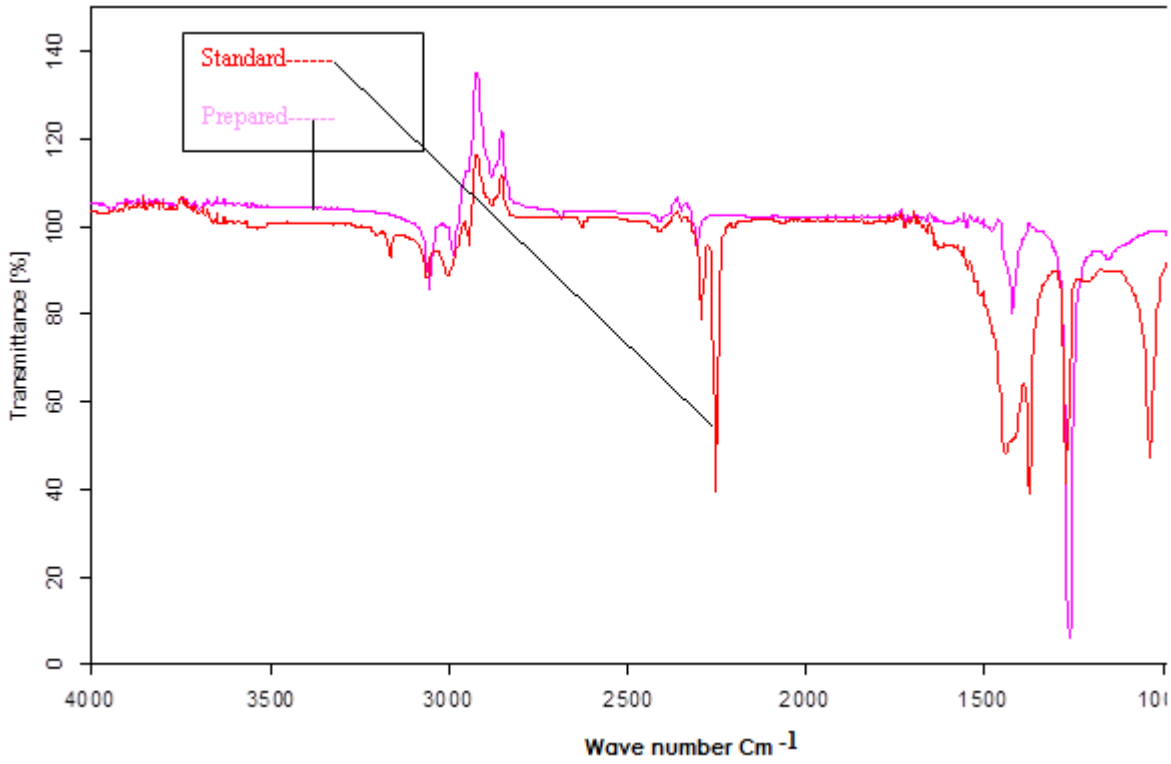

Figure 3.25. FTIR charts for the comparison between standard and produced 9,10-Anthraquinone

3.4.1. Degradation of 9,10-Anthraquinone

Several samples were analysed by GC during this part of work in same conditions, such as; initial concentrations of 9,10- anthraquinone, the temperature of the reactor, the pH of the solution and the light intensity of the UV light. Figures 3.26 and 3.27 show the GC chromatogram and mass spectra for the standard compound that was prepared before exposure to the UV light under the following conditions: a concentration of the compound of 25ppm, a titanium dioxide concentration of 175 mg/100ml, the temperature of the reactor equal to 298.15 K, a pH of 6.8, and light intensity equal to 2.5 $mW.cm^{-2}$. Figures 3.28 and 3.29 show the GC chromatogram and mass spectra for the standard compound that was prepared after exposure to the UV light. Figure 3.30 shows the reduction of the concentration during exposure to the

UV light; this Figure illustrates the degradation progress with increases in the times of illumination.

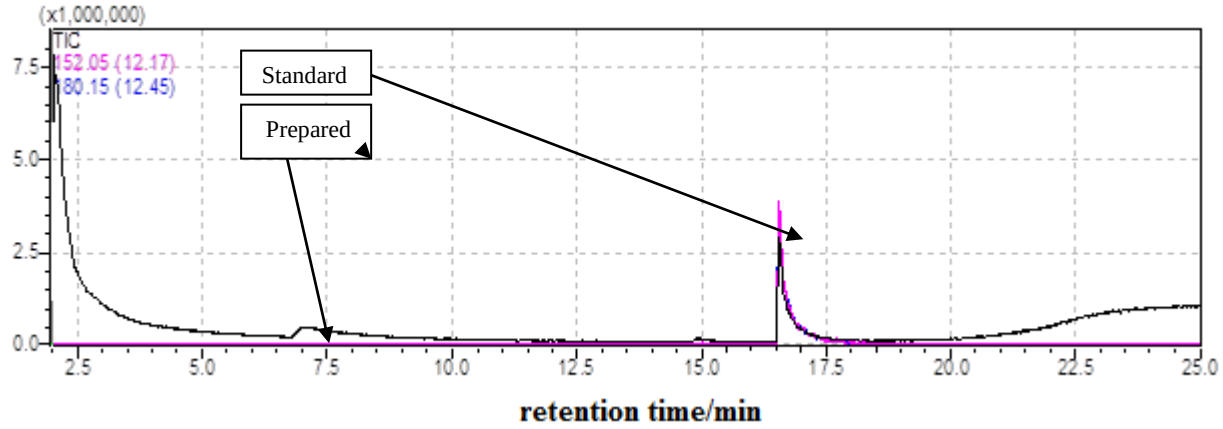

Figure 3.26. Chromatogram of GC –MS for standard9,10-Anthraquinone before exposure to UV light

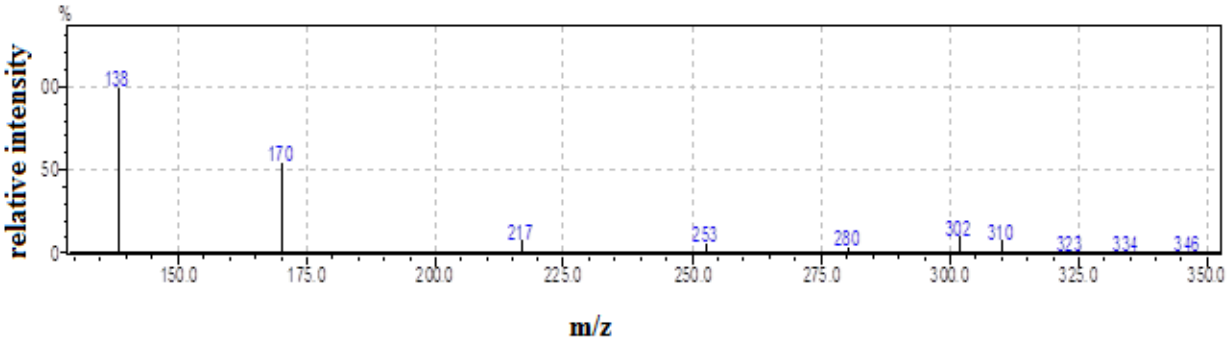

Figure 3.27. Mass spectra for standard 9,10-Anthraquinone before exposure to UV light

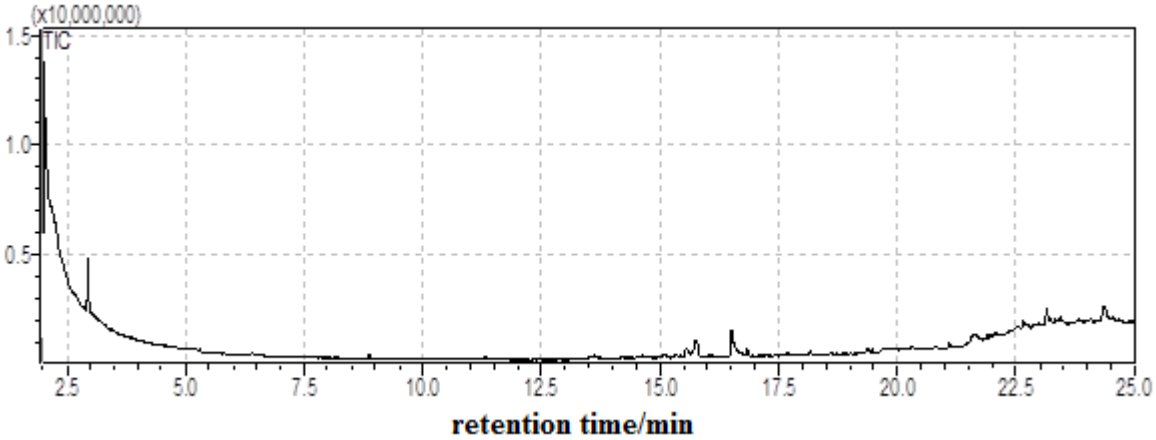

Figure 3.28. Chromatogram of GC –MS for standard 9,10-Anthraquinone after exposure to UV light

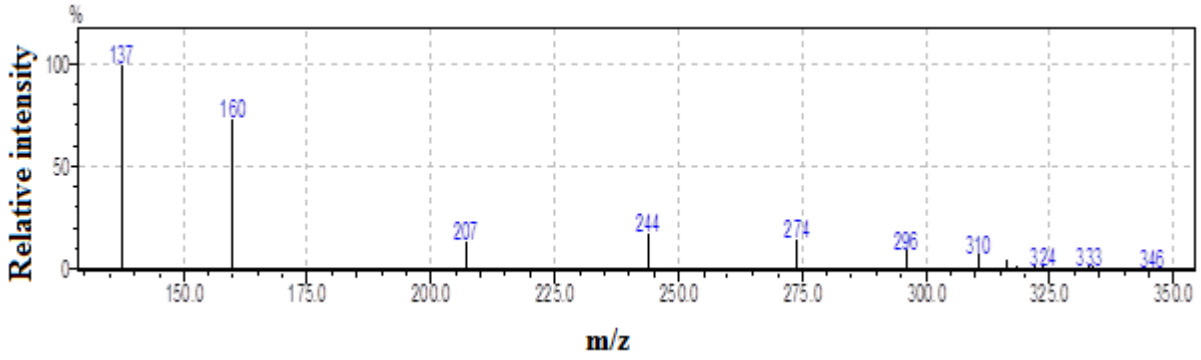

Figure 3.29. Mass spectra for standard 9,10-Anthraquinone after exposure to UV light

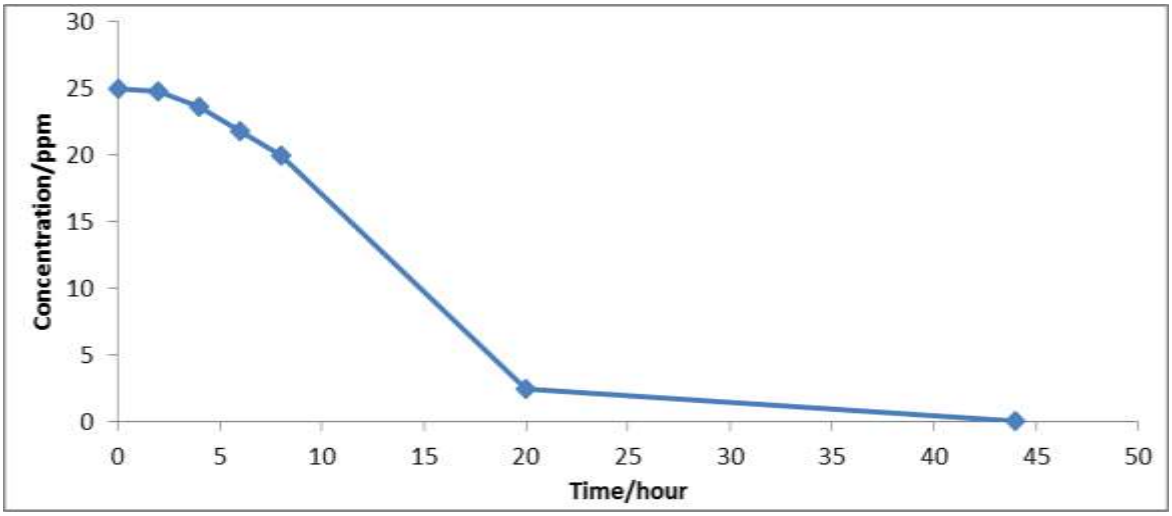

Figure 3.30. Effects of time on the reduction of the concentration of 9,10-Anthraquinone during UV light exposure

CHAPTER FOUR

DISCUSSION

٤.1. Physicochemical properties of water

Rivers that flow through agricultural, urban industrial area carry a great number and variety of contaminants, therefore the examination of different properties is very important. The results of present study referred that the lowest value of air temperature was recorded during December 2011; while the highest value was recorded in July 2012, .This is related to Iraqi climatic nature. Local variation of surface water temperature attributes to difference in the time of measurement, especially if take in consideration the number of sampling stations (fourteen sites).

The pH values recorded in the present study are within the narrow range and tend to be alkaline as it is frequent in Iraqi inland water. This is due to buffering capacity of Iraqi natural waters, due to the relatively high content of calcium bicarbonate.

Electrical conductivity of water referred to the dissolved salts, so high correlation occurred between total dissolved solids and Electrical conductivity. The Electrical conductivity values were ranged between 819–1250 µS/cm. The highest value was recorded during cold months probably related to high precipitation and soil leaching processes or due to effluent loaded by salts and dissolved material. In addition,

increase in the concentrations of total hardness causes increase in EC concentrations. [196].

4.2. PAHs in surface water samples

Due to the urbanization and industrialization, several types of contaminants find their way into all parts of the environment. PAHs are may be formed and released to the environment as a result of incomplete burning or pyrolysis of organic matter, during industrial processes and other human activities [197]. Water contamination by PAHs compounds is associated with the anthropogenic activities that represent the major source of PAHs compounds in addition to natural source. PAHs compounds are of special interest due to their potential hazard to human life and natural life. Therefore, the determination of PAHs in the aquatic ecosystem is quite essential and provides very important information on the anthropogenic input into the study area. Levels of the PAHs in previous study were reported petrogenic origin and closely related, due to their molecular weights [198].

The mean concentrations of all 16 PAHs for every site as shown in table 4.1. Two ring PAHs include naphthalene, three-ring PAHs include acenaphthylene, acenaphthene, fluorene, phenanthrene and anthracene, four-ring PAHs include fluoranthene, pyrene, benzo(a) anthracene and chrysene, five-ring PAHs include benzo(b)fluoranthene, benzo(k)fluoranthene, benzo(a)pyrene and dibenzo(a,h)anthracene, six-ring PAHs include indeno(1,2,3-c,d)pyrene and benzo(g,h,i)perylene.

Many researchs have dealt with PAH compounds in water of other rivers in the world [199-215]. The concentrations of PAHs in those polluted areas were variant from site to site. Although a direct comparison of literature data is difficult because of the difference in the phase analyzed (particulate, dissolved or both), the compounds considered in each study and the analytical method. The comparative levels of the total PAHs in surface water from different locations are shown in table 4.2.

Naphthalene exhibited large differences between the twelve months at most sampling sites, with higher mean concentrations shown in site five 7.73 ppb. The mean concentration of lowest molecular weight PAHs two-ring (Naphthalene) was 2.23 ppb . This concentration is lower than those found in different aquatic systems (5.02 and 2.75) ppb in Lake Chaohu and Hun River, China respectively, but higher than those found in Raba River, Hungary and in the Hungarian upper section the Danube River (0.023 and 0.006) ppb respectively.

The mean concentration of Acenaphthylene in Shatt Al-Hilla River was 3.78 ppb , this concentration is much higher than those found in Danube River, Raba River and Hungarian upper section the Danube River and the Moson Danube branch were (0.003, 0.001 and 0.002) ppb respectively.

The mean concentration of Acenaphthene in Shatt Al-Hilla River was 1.78ppb , this concentration is higher than those detected in surface samples of the Jialing River and surface samples of the Japan sea (0.058 and 0.001) ppb respectively.

Table 4.1. Mean concentrations of individual PAHs in surface water of Shatt Al-Hilla River

Site No. / PAHs ppb	S1	S2	S3	S4	S5	S6	S7	S8	S9	S10	S11	S12	S13	S14
Nap	1.20	1.97	3.89	0.11	7.73	ND	1.05	6.39	0.36	0.02	0.15	7.13	0.63	0.54
AcPY	0.47	2.90	11.22	5.13	5.57	3.03	1.21	10.90	1.40	0.51	2.51	3.85	1.14	3.16
AcP	2.95	0.37	1.97	1.80	0.08	1.49	0.72	2.99	10.86	0.72	0.04	0.57	0.13	0.26
Flu	3.90	6.59	14.80	10.88	6.01	18.99	10.57	14.83	13.79	9.42	5.61	11.43	5.13	9.33
Phe	6.70	1.01	0.87	1.30	2.36	3.58	3.27	0.40	2.88	7.37	0.29	0.24	4.25	17.14
Ant	6.64	6.32	0.47	1.62	7.88	1.06	3.05	1.51	0.08	5.39	10.26	1.16	4.19	1.13
FL	3.26	5.77	9.35	3.13	7.42	3.81	1.31	5.73	2.50	9.99	3.29	17.46	7.24	15.20
Pyr	0.24	8.53	30.11	0.37	1.57	4.42	ND	0.27	0.40	0.54	ND	5.44	2.66	6.21
BaA	2.23	6.81	12.54	1.59	18.16	2.75	8.28	9.12	17.41	12.16	7.90	1.75	3.41	2.50
Chr	1.48	15.43	1.49	0.82	0.20	3.10	1.06	3.82	0.01	0.01	1.52	0.20	0.01	3.90
BbFl	4.91	3.68	13.45	6.19	6.74	2.87	1.56	1.98	4.50	15.30	3.58	11.74	4.52	2.56
BkFl	2.62	0.38	1.71	0.75	9.01	6.72	0.35	9.67	8.39	9.90	6.46	6.03	17.25	8.99
BaP	ND	4.56	5.70	0.68	0.08	50.17	2.44	0.33	2.31	0.85	0.35	1.36	3.06	0.69
InP	24.34	2.37	3.73	1.31	3.60	15.27	0.69	0.44	6.50	1.82	0.03	ND	6.79	ND
DbA	25.02	5.56	1.47	3.13	1.53	14.29	2.32	0.55	5.17	1.32	2.60	2.43	3.37	2.07

BghiP	**11.88**	**8.82**	**0.36**	**1.33**	**0.73**	**7.32**	**6.06**	**0.96**	**1.00**	**0.06**	**ND**	**4.83**	**11.41**	**6.70**
PAH16∑	**97.84**	**81.07**	**113.13**	**40.14**	**78.67**	**138.87**	**43.94**	**69.89**	**77.56**	**75.38**	**44.59**	**75.62**	**75.19**	**80.38**

ND: no detection

The mean concentration of Fluorene in Shatt Al-Hilla river was 10.09 ppb is higher than those found in Qiantang River, China and Hangzhou Canal, China (0.52 and 2.38) ppb respectively [204]. The mean concentration of Phenanthrene in Shatt Al-Hilla river was 3.69 ppb is also higher than those measured in Inland river, China and West Lake, China (0.62 and 0.48) ppb respectively [204].

Table 4.2. Comparative levels of total PAHs in water samples collected from different locations

Location	Mean of PAH_{16} ppb	Range ppb	No. of PAHs	Date of sampling	Reference
Shat Al-Hilla River, Iraq	**77.97**	**40.14 - 138.87**	**16**	**2011-2012**	**This study**
Lake Chaohu,China	**0.18±0.07**	**0.37-0.95**	**16**	**2009**	**Qin et al., 2013[203]**
Hangzhou City, China	**5.538**	**0.98- 9.66**	**16**	**2002**	**Chen et al., 2004[[204]**
Raba River, Hungary	**0.11 ± 0.07**	**0.04 - 0.43**	**17**	**2008-2011**	**Nagy et al., 2013[205]**
Hun River, Northeast China	**0.28**	**0.12 – 0.43**	**16**	**2009**	**Zhang et al., 2013[206]**
Jialing River, China	**1. 00**	**0.81 – 1.58**	**16**	**2009-2010**	**Xiao et al., 2012[207]**
Danube River, Hungary	**0.12±0.13**	**0.01-0.02–**	**16**	**2001–2010**	**Nagy et al., 2013[208]**
Niteroi City, Rio de Janeiro State, Brazil	**--**	**0.004–0.870**	**15**	**2008-2009**	**Riberio et al.,**

					2012[209]
Gomti river, India	**10.33 ± 19.94**	**0.06 – 84.21**	**16**	**2004-2006**	**Malik et al., 2011[210]**
Sacramento River, California	**0.16±0.06**	**0.19 - 3.78**	**16**	**2004 - 2005**	**Kim et al., 2009[211]**
Japan Sea	**0.01**	**0.007 – 0.01**	**13**	**2010**	**Chizhova et al., 2013[212]**
Danube River, Hungarian upper section	**0.09 ± 0.05**	**0.02 - 0.35**	**16**	**2007-2010**	**Nagy et al., 2012[213]**

The mean concentration of Anthracene in Shatt Al-Hilla river was 3.62 ppb , this concentration is higher than those found in Tianjin, China 0.006 ppb. [214]. The main concentration of Fluorene in Shatt Al-Hilla River was 6.81ppb is higher than those were found in Raba River, Hungary and Hun River, China (0.123 and 0.341) ppb respectively. The concentration of pyrene in Shatt Al-Hilla River was 4.34 ppb is higher than those found in Qiantang River, Chine and Hangzhou Canal, China (0.52 and 2.38) ppb respectively. The mean concentrations of Benzo (a) anthracene, chrysene, benzo(b)fluoranthene, benzo (k) fluoranthene, benzo (a) pyrene, dibenzo (a,h) anthracene, indeno(1,2,3-c,d)pyrene and benzo (g,h,i) perylene in Shatt Al-Hilla river were higher than those found in different locations mentioned in Table 4.2.

Table 4.3 illustrates the mean concentrations of PAH which are classified according to number of rings. The lowest percentage was for 2-ring PAHs (Naphthalene) 2.85%, while the highest percentage (29.37%) was recorded for 3-ring PAHs were the most abundant than the others

(3-ring PAHs > 5-ring PAHs > 4-ring PAHs > 6-ring PAHs > 2-ring PAH), these arrangement is similar to those found by Zhang et al., 2013[215].

Table4.3. Mean concentration of PAHs classified according to number of rings and representative percentage

∑ of Mean concentration ppb	**No. of ring**				
	Two-ring	**Three-ring**	**Four-ring**	**Five-ring**	**Six-ring**
	2.22	**22.96**	**21.12**	**22.22**	**9.44**
Percentage	**2.85%**	**29.48%**	**27.11%**	**28.53%**	**12.12%**

abundance					

The compositional pattern of PAH by rings number of the total contamination gradient of the Shatt Al-Hilla River are listed in Table 4.3. It is clear that 3-ring PAHs are the most abundant PAHs, and 5-ring PAHs take second. Naphthalene was the less dominant component in the period of study 2.85% of $\sum PAHs_{16}$.

PAHs enter surface waters mainly via atmospheric fall out, municipal/industrial effluents, urban runoff and oil spillage or leakage (H. Zhang and references therein) [206]. In general, relative concentration values of PAH compounds with different molecular weights were used frequently to distinguish the PAHs sources. PAHs were regarded as two types, including high-rings of 4-6 rings (high relative molecular weight, HMW) and low-rings of 2-3rings (low relative molecular weight LMW). The results in table 4.3, show that the PAH concentrations HMW are higher than those of LMW (52.78 and 25.1) ppb respectively from fourteen sampling positions. Special PAH compound ratios, such as Phenanthrene/Anthracene, Flurene/Pyerene, LMW/HMW and Fluorenthenel / (Fluorenthene+Pyrene), are widely used to identify the sources of PAH compounds in surface water. Previous researchers were suggested that the possible sources of PAHs are petroleum when the ratio of Phenanthrene/Anthracene > 10, while the possible input of PAHs is incomplete combustion of fuel such as coal and oil when Phenanthrene/Anthracene <10. Meanwhile, according to the conclusions of other researchers, when the rate of Fluoranthene/(Fluoranthene+Pyrene) <0.5, it was frequently considered as an indicator of petroleum; when the rate of Fluo/(Fluo+Py)>0.5, it was usually considered as an indicator of combustion [207].

In this work, the ratios of Phenanthrene/Anthracene and Fluoranthene/(Fluoranthene+Pyrene) were used to identify the possible sources of PAHs in surface water of Shat Al-Hilla River.

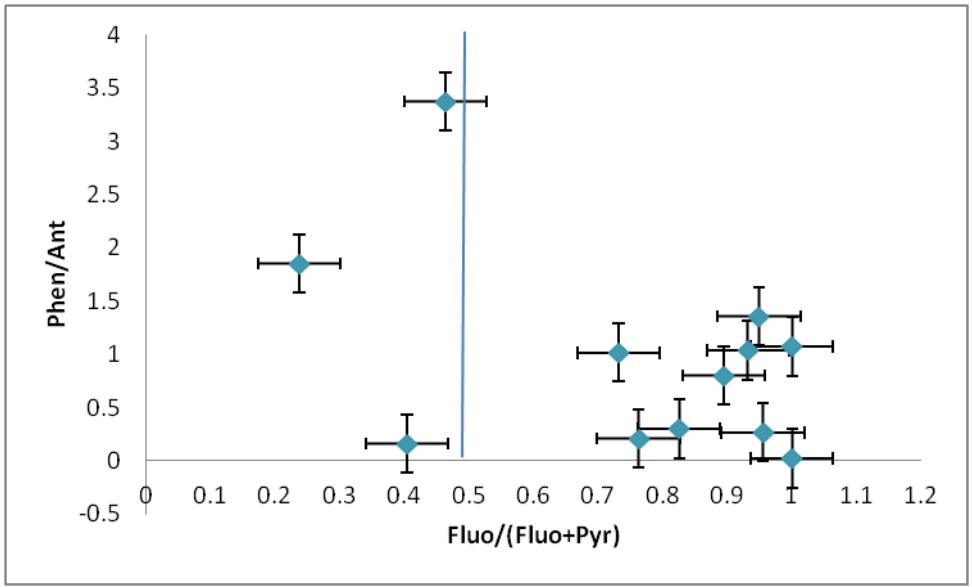

Figure4.1. Phen/Ant and Fluo/(Fluo+Py

r) ratios for source identification of PAHs

Figure 4.1 and Table 4.4, show the ratio of LMW/HMW. Figure 4.2 illustrates the source water identification of PAHs for average concentration of mentioned PAHs (Anthracene, Phenanthrene, Fluorenthene and Pyrene) along the Shatt Al-Hilla River using the ratio of Phen/Ant and Fluo / (Fluo + Pyr). The results show that the ratios of Phen/Ant are almost in the range of 0.020 to 3.377, which indicate that the sources of PAHs are from incomplete combustion of fuel. The ratios of Fluo/ (Fluo+Py) were almost range of 0.236 to 1.000, which indicate that the sources of PAHs are from incomplete combustion and from petrol.

The results illustrated that the water samples are strongly polluted by pyrolytic PAHs. Normally, pyrolytic PAHs were mainly from heavily polluting works near the river as mentioned in chapter two (2.3 the study area). The petroleum input of PAHs is possible too in surface water of Shatt Al-Hilla River.

Table4.4. Ratio of LMW/HMW of the Average of PAHs

Phen/Ant	Fuo/Fluo+Pyr
1.037	**0.931**
0.159	**0.403**
1.851	**0.236**
0.802	**0.894**
0.299	**0.825**
3.377	**0.462**
1.072	**1.000**
0.264	**0.955**
1.360	**0.862**
0.020	**0.948**
0.206	**1.000**
1.014	**0.762**

4.3. Treatment of Anthracene

4.3.1. Direct photolysis

Figure 3.1, shows the degradation of Anthracene by direct photolysis by plotting the concentration against time for Anthracene degradation. This figure shows that the consumption time is 360 min for reduce the concentration of Anthracene from 25.00 ppm to 2.90 ppm, this time is considered long compare with other degradation methods.

4.3.2. Treatment of Anthracene by AOPs

4.3.2.1. Effect of TiO_2 type

Figure 3.2 shows the comparison between both types of Titanium dioxide P25 and UV100. P25 is shown to be more efficient than UV100, recent studies have proved that due to the particle size of P25 which consist of 80% anatase and 20% of rutile, this percentage gives this type of titanium dioxide perfect performance due to the wide surface area available for adsorption.

4.3.2.2. Effect of Anthracene Concentration

The effect of the initial concentration of anthracene on the photocatalytic degradation was studied by varying the initial concentration over a wide range. At a fixed pH and amount of catalyst, photocatalytic experiments were carried out at different initial concentrations of anthracene. The results in Figure 3.3 shows a plot of $In(C_o/C_t)$ against time for different anthracene concentrations, where C_O is the initial concentration and Ct, is the concentration at time t. The rate of photodegradation increased with increasing the initial anthracene concentration [216, 217]. The study was carried out for the concentrations greater than that detected in the water surface. Figure 3.4 shows the effect of initial anthracene concentration on rate constant by TiO_2, by this Figure it is concluded that the rate of degradation is increased with increasing initial concentration of Anthracene.

4.3.2.3. Effect of Light Intensity

The effect of light intensity on the degradation efficiency for anthracene was examined at constant initial anthracene concentration (25 ppm). It is found that the percentage of degradation and photodegradation for anthracene increases with increasing the light intensity as shown in Figures 3.5 and 3.6. The light intensity was studied in the range (1-2.5) $mW.cm^{-2}$ by changing the height and lowering the lamps. From these results, it is found that the degradation rate for anthracene increases with increasing the light intensity, this result in agreement with previous study [218]. This behavior can be explained that the UV irradiation production of the photons required for the electron transfer from the valence band to the conduction band in the catalyst. Photocatalyst and the energy of a photon is related to its wavelength and the overall energy input to a photocatalytic process is dependent on light intensity. The rate of degradation for anthracene increases when more radiations fall on the catalyst surface and hence more ·OH radical is generated on catalyst surface [219,220].

4.3.2.4. Effect of pH

The results in Figures 3.7 and 3.8 are showing that the photodegradation efficiency of anthracene at different pH value of solution in the presence of TiO_2 (Degussa P25). The production of hydroxyl radicals is also a function of pH. Therefore, pH is an important parameter in photocatalytic reactions. The photodegradation of anthracene was studied at different pH. In all experiments, pH was adjusted by using appropriate amounts of base (NaOH) or acid (HNO_3) solutions [221-224]. The zero point charge

(ZPC) is equal to 6.8 for TiO_2 (Degussa P25) and the semiconductor surface will remain positively charged in acidic medium and negatively charged in alkaline medium, due to the ionization state of the surface of semiconductor according to the following reactions in equations 4-1 and 4-2:

$$TiOH + H^+ \longrightarrow TiOH_2^+ \quad .....4-1$$

$$TiOH + OH^- \longrightarrow TiO^- + H_2O \quad .....4-2$$

4.3.2.5. Effect of Temperature

The effect of temperature on photocatalytic degradation of anthracene in water solution was investigated in the range of 278.15-308.15K. The results in Figure 3.9 show that the degradation efficiency of anthracene gradually increased with increasing temperature. The increases in temperature would lead to generate the free radicals [225]. Therefore, the rise in temperature helps the degradation reaction to compete with more efficiently than electron–hole recombination [226]. The increasing of temperature may increase the oxidation rate of anthracene, also, reduces the adsorption capacities associated with anthracene and dissolved oxygen [227, 229]. Generally, the rise in temperature can affect the amount of adsorption [228]. Arrhenius plot shows that the activation energy for photocatalytic degradation of anthracene is equal to12.76 kJ mol^{-1} for TiO_2 as shown in Figure 3.10.

4.3.3. Effect of addition of H_2O_2

Hydrogen peroxide (H_2O_2) plays an important role in the production of hydroxyl radicals. The effect of addition of hydrogen peroxide H_2O_2 on the degradation rate was studied for photocatalytic degradation of the anthracene. The results in Figure 3.11 shows that the degradation rate decreases with increasing concentrations of hydrogen peroxide H_2O_2 from 5.00 to 100.00 mmol/L, this result is in agreement with pervious work [230]. This behavior is due to the high concentration of hydrogen peroxide H_2O_2 the photocatalytic processes decreases because of its hydroxyl radical scavenging effect, according to the following equations [231,232].

$$H_2O_2 + {}^{\bullet}OH \longrightarrow H_2O + HO_2^{\bullet} \quad \text{.....4-3}$$

$$HO_2^{\bullet} + {}^{\bullet}OH \longrightarrow H_2O + O_2 \quad \text{.....4-4}$$

Under UV irradiation, H_2O_2 are photolyzed to form two hydroxyl radicals ($2OH^{\bullet}$) that react with organic contaminants [233,234]. Previous study was documented that H_2O_2/UV process was more effective in an acid medium (pH 3-4) [235]. Reduced efficiencies for H_2O_2/UV processes in presence of suspended material like titanium dioxide can also result during photocatalytic treatment, since a fraction of irradiated energy is scattered by these particles.

4.3.4. Chemical Fenton

4.3.4.1. Effect the initial concentration of Anthracene on degradation.

Thinking about the possibility to apply this method for treatment the contaminated water sample, it's very important to study the initial concentration of anthracene as the first step in this method. Therefore, it is essential to determine the suitable amount of anthracene that would be degraded with a fixed reagent concentration. As shown in Figure 3.13, the reaction occurs quickly in the first 45 minute with 16 ppm of anthracene, and then gradually increases the degradation rate with increasing time of reaction. The explanation for this phenomenon may be attributed to the suitability of this amount of anthracene (16 ppm) with those addition like H_2O_2 and $FeSO_4$.

4.3.4.2. Effect of $FeSO_4$ mass

Experiments are conducted in order to investigate the influence of ferrous ion concentration as (catalytic agent) on the process. Figures 3.14and 3.15 show the relationship between the degradation extent and the amount of ferrous ion [236].

The results show increasing degradation with the ferrous ion concentration increase. At all concentrations of ferrous the degradation occurs quickly in the first 15 minute except at 30mg it needed to 30 min, significant differences are found between 30mg and 120mg.

4.3.4.3. Effect of H_2O_2

The experiments were carried out with initial concentration of anthracene of 16ppm. Experiments were performed to determine the influence of hydrogen peroxide concentration on the process. The degradation rate of anthracene versus hydrogen

peroxide concentration is shown in Figure 3.16, which indicates that the reaction followes pseudo first order kinetics [237].

Additions of 200mg/L and 150 mg/L show that the degradation increase quickly within the first fifteen minute of reaction, while in 100mg/L and 50mg/L addition the degradation need 30 min to increase. Figure 3.16 shows that the increase of H_2O_2 concentration from 50 to 200 mg/L yield highest efficiency of anthracene removal. Figure 3.17 illustrates effect of concentration of H_2O_2 on rate constant.

4.3.4.4. Effect of pH

The Fenton's reaction is depending on the pH value, because this value affects the hydroxyl radical generation and consequently, the efficiency of degradation [238]. pH change effects the adsorption quantity of organic pollutants and the ways of adsorption on the surface of photocatalyst (coordination)[239]. For this oxidation process, the optimal pH ranged mentioned in previous studies is 3 to 6.

In our present work the range of pH (2-5) values were studied and the results are shown in Figure 3.18. It can be observed that the removal efficiency was significantly changed with pH change. At all pH values the degradation occurred quickly in the first 15 minute. Comparing the results of degradation at different pH values exhibit that the reaction at pH=4 is fastest than others about five times. The most rapid elimination of anthracene from the reaction mixture occurred at pH=4. Figure 3.19. shows the effect of initial pH of solution on rate constant, it is clear that the zero point charge is at pH=4.

4.3.4.5. Effect of temperature

Experiments were conducted under the same conditions such as (amount of initial concentration of anthracene, amount of ferrous ion, pH value, Hydrogen peroxide concentration) at four different temperatures between 293.15-323.15 K to investigate the effect of these temperatures on the degradation rate of aqueous solution of anthracene. The results are illustrated in Figures 3.20 and 3.21. An enhancement in the rate and even in the extent of degradation efficiency was observed with temperature increase. As known, at higher temperatures the thermal decomposition of PAHs increase and the hydrogen peroxide decomposition also accelerate resulting a decrease of the concentration of hydroxyl radicals, despite of this fact, the degradation reaction increased with temperature. Results show high differences between results at temperature 50 with others, the degradation being more than two times at fifteen minute comparing with other temperatures. Generally at all temperatures observed that the degradation increase quickly within the first fifteen minute of reaction.

4.3.5. Photo Fenton

4.3.5.1. Effect of light intensity

The effect of UV light intensity on the degradation of PAHs was investigated as shown in Figures 3.22 and 3.23. The intensity of light was adjusted by changing the height of the lamps from the reactor and measuring by UV light meter. The UV light intensity shows a significant influence on the PAHs degradation ratio in photo-Fenton reaction. The degradation ratio of PAHs increased while increasing the intensity of the UV light. The UV light absorbed by the catalyst plays an important role in the course of reaction [240].

So increasing the UV light intensity increase, the number of incident photons then increasing the number of released hydroxyl radicals from the heterogeneous photo-Fenton reaction. Then, the degradation ratio of anthracene is increased. The highest degradation ratio was appeared at 3.0 mW/cm^2 and then at (2.0, 1.5 and 1.0) respectively.

4.3.6. Ozonation of Anthracene

Anthracene is frequently used as a model PAH and its reaction with ozone on various organic compounds has been widely investigated. Most previous researchers were focused on the heterogeneous reactions of PAH in carbonaceous aerosol [241].

Figure3.24 shows the results of experiments are applied for anthracene degradation: in presence of UV alone; ozone alone; UV and TiO_2; in synergy between ozone and H_2O_2 in presence of UV; and synergy between ozone and TiO_2 in presence of UV.

Previous study proved that the synergy between ozone and H_2O_2 in presence of UV is increase the surface area of titanium dioxide and then increase the efficiency of degradation [242].

Ozone is stronger oxidant than oxygen, when it is adsorbed on the surface more easily reduced by electron that generated from reduction band of TiO_2. Equations a and b illustrate production of ozonide radical anion, which in the next steps generates hydroxyl radical equations c and d. Also the recombination between holes and electrons of TiO_2 is minimized due to the more efficiency trapping of photogenerated electrons by ozone.

$$TiO_2 + h\nu \longrightarrow TiO_2\ (e^- + h^+) \quad \ldots\ldots\ldots\ldots (a)$$

$$TiO_2 + O_3 \longrightarrow O_3^{-\bullet} + TiO_2 \quad \ldots\ldots\ldots\ldots (b)$$

$$O_3^{-\bullet} + H^+ \longrightarrow HO_3^{\bullet} \quad \ldots\ldots\ldots\ldots (c)$$

$$HO_3^{\bullet} \longrightarrow O_2 + HO^{\bullet} \quad \ldots\ldots\ldots\ldots (d)$$

4.4. Comparison between direct photolysis and photocatalytic processes

Direct photolysis (in the absence of catalyst) shows slower degradation process for anthracene compared to that in the presence of titanium dioxide as a catalyst, this is ordinary due to the efficiency of titanium dioxide as supplier for oxidation electrons from conductive band for this catalyst. However the oxidation process which produce hydroxyl free radicals, which it contribute by attack on the anthracene molecule to be degraded in short time comparing with direct photolysis. Figure 4.3, shows the comparison between direct photolysis and photocatalysis. It is found that anthracene was slightly degraded after 180 minutes of irradiation.

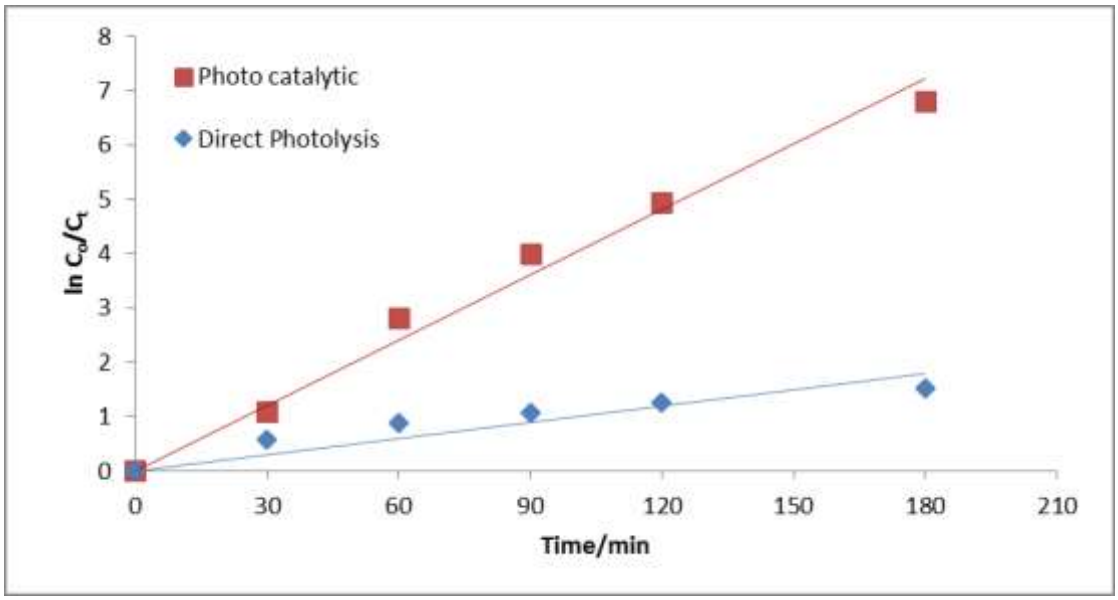

Figure 4.2. Comparison of direct photolysis and photocatalysis of anthracene

4.5. Photocatalytic transformation of Anthracene

During the photocatalytic degradation experiments with anthracene only 9,10-anthraquinone was found as an intermediate, in agreement with Theurich et al., [243]. The mechanism of photocatalytic degradation, as presented in Scheme 4.1and 4.2, involves an $OH^{\cdot}$ radical attack at the 9-position (reactions 4-5and 4-21) followed by an oxidation with O_2 (reactions 4-6 and 4-22) at the weakened 10-position resulting in a hydroxyperoxyl radical (3). Compound (3) will probably decay in two different pathways. On the one hand, an initial abstraction of a hydrogen atom (reaction 4-23), followed by a loss of water (reaction 4-24) and a second oxidation via an ·OH-radical leading (after the loss of water, reaction 4-25) to the semiquinone radical of anthracene (10) which is readily oxidized to anthraquinone (7) (reaction 4-26). On the other hand, the elimination of $HO_2^{\cdot}$ (reaction 4-7) will result in the formation of anthranol (4) which is the meta stable tautomeric enol-form (4-8) of anthrone (5). The

latter will be easily oxidized (reaction 4-9 and 4-10) via an unstable peroxide of anthrone (6) to anthraquinone (7).

4.5.1. Suggested mechanism (Scheme 1)[243]

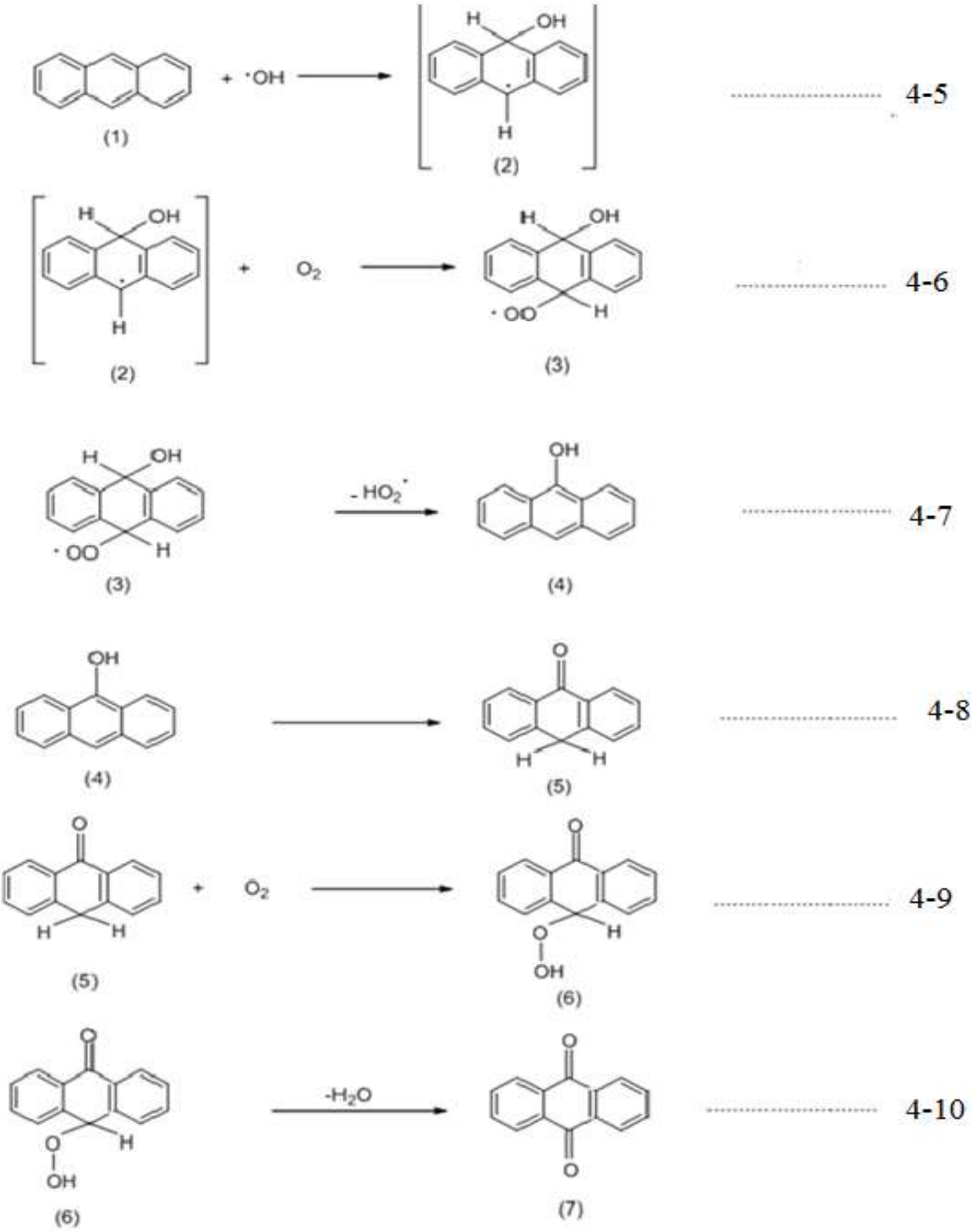

Scheme 4.1. Mechanism of photocatalytic degradation of anthracene

Suggested mechanism of the Titanium dioxide excited by UV-A (365nm).

$$TiO_2 \xrightarrow{h\nu} TiO_2\ (e^-_{cb}, h^+_{vb}) \quad \text{.....4 – 11}$$

$$TiO_2\ (e^-_{cb}, h^+_{vb}) \longrightarrow h^+ + e^- \quad \text{.....4 – 12}$$

$$H_2O \longrightarrow HO^- + H^+ \quad \text{.....4 – 13}$$

$$TiO_2\ (h^+_{vb}) + H_2O \longrightarrow TiO_2 + HO^\bullet + H^+ \quad \text{.....4 – 14}$$

$$TiO_2\ (e^-_{cb}) + O_{2_{ads}} + H^+ \longrightarrow TiO_2 + HO^\bullet_2 \quad \text{.....4 – 15}$$

$$TiO_2 + HO^\bullet_2 \longrightarrow O^{\bullet -}_2 + H^+ \quad \text{.....4 – 16}$$

$$2HO^\bullet_2 \longrightarrow H_2O_2 + O_2 \quad \text{.....4 – 17}$$

$$H_2O_2 + O^{\bullet -}_2 \longrightarrow HO^\bullet + O_2 + HO^- \quad \text{.....4 – 18}$$

$$H_2O_2 + h\nu \longrightarrow 2HO^\bullet \quad \text{.....4 – 19}$$

$$H_2O_2 + TiO_2\ (e^-_{cb}) \longrightarrow HO^\bullet + HO^- \quad \text{.....4 – 20}$$

4.5.2. Suggested mechanism (Scheme 2)[243].

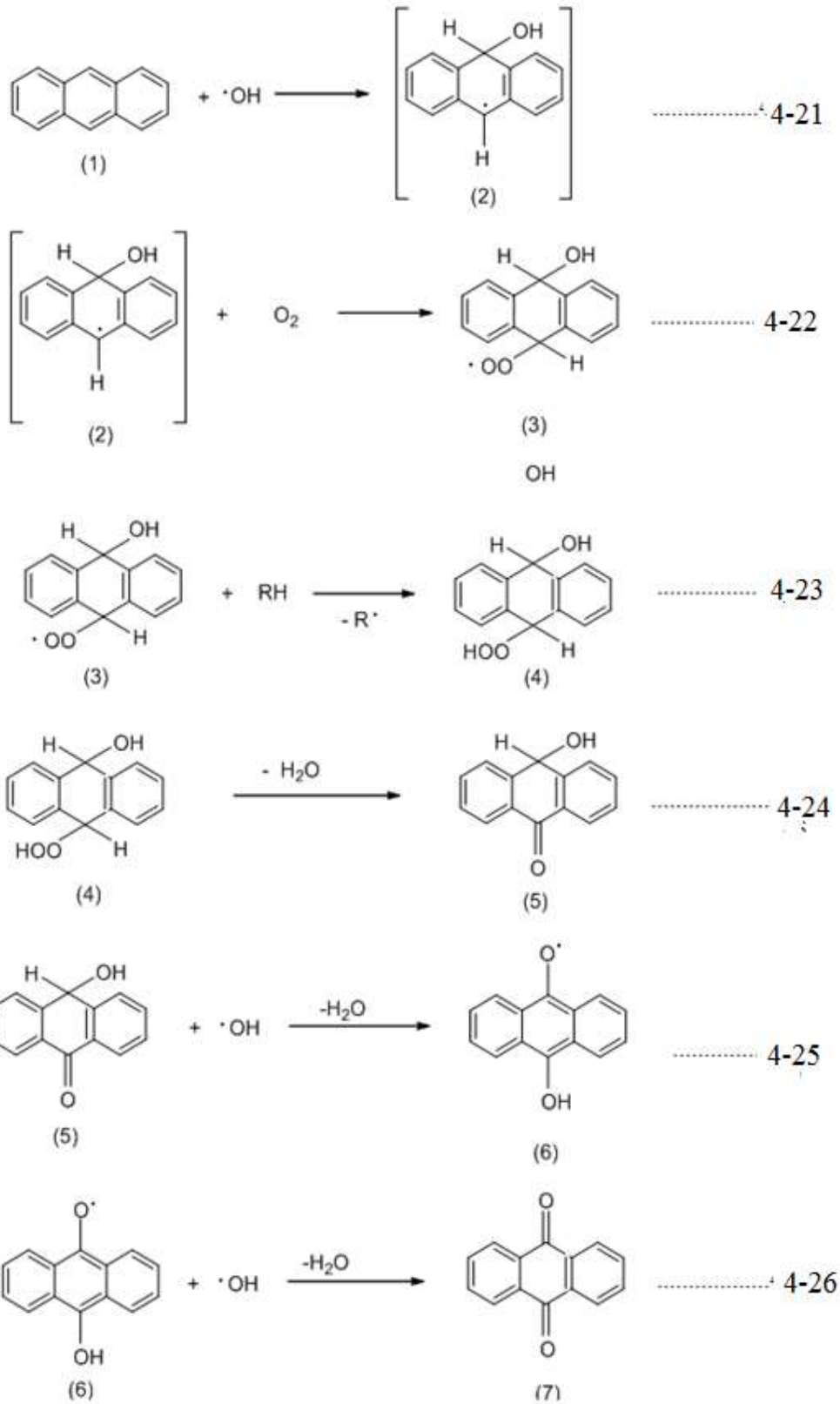

Scheme 4.2. Mechanism of photocatalytic degradation of anthracene

4.6. Degradation of 9,10-Anthraquinone

Figures 3.26 and 3.27 shows the GC chromatogram and mass spectra for the standard compound before exposure to the UV light. Figures 328 and 3.29 are show in GC chromatogram and mass spectra for the standard compound that prepared after exposure to the UV light. Figure 3.30 shows the reduction of the concentration during exposure to the UV light, this Figure illustrate the degradation progress with increasing the time of illumination.

4.7. Conclusions

This study focused on monitoring of the concentrations of PAHs in surface water of Shatt Al-Hilla river for one year. Treatment of PAHs by different methods also was studied through this study. The main conclusions can be summarized as follows:

1- The surface water of Shatt Al-Hilla is polluted with PAHs.

2- The concentrations of PAH exhibit spatial and monthly variation.

3- The lowest percentage for 2-ring PAH (Naphthalene) among total PAH found is 2.85%, while the highest percentage for 3-ring (Acenaphthylene, Acenaphthene, Fluorine, Phenenthrene and Anthracene) PAHs is (22.85%).

4- The ratios of Phen/Ant are almost in the range of 0.020 to 3.377, which indicated that the sources of PAHs are incomplete combustion of fuel. The ratios of Fluo/ (Fluo+Py) are almost range between 0.236 to 1.000, which indicate that the sources of PAHs are incomplete combustion and of petrol.

5- Solid phase extraction is more efficient than liquid-liquid extraction due to it is cheaper, safer, more accurate and higher sensitivity.

6- The photocatalytic oxidation for Anthracene proves that it is more efficient than direct photolysis.

7- Titanium dioxide (P25) is better than titanium dioxide (UV100), during oxidation processes for Anthracene.

8- The optimum conditions of photocatalytic oxidation of Anthracene are: ; perfect concentration of Anthracene is 25 ppm, 2.5 mW. cm^{-2} of light intensity, pH of 6.8 is the best medium for Anthracne, 308.15K is the appropriate degree of temperature and degradation rate of Anthracene without addition of hydrogen peroxide is fastest.

9- Treatment of Anthracene by Fenton and photo Fenton shows the optimum conditions are as follows; 16ppm of Anthracene is better than 4ppm, 120 mg of ferric iron is the best, 200mg/L of hydrogen peroxide is more efficient, pH =4 is the most appropriate medium for oxidation, 323.15K is the fastest degree for degradation and 3.0 mW. cm^{-2} is the best intensity of light.

10- The competitive degradation study using ozone with or without addition oxidation methods shows the following arrangement:

$UV+O_3+TiO_2 > UV+O_3+H_2O_2 > UV+TiO_2 > UV+O_3 > O_3 > UV$

11- Complete degradation of 9,10-Anthraquinone needs about 44 hours duration in the same conditions used for degradation of anthracene.

4.8. Recommendations

1- Development of experimental and theoretical models for estimation of the PAHs in surface water in all Iraq's rivers.

2- Development of analytical methods and additional characterization of concentrations of a broader range of PAHs in ambient air, drinking water and sediments.

3- Encouragement of Governmental authorities for using the green and renewable energy for electric generation and for irrigation to reduce the amount of pollutants that emitted in atmosphere.

4- Periodical evaluation for PAHs concentration in surface water in all Iraq's rivers.

Publications

1- Faiq F. Karam, Falah H. Hussein, Sadiq J. Baqir and Fadhil M. Abed, Determination of polycyclic aromatic hydrocarbons in surface water of Shatt Al-Hilla River, Asian Journal of Chemistry; Vol. 24, No. 12 (2012), 5589-5591.

2- Falah H. Hussein, Faiq F. Karam and Sadiq J. Baqir, Monitoring of PAHs in Surface Water of Shatt Al-Hilla River, A-case study, Asian Journal of Chemistry; Vol. 26, No. 15(2014), manuscript No. 1600, under printing.

3- Falah H. Hussein, Faiq F. Karam and Sadiq J. Baqir, Determination of Benzo(a)anthracene in Surface Water of Shatt Al-Hilla River by Solid
Phase Extraction and High Performance Liquid Chromatography A-Case Study, Asian Journal of Chemistry; Vol. 26, No.15(2014), manuscript No 1061. under printing.

4- Falah H. Hussein, Faiq F. Karam and Sadiq J. Baqir, Determination of Benzo(a)Pyrene in surface water of Shatt Al-Hilla River A-case study, Asian Journal of Chemistry: Vol.26 (2014), manuscript No. 17162/2014, under printing.

5- Faiq F. Karam, Falah H. Hussein, Sadiq J. Baqir, Ahmed F. Halbus, Ralf Dillert and Detelf Bahnemann, Photocatalytic degradation of Anthracene in closed system reactor, International journal of Photoenergy, Volume 2014, Article ID 503825, 6 pages.

Conferences

1- Faiq F. Karam, Falah H. Hussein and Sadiq J. Baqir Determination of polycyclic aromatic hydrocarbons in surface water of Shatt Al-Hilla River. A poster presented at the ICGTCS- conference held at Udaipur, India during 3-4th **March 2012**.

2- Faiq F. Karam, Falah H. Hussein and Sadiq J. Baqir attendance in Nano day 2012, which held in 27th **September 2012** in Leibniz University, Hannover /Germany.

3- Faiq F. Karam, Falah H. Hussein and Sadiq J. Baqir, Treatment of Anthracene contaminated waters by Fenton process. A poster presented at 3ed European Conference on Photocatalysis which held in 25-27 **September, 2013**, Portoroz, Slovenia.

4- Faiq F. Karam, Falah H. Hussein and Sadiq J. Baqir, Treatment methods of Anthracene, the Ninth Scientific Symposium for Post Graduate Studies, oral presentation in college of Science, University of Babylon, **May 2013**.

5- Faiq F. Karam, Falah H. Hussein and Sadiq J. Baqir, Determination of polycyclic aromatic hydrocarbons (PAHs) in surface water of Shatt Al-Hilla River: Analytical methods, Environmental concerns and Treatment methods, the Ninth Scientific Symposium for Post Graduate Studies-PhD, oral presentation in college of Science, University of Babylon, **May 2013**.

Poster Presentations

1- Faiq F. Karam, Falah H. Hussein and Sadiq J. Baqir "Determination of polycyclic aromatic hydrocarbons in Shatt Al-Hilla River", **December 2011**, College of Science, Chemistry Department, Babylon University-Iraq.

2- Faiq F. Karam, Falah H. Hussein and Sadiq J. Baqir, "Determination the physicochemical properties of surface water of Shatt Al-Hilla River", **March 2012**, International Conference On Global Trends In Pure And Applied Chemical Sciences(ICGTIACS-2012), **3-4 March 2012**, Udaipur (Rajasthan) India.

.

3- Faiq F. Karam, Falah H. Hussein and Sadiq J. Baqir, "Photocatalytic degradation of Anthracene by titanium dioxide", **February 2013**, College of Science, Chemistry Department, Babylon University-Iraq.

4- Faiq F. Karam, Falah H. Hussein and Sadiq J. Baqir, " Treatment of anthracene contaminated waters by Fenton process ", 3ed European Conference on Photocatalysis which held in **25-27 September, 2013**.

5- Faiq F. Karam, Falah H. Hussein and Sadiq J. Baqir, "Treatment of anthracene by ozonation", **January 2014**, Chemistry Department, College of Science, Babylon University-Iraq.

6- Faiq F. Karam, Falah H. Hussein and Sadiq J. Baqir, Determination of polycyclic aromatic hydrocarbons (PAHs) in surface water of Shatt Al-Hilla River", **April 2014**, Chemistry Department, College of Science, Babylon University- Iraq.